Titre: Title:	Validation of a Test Protocol for Navigation Surgery in Total Knee Arthroplasty
Auteur: Author:	Atefeh Zarei
Date:	2022
Type:	Mémoire ou thèse / Dissertation or Thesis
Référence: Citation:	Zarei, A. (2022). Validation of a Test Protocol for Navigation Surgery in Total Knee Arthroplasty [Master's thesis, Polytechnique Montréal]. PolyPublie. https://publications.polymtl.ca/10359/

POLYTECHNIQUE MONTRÉAL
affiliée à l'Université de Montréal

Validation of a Test Protocol for Navigation Surgery in Total Knee Arthroplasty

ATEFEH ZAREI
Institut de génie biomédical

Mémoire présenté en vue de l'obtention du diplôme de *Maîtrise ès sciences appliquées*

Génie biomédical

Mai 2022

POLYTECHNIQUE MONTRÉAL
affiliée à l'Université de Montréal

Ce mémoire intitulé :

Validation of a Test Protocol for Navigation Surgery in Total Knee Arthroplasty

présenté par **Atefeh ZAREI**
en vue de l'obtention du diplôme de *Maîtrise ès sciences appliquées*
a été dûment accepté par le jury d'examen constitué de :

Carl-Éric AUBIN, président
Delphine PÉRIÉ-CURNIER, membre et directrice de recherche
Karine DUVAL, membre et codirectrice de recherche
Jean THURIET, membre et codirecteur de recherche
Nicola HAGEMEISTER, membre

DEDICATION

To my daughter Adrina,
My inspiration and my life...

À ma fille Adrina,
Mon inspiration et le but de ma vie...

ACKNOWLEDGEMENTS

"Let us be grateful to the people who make us happy; they are the charming gardeners who make our souls blossom."

- Marcel Proust

The completion of this master's thesis was indeed a meandering road, which would have never been possible without the support of a number of amazing people, whom I was lucky enough to cross paths with.

First and for most, I owe a great debt of gratitude to my mentor and supervisor for the past three years, Prof. Delphine Périé-Curnier, who has always fascinated me by her dedication, intelligence, and professionalism.

Then, special thanks go to my research co-supervisor, Karine Duval, for her trust and her patience, who kindly supported me trough the past three years.

Next, I would like to express my deep gratitude to my mentor and second co-supervisor Jean Thuriet. He showed me how to be a big-picture thinker yet a detail-oriented researcher. He always guided me away from incremental research and showed me how to explore the unknown, how to structure innovative research, and how to set milestones and achieve them efficiently.

The past three years at Zimmer Cas have been a great experience both educationally and socially. I would like to take this opportunity to appreciate the engineers and staff members of ZimmerCas. In particular, I thank Dr. Emmanuel Gaillard, Nathalie Godin, and Marie-Claude Rasetti for their kind support during my master's study. I also thank the incredible friends I've made from the iAssist team at Zimmer.

During the past three years I took couple of courses at Polythechnique, where I was fortune enough to learn a lot from my Professors and classmates.

I would also like to thank Mitacs organisation for offering me la bourse Mitacs Accélération and supporting this work.

My sincere gratitude goes to the jury members of my master's thesis, Prof. Carl-Éric Aubin and Prof. Nicola Hagemeister for their time and effort in evaluating my thesis.

9,428 km away from home I would like to appreciate all my mentors, from whom I had learned a lot throughout my educational journey in my beloved country, Iran. Unfortunately,

these lines are too short and my memory is too limited to remember and name all and put in words how important their role has been. Nevertheless, I would like thank Dr. Amin Ebrahimzadeh, Dr. Sabalan Daneshvar and Mrs. Hassanzadeh, my high school teacher, who made me interested in biomedical engineering. Also, I would like to thank my friends from my hometown, Tehran, for their true friendship and encouragement.

Last but not least, special thanks goes to my parents, my family, my lovely daughter, Adrina, and my beloved husband (yol arkadaşım), Amin, for their endless, unconditional love and support. I am blessed beyond words to have had their love, encouragement, and support in ups and downs of this journey.

Atefeh Zarei

Montréal, Canada

May 2022

RÉSUMÉ

Reconnue comme l'une des procédures orthopédiques les plus réussies avec un taux de survie de plus de 90 % au cours des 15 dernières années, le remplacement total du genou, également appelé arthroplastie total du genou, vise à remplacer les articulations du genou endommagées (ex. cartilage) avec un genou artificiel. Le succès d'une procédure de remplacement de genou dépend principalement du placement précis de la prothèse et de l'alignement du membre inférieur. Pour augmenter la précision du remplacement de genou, l'application de la robotique en chirurgie orthopédique a récemment émergé, laissant la place à un groupe de systèmes intervention humaine dans la boucle, qui combinent la dextérité des chirurgiens humains et la précision des robots. Un exemple de tels systèmes est le système de genou iAssist, qui est bien connu pour ses avantages, tels qu'un temps de chirurgie plus court par rapport aux systèmes assistés par ordinateur à grande console, un coût réduit et des complications post-chirurgicales réduites. Une nouvelle version d'iAssist a récemment été conçue avec des mises à jour du système, ce qui oblige à revalider l'ensemble du système en termes de précision et de sécurité. L'objectif de cette recherche est de concevoir un protocole de test pour valider la précision de la nouvelle version d'iAssist pour la procédure fémorale. L'objectif principal de cette étude peut être divisé en sous-objectifs suivants: (i) développer un protocole de test ainsi que la conception d'un spécimen artificiel, (ii) caractériser l'efficacité du protocole de test proposé, (iii) mesurer la déviation des angles de résection cruciaux, (iv) valider qu'iAssist est aussi précis que la méthode conventionnelle. Notre méthode de validation proposée repose sur l'utilisation d'une machine de mesure de coordonnées (FaroArm), ainsi qu'un spécimen de fémur artificiel spécialement conçu. Après avoir défini toutes les étapes de la procédure de test avec le FaroArm, une évaluation détaillée a été effectuée pour prendre en compte les sources d'erreurs possibles et pour caractériser la précision de la procédure de mesure. Les résultats ont montré que la méthode de mesure proposée est 6 à 7 fois plus précise que la précision estimée d'iAssist, ce qui est une performance élevée pour une prototype. La méthode de mesure étant suffisamment précise, nous avons donc procédé à la mesure de la précision d'iAssist. La précision d'iAssist pour la procédure fémorale est définie par la précision avec laquelle iAssist localise le plan de résection fémoral, par rapport aux angles varus/valgus et flexion/extension spécifiés par le chirurgien. Ces angles qui définissent le plan de résection sont déterminés avec l'axe mécanique du fémur. L'axe mécanique, par définition, est une ligne passant par deux repères anatomiques : le centre de l'articulation du genou (entre le condyle latéral et médial) et le centre de la sphère fémorale. La précision de la procédure fémorale avec iAssist n'est validée que si la précision de la résection fémorale

distale pour d'angle varus/valgus se situe à ±3° dans 83.6 % des cas et pour l'angle de flexion/extension à ±3° dans 65.7 % des cas, selon les exigences du système et la précision de la méthode conventionnelle. Comme le résultat de notre étude démontre que la précision globale d'iAssist obtenue par notre technique de mesure était de [-2,21, +2,84] dans 96.6% des cas pour l'angle V/V, et de [-2.06, +2.93] dans 86.6% pour l'angle F/E. Les résultats de cette étude ont montré que nous avons atteint l'objectif principal de cette thèse et défini un protocole de test pour mesurer la précision du système de genou iAssist. L'amélioration de la procédure de test sera possible en améliorant la conception du modèle de recherche ou les autres aspects de la méthode de test. L'ajout de poids, pour simuler les poids des tissus mous sur l'os (par exemple, les muscles et les tendons) est suggéré pour améliorer le modèle de recherche. Une autre suggestion est d'exécuter le protocole de test par des chirurgiens experts, afin d'améliorer d'autres aspects de la méthode de test.

ABSTRACT

Known as one of the most successful orthopaedic procedures with a survival rate of more than 90% in the past 15 years, total knee replacement, also referred to as total knee arthroplasty (TKA), aims to replace damaged knee joints (i.e., bone and cartilage) with an artificial one. Successful outcome of a TKA procedure mainly depends on the accurate placement of the prosthesis and the alignment of the lower limb. To increase the accuracy in TKA, the application of robotics in orthopedic surgery has recently emerged, giving way to a group of human-in-the-loop (HITL) systems, which combine the dexterity of human surgeons and accuracy of robots. An example of such systems is the iAssist Knee System, which is well known for its advantages, such as a shorter time of surgery in comparison with large console Computer Assisted Systems, reduced cost, and reduced post-surgical complications. A new version of iAssist has recently been designed with system updates, which mandates the need to re-validate the whole system in terms of accuracy and safety. The objective of this research is to design a test protocol to validate the accuracy of the new version of iAssist for the femoral workflow. The main objective of this study can be divided into the following sub-objectives: (i) to develop an accuracy test protocol along with designing an artificial specimen, (ii) to characterize the efficiency of the proposed test protocol, (iii) to measure the deviation of the crucial resection angles, (iv) to validate that iAssist is as accurate as the conventional method. Our proposed validation method relies on using a coordinate measuring machine (FaroArm), along with a specifically designed artificial femur specimen. After defining all the steps of the test procedure with the FaroArm and specimen, a detailed assessment has been done to take into account the possible sources of errors and to characterize the accuracy of the measuring procedure. The results has shown that the proposed measuring method is 6.5 to 7.3 times more accurate than the estimated accuracy of iAssist, which is a high performance for a prototype. Since the measuring method was accurate enough, thus we had proceed with measuring the accuracy of iAssist. The accuracy of iAssist for the femoral workflow is defined by how accurately iAssist locates the femoral distal cut plane, relatively to the varus/valgus and flexion/extension angles specified by the surgeon. These angles that define the cut plane are determined with the mechanical axis of the femur. The mechanical axis, by definition, is a line passing two anatomical landmarks: the center of knee joint (between the lateral and the medial condyle) and center of the femoral sphere. The accuracy of the femoral workflow with iAssist is validated only if the accuracy of the distal femoral cut for varus/valgus angle falls within $\pm 3^\circ$ in 83.6% of all cases and for flexion/extension angle falls within $\pm 3^\circ$ in 65.7% of all cases, as per the system requirements and the accuracy of conventional method. As the

result of our study demonstrate the overall accuracy of iAssist obtained by our measuring technique was [-2.21, +2.84] in 96.6% of the cases for varus/valgus angle, and [-2.06, +2.93] in 86.6% for flexion/extension angle. The results of this study has shown that, we achieved the main objective of this thesis and defined a test protocol to measure the accuracy of iAssist knee system. Improvement of the test procedure will be possible by improving the design of the research model or other aspects of the test method. Applying weight, to simulate the weights of the soft tissues on the bone (e.g. muscles and tendons) is suggested to improve the research model. In addition to improvement of the research model, executing the test protocol by expert surgeons is suggested to improve other aspect of the test method.

TABLE OF CONTENTS

LIST OF TABLES

LIST OF FIGURES

LIST OF SYMBOLS AND ACRONYMS

CAS	Computer Assisted System
TKA	Total Knee Arthroplasty
TKR	Total Knee Replacement
V/V	Varus/Valgus angle
F/E	Flexion/Extension angle
MA	Mechanical Axis
ASME	American Society of Mechanical Engineers
RP	Resection Plate
MAEP	Mechanical Axis Entry Part

LIST OF APPENDICES

CHAPTER 1 INTRODUCTION

Arthroplasty is an orthopedic surgical technique with the aim of rehabilitating the function of joints by remodeling, realigning, or replacing the articular surface of musculoskeletal joints. The three most commonly executed types of arthroplasties are shoulder arthroplasty, hip arthroplasty and knee arthroplasty [1]. Patients undergoing these types of surgeries usually suffer from degenerative joint disease, which may eventually lead to loss of cartilage in the joints. Osteoarthritis is one the most common degenerative joint diseases that has affected 240 million people globally in 2016. Among these, knee is one of the most commonly affected joints [2]. Therefore, total knee arthroplasty (TKA), also known as total knee replacement, is one of the most interesting topics in biomechanics and biomedical research and studies. The main idea behind the TKA is to replace the damaged knee joint (i.e., bone and cartilage) with an artificial knee (prosthesis), which is typically made of metal, plastics, or polymers. The experience of the patients who underwent TKA is often positive in terms of functional and clinical outcomes. Based on patient-reported outcomes, satisfaction rate among the patients was reported around 70%-93% [3].

1.1 Basic Concepts and Definitions

The success of TKA depends on the selection of alignment technic and how the procedure achieves the main objectives of the TKA, which include restoration of function, provision for stability and durability, and, importantly, pain relief [4].

The terms of alignment corresponds to, three important steps during a TKA procedure:

- The resection angle of the damaged tissue (femoral distal cut and tibial proximal cut,
- Placement of the tibial and femoral components of the prosthesis and the alignment of them with each other,
- Alignment of the lower limb (Hip Knee Ankle).

1.1.1 Basic Concepts

There are different conventional approaches to achieve a successful TKA procedure:

1. Systematic approach: “A systematic approach means that this alignment strategy is used on every patient homogeneously. Currently, a systematic mechanical alignment

strategy is most widely used by knee surgeons" [5]. Mechanical alignment and anatomical alignment technics fall within the category of systematic approaches [5].

2. Patient-specific approach: A patient specific approach is a method based on the restoration of the constitutional anatomy and inherent kinematics of the patient's knee. In this technique, surgical plans vary based on the characterization of each individual knee. Kinematic Alignment (KA) and Unicompartmental Knee Arthroplasty (UKA) are the mostly performing surgery from this category [6].

3. Hybrid approach: Integration of different alignment techniques from different approch falls in the category of hybrid approach. Restricted Kinematic Alignment (rKA) and Adjusted Mechanical Alignment (aMA) are the examples for this category of total knee arthroplasties [7].

In the past decades, TKA has gone through lots of changes and improvements compared to the early stages. In particular, the advances in TKA have been seen in different elements of TKA such as computer navigation, cutting guidance based on MRI and CT, enhancement of the recovery programs, design of the implant and material, and also patient-specific implants [3]. The importance of computer navigation systems during TKA procedure, give rise to the use of different motion tracking methods to achieve a navigation system with higher accuracy. One of these interesting navigation systems is iAssist Knee System, an inertial based navigation system [8]. Figure 1.1 shown a Femoral workflow of a TKA procedure in the help of iAssist. Later in the problematic section, the iAssist Knee system is explained in details.

1.1.2 Definations

In this section, short summaries of essential concepts related to the research topic are presented:

Mechanical Axis (MA) of the Femur: An imaginary line passing from the center of the proximal femoral head (femoral sphere) to the center of knee joint on the distal femur, as shown in Figure 1.2.

Mechanical Axis (MA) of the Tibia: An imaginary line passing by the center of knee joint on the proximal tibial and the center of ankle on the distal tibia, as shown in Figure 1.2.

Mechanical Axis (MA) of the Lower Limb: An imaginary line passing from the center of the proximal femoral head (femoral sphere), the center of knee joint (distal femur) and the center of ankle on the distal tibia, as shown in Figure 1.2.

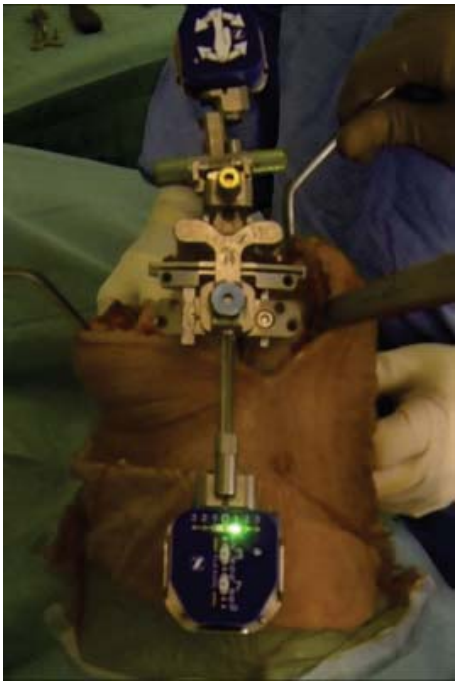

Figure 1.1 An illustration of using iAssist during a TKA procedure [9]

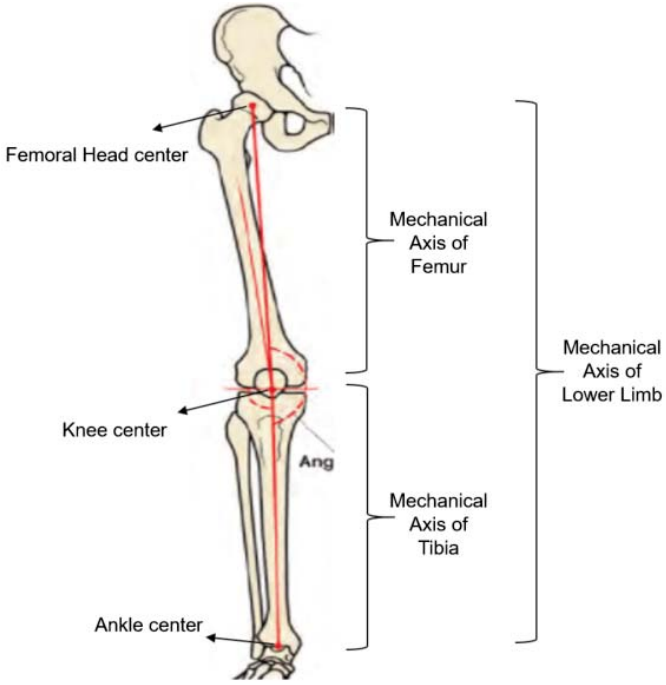

Figure 1.2 An illustration of mechanical axis of lower limb [10]

Femoral Distal Cut: Femoral distal cut is made perpendicular to the mechanical axis of the femur, as shown in Figure 1.3.

Tibial Proximal Cut: The tibial proximal cut is made perpendicular to the mechanical axis of the tibia, as shown in Figure 1.3.

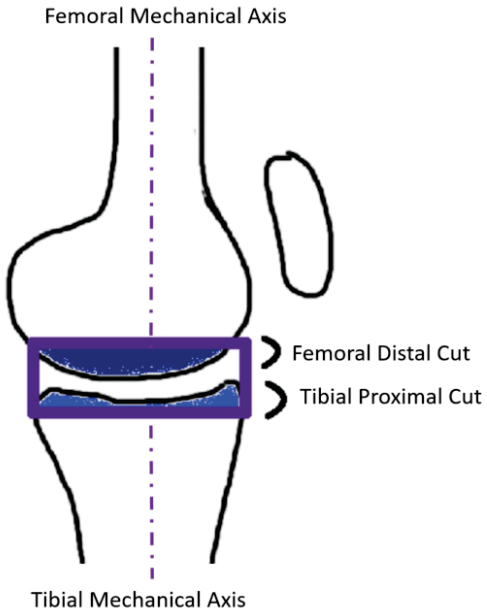

Figure 1.3 An illustration of the cuts in Total Knee Arthroplasty [11]

1.2 Problematic

Over the past years, accurately aligning the components of the prosthesis has been reported as the determinant key of a survival total knee arthroplasty [12] [13].

The conventional methods of TKA use the femoral intramedullary guide and the tibial extramedullary guide for component placement and alignment in TKA. The two serious shortcomings of these techniques are as follows:

1. having a limited degree of accuracy especially for the femoral distal cut [14].
2. injury of the intramedullary canal of the femur due to use of the intramedullary rod which leads to a higher blood loss [14].

In order to overcome these shortcomings, computer assisted navigation systems were developed. Involvement of navigation systems in orthopedic surgery started with total hip arthroplasty.

The first TKA procedure with the involvement of a navigation system took place in 1997 [12] [15] [16]. To navigate surgeons through TKA procedure, there are various techniques of computer assisted system (CAS) depending on the underlying tracking method.

Motion trackers help users in navigation by providing position and orientation control of the desired object and let users to match the virtual computer graphics representations of the objectives with their physical counterparts [17].

The currently used navigation systems in the TKA field are optical navigation, image-based navigation, fluoroscopy-based navigation, imageless navigation, and electromagnetic navigation [12].

The results of many studies and publications demonstrate the accuracy of computer assisted navigation in TKA is significantly higher compared to the conventional methods [18]. It has been reported that the assistance of the computer navigation systems in restoration of the mechanical axis of the lower limb is $\pm 3^{\circ}$ is 98% to 100% of the TKA procedures, whereas in conventional methods, this figure is 90% to 92% of TKA procedures [4].

These results demonstrate that the computer navigation systems are able to achieve the primary goal of TKA, which is to minimize the malalignment of the lower limb and to enhance the component placement [4]. The benefits of using the navigation systems in the TKA procedure is not limited to accurately aligning the components of the implant and lower limb. In fact, it has other advantages such as postoperative recuperation, more precise and reproducible bony resection, low blood loss and ligament balancing [14] [16].

Although the use of navigation systems has overcome the issue of accuracy in TKA, some inconveniences and complexity have been added to the field such as:

1. Dependence on the inputs from the surgeon [4].
2. Incurring of additional time [4].
3. Cost In clinical field and surgical procedures [4].
4. Pin loosening and fracture [4].
5. Requiring a learning phase [19] [4] [20].

Due to the aforementioned shortcomings discussed above the involvement rate of the navigation system in TKA is about 5% of the overall number of TKA surgical workflow [12]. Toward this end, the attempt of combining the accuracy associated with large console computer-assisted systems and convenience of conventional systems without the need for large computers to assist surgeons has been proposed by Zimmer Biomet company [14] [5].

iAssist was introduced the field in 2012 [14]. In fact iAssist is less invasive compared to conventional methods, the small spike in iAssist with the help of electronic navigation pods plays a role as the femoral intramedullary rod in conventional methods. As iAssist is not a large console computer-assisted-system therefore the additional operation time in surgical procedure with iAssist is less than other navigation systems. Thus the initial setup cost of the navigation systems no longer exist in the TKA with iAssist knee system [14].

In addition, the pin site location problem is less challenging compare to the other navigation methods [14] [19]. The other important feature in iAssist knee system is the ability to intra-operatively validate the resection for femur and tibia with validation tools and validation pods.

The results of [21] a meta-analysis on clinical outcomes of iAssist, showed that 89.1% of surgeries in the help of iASSIST were within $\pm 3^{\circ}$ of neutral MA of the lower limb. In the conventional treatments only 70.96% of the surgeries were within $\pm 3^{\circ}$ of neutral MA lower limb. The result of this study, establish that, the iASSIST navigation system provides more accurate prosthesis implantation compare to the conventional methods.

Recently, the fact of continuous improvement procedure in the company give rise to design of a new version of iAssist with system updates. The fact that new technics should be extensively tested before being used on patients, mandates the need to revalidate the whole system in terms of accuracy and safety [22].

The new version of iAssist knee system has been evaluated with frozen human cadaver as research models. In the cadaveric validation lab the optical system has been selected as gold standard for measuring the accuracy of iAssist.

Executing accuracy validation tests on cadavers has some inconveniences and the company faced some challenges during the cadaveric validation lab, here the challenges are pointed out:

1. Cost: The high cost for the cadaveric lab partly was due to cadaver specimens and the environment. Buying cadavers for using them as research model is expensive. The use of cadavers as specimens requires a testing environment compatible with the cadaver for instance an adequate temperature. Preparing and maintaining this type of environment adds extra cost to the research.

2. Time consumption: As discussed previously, since the cadaveric need a specific environment, providing this condition and setting up the desirable circumstances imposed extra time to the study.

3. Complexity of use: Using cadavers as specimens requires numerous administrative works and standard processes.

4. Measuring tool: As mentioned previously the optical system has been selected as gold standard in the cadaveric study. The results of iAssist have been compared with the results of the optical system. Therefore validating the accuracy of iAssist knee system has been done relatively to the accuracy of optical system. As the result of [9] demonstrate, the first version of iAssist in 95% of cases was as accurate as the optical navigation system. We expect that the accuracy of the new version will be close to the accuracy of previous version. Validating the accuracy of new version of iAssist by comparing it with optical system which has more or less the same accuracy as iAssist, it is sufficient. However, having a system 10 times more accurate as estimated accuracy of iAssist system is the best strategy for validating the iAssisy knee system [23].

The motivation of this study is to overcome the challenges which are related to the validation cadaveric lab. Thus, the company decided to conduct a new measuring protocol for validating the accuracy of iAssist.

1.3 Research Objectives

The main objective of this study is to design a test procedure in order to validate the accuracy of the new version of iAssist knee system. This objective is divided into the following sub-objectives:

(i) To define the accuracy test protocol and develop a compatible specimen for performing the test method on it.

(ii) To validate the performance of the designed test procedure as well as the equipment involved in the test procedure and characterize the upcoming contributed errors in different steps and the use of different equipment during the test procedure.

(iii) To measure the deviation of crucial resection angle (femoral distal cut angle) during the surgical procedure with iAssist for the femoral workflow.

(iv) To validate that iAssist knee system is at least as accurate as the conventional method.

Figure 1.4 illustrates the workflow of the designing the accuracy test protocol for validating accuracy of iAssist.

The definition of validation in our study is customer oriented which means assessing the achievement to the design inputs and the user needs of the design of the iAssist knee system.

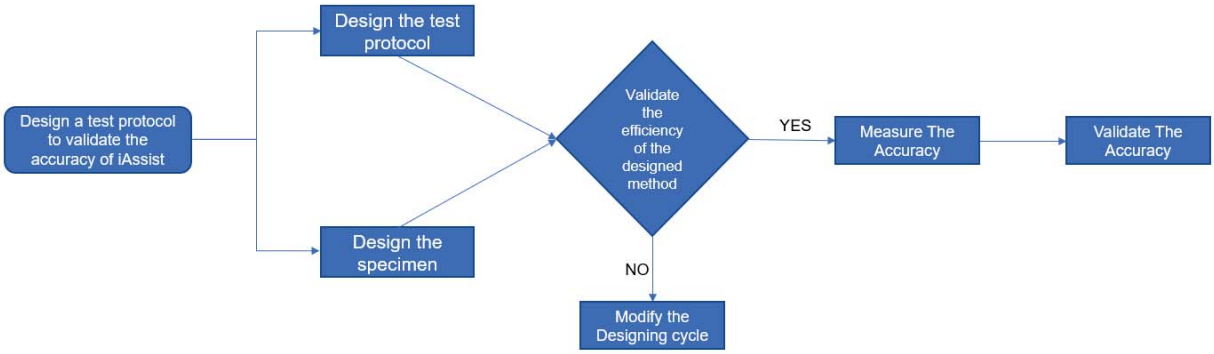

Figure 1.4 Flowchart of the proposed test protocol design.

The user needs and the design inputs of the iAssist knee system has been gathered from the needs of surgeons and physician during a surgical procedure, Zimmer Biomet sales associate, and company designers. We have selected accuracy among many other user inputs such as, usability, safety, ease of use, and compatibility. The reasons why we select accuracy to validate the iAssist Knee system are as follows:

(i) **Time**: Since my study is a master's project and validating the accuracy requires shorter time than other features (i.e. usability, safety, etc) so it fits well with a master's project.

(ii) **Proof of Concept**: In order to demonstrate the ability of the iAssist knee system in accurately recognizing the angles of the femoral distal cut.

(iii) **Quantitative Feature**: Validating a quantitative feature is simpler and sharper than a qualitative feature.

1.4 Thesis Outline

Chapter 1 of this thesis introduces the main principles of total knee arthroplasty, causes of undergoing knee surgical procedure, and objectives of TKA. Different methods for achieving the objectives of the TKA were explained. Further, we also discuss the motivation and thesis objectives.

In Chapter 2, a detailed literature review is presented on the computer assisted systems and motion tracking systems.

Chapter 3 is about the proposed test method, designing the different involved equipment of the test procedure and characterize the contributed errors during the execution of proposed method.

Chapter 4 will be dedicated to the results and the statistical analysis of the outcome of the developed test procedure and validating the accuracy of proposed test method.

In Chapter 5, we discussed the challenges and limitations of the proposed test method as well as the drawbacks and the uncertainties in measurements.

In the last chapter (conclusion), we present some concluding remarks along with a few interesting research directions to be explored. In this chapter also some possible future works in order to overcome the challenges and limitations of this research will be provided.

CHAPTER 2 LITERATURE REVIEW: ARTICLE 1: A REVIEW OF MEDICAL ROBOTICS AND MOTION TRACKING SYSTEMS FOR TOTAL KNEE ARTHROPLASTY

2.1 Presentation of the Article

The article presented in this chapter reviews different robotic techniques which has been used in TKA procedures. It also consists a review on different tracking systems applied in robotic systems involved in TKA. These reviews are necessary for a good understanding to better answering the matter of gold standard choice to validate the accuracy of iAssist.

This article, entitled "A Review of Medical Robotics and Motion Tracking System for Total Knee Arthroplasty", was submitted to the journal "Orthopaedics & Traumatology: Surgery & Research" in October 2021. The contribution of the first author to the preparation and writing of the item is valued at 75%

2.2 Beginning of the Article

TITLE: A REVIEW OF MEDICAL ROBOTICS AND MOTION TRACKING SYSTEMS FOR TOTAL KNEE ARTHROPLASTY

Authors:

Atefeh Zarei†

Jean Thuriet*

Emmanuel Gaillard*

Delphine Périé†

Affiliations:

†Polytechnique Montréal, 2500 Chem. de Polytechnique, Montréal, H3T 1J4, QC, Canada

*Zimmer Biomet Montréal, 75 Rue Queen, Montréal, H3C 2N6, QC, Canada

Corresponding author:

Delphine Périé-Curnier

Address: C.P. 6079, Succ. Centre-ville, Montréal, Québec, Canada, H3C 3A7

Phone: (1) 514-340-4711 #4437

Fax: (1) 514-340-5264

E-mail address: delphine.perie@polymtl.ca

Abstract

Total Knee Arthroplasty (TKA) is known as one of the most successful procedures among all orthopedic surgical procedures. The accuracy of the placement of the prosthesis is key to high survival rate of TKA. Medical robots have recently emerged to help the surgeons get the procedure done more accurately. The most important component of medical robots is the so-called tracking system, which has a direct impact on its accuracy. In this paper, after reviewing different techniques of surgical assistant robots in TKA, we present a comprehensive survey of motion and object tracking systems. Our comparison of the different techniques is carried out based on three criteria of accuracy, compatibility with minimally invasive surgery (MIS), and complexity of use. We also explain how iAssist Knee System can serve as a contemporary human-in-the-loop robotic system, which relies on an inertial motion tracking system to achieve a relatively high accuracy and desirable outcome.

Introduction

Total knee arthroplasty (TKA) or total knee replacement is a surgical procedure with the aim of replacing damaged knee joints (i.e., bone and cartilage) with an artificial (prosthesis) knee made of metal, plastics, or polymers. Nowadays, TKA with a survival rate of more than 90% in the past 15 years is one of the most successful orthopaedic procedures [24]. The impact of component malalignment varies from a patient to another, depending on various factors. Instability and aseptic loosening, polyethylene wear, and patellar dislocation, causing unpleasant perceptions by patients are some types of the implant failures [24] [25]. Degeneration of cartilage is the main cause of the need of TKA. This phenomenon is coming from Osteoarthritis or leg deformity which is a congenital physical abnormality [26]. In 2016, Osteoarthritis (OA) affected 240 million people worldwide. In the United States, 27 million people were diagnosed with OA, the most commonly affected area is knee. The risk of development of OA is higher among individuals older than 45 years old [27]. The statistical reports from Canada show that between 2017 and 2018, a total of 128,994 joint replacements were performed. During the same period, a total of 58,492 hip replacements and 70,502 knee replacements were done. The results of this study demonstrate an increase of 17.0% on the executed total knee arthroplasty in the five past years. "These joint replacement surgeries have an average acute length of stay of 4.5 days and also account for more than 585,000 acute care bed days" [28]. From a cost perspective, each joint replacement surgery would cost around 10,000 USD as the inpatient cost. It should be mentioned that the rehabilitation costs and physician payments are excluded from this amount. As the statistical studies represent, every year the spend on such surgery is more than 1.2 billion USD [28].

The growth of the demand for TKA highlights its importance in the quality of life of a large population. A large number of clinical studies and observations were done on the postoperative state of patients undergoing total knee surgery. The results of these works demonstrate the safety and efficiency of TKA including pain reduction, improvements in the quality of life, enhancement of the motion ranges, and functional status improvements for the older population. Research reveals a range between 75% to 89% of satisfaction rate among the patients treated by a total knee replacement [29] [30]. The key factors in executing a successful TKA are as follows: (i) an ideal preoperative status of patient, (ii) choosing the suitable component, and (iii) choosing a proper surgical method. Generally, the surgical technique consists of the following three steps. First, the angles of the distal cut in femur bone are determined. Next, the angles of the proximal cut in tibia bone are determined. Then, femur and tibia are adjusted in order to neutrally align the leg [31].

Obtaining a hip-knee-ankle (HKA) angle of zero degree is the most important factor in getting the best clinical outcome. The greater the HKA angle is, the more severe the leg deformity (varus and valgus) becomes. This, as a result, leads to a short lifetime of the prosthesis and eventually the failure of TKA surgery [32]. The feasibility of controlling the aforementioned three steps, especially femoro-tibial alignment, caused the factor of choosing a proper surgical method to become the easiest element to control. There exists a variety of techniques for alignment of the femoro-tibial joint. Mechanical Alignment (MA), Anatomical Alignment (AA), and Kinematic Alignment (KA) are some of the widely used techniques, among others [31].

The application of robotics in the medical field goes back to 1985, when the so-called PUMA 200 was used to increase the accuracy of needle replacement in a computerized tomography (CT)-guided brain biopsy [33]. Puma 200 was designed to work alongside humans and had an accuracy of 0.05 mm. The application of robotics in orthopedic surgery emerged in the mid-1980s with the development of the ROBODOC (Integrated Surgical Systems, Inc., Sacremento, CA), which aimed to obtain an accurate fit for the prosthesis using an image-guided robot for preparing femoral canal in total hip arthroplasty (THA) [34]. After clinical trials on dogs, ROBODOC was first used in human subjects in 1992 and then shortly after was adapted to be used in TKA surgery. Despite the high accuracy and stability achieved by ROBODOC, conflicting results were reported on the amount of soft tissue problems and gait anomalies. Other evident disadvantages include increased theatre time, increased cost, and necessity for a pre-operative CT-based plan [35]. Not long afterwards, a number of robotic systems emerged. The active constraint robot (ACROBOT) (Imperial College, London, UK) underwent the first series of clinical trials in 2002 and showed consistent and accurate placement of implants in unicondylar knee arthroplasty (UKA) [36]. Later in 2008, the US food and drug administration (FDA) approved the MAKO robotic arm (Stryker, Mahwah, NJ, USA). In 2012, iAssist (Zimmer, IN, USA) computer assisted navigation system was introduced to be used in TKA. iAssist can help the surgeon obtain the best operation plan via calculating the right resection of tibia and femur. More recently, ROSA (Zimmer Biomet) has emerged, which is a surgical assistant robot using X-ray-based imaging systems. Figure 2.1 illustrates the timeline of surgical robotic systems.

Depending on the amount of involvement of human surgeon in the whole procedure, surgical robotic systems can be categorized as (i) fully-autonomous, (ii) semi-autonomous, and (iii) passive systems. After receiving the resection plan, autonomous robotic systems are able to perform the remaining operation independently. In contrast, semi-autonomous systems require limited involvement of the surgeon. In passive robotic systems, on the other hand, the surgeon has a full control on the entire procedure with the computer-aided navigation

guidance provided by the robot [37]. In this paper, we present a comprehensive survey on the aforementioned robotic systems and compare them in terms of the following criteria: (1) accuracy, (2) invasiveness, and (3) ease of use. Furthermore, we focus on the passive robotic systems, especially given that such systems tend to keep human in the loop, thus leveraging not only the unique skill-sets of human surgeons, but also the extra precision of robotics. As a fundamental component of passive systems, we compile the research work on different tracking systems and compare them in terms of accuracy, applicability in minimally invasive surgeries, and complexity of use. As a practical example of state-of-the-art passive systems, we discuss the performance and recent achievements of iAssist navigation system.

The remainder of this paper is organized as follows. In Section II, we detail the different types of autonomous systems and then narrow our focus on semi-autonomous systems and review the commonly used tracking systems. In Section III, after presenting a performance comparison between different robotic systems in terms of accuracy, invasiveness, and ease of use, we outline their advantages ad disadvantages. In Section IV, we present the discussion on the topic and summarize the review. Finally, we draw the concluding remarks in Section V.

II. Methods of Robotic Systems

Fully-autonomous, semi-autonomous, and passive robotic systems

In fully-autonomous robotic systems, the role of the human surgeon is limited to establishing and determining the plan of resection, positioning, and sizing. In such systems, the robot is capable of performing the operation independently with surgeon oversight. Autonomous systems did not succeed mainly due to issues with incurring injuries to nerve and other soft tissues. Examples of fully-autonomous robotic systems include ROBODOC (Curexo Technology Corporation, Fremont, CA) and CASPAR (Ortho-Maquet/URS, Schwerin, Germany). ROBODOC was the first robot used clinically in orthopedic surgery. ROBODOC was approved by European Union for sale in 1994, first being used in Germany. Similar to its early design, ROBODOC system is still CT-based. However, it is now a computer-aided robotic milling device, which allows surface preparation for TKA. In [38], it is demonstrated significant differences in the coronal femoral component angles, sagittal femoral angles, and sagittal tibial angles between the robotic assisted and conventional groups. The key feature of the ROBODOC system is the accuracy for dimension and positioning as well as the ability to see where the robot is milling, thus achieving a more consistent outcome. CASPAR was an image-guided robot aiming to improve and decrease the variability in the mechanical axis

in THA and TKA procedure [39]. The authors of [40] showed improved tibiofemoral alignment using the CASPAR system. Both ROBODOC and CASPAR rely on CT imaging for preoperative planning, meaning that they require the creation of a three-dimensional (3D) plan derived from CT-scan or MRI. Both systems have shown to obtain a greater precision with mechanical axis alignment in comparison with conventional techniques. However, these systems suffer from a number of detriments, namely, additional time for preoperative planning and registration, lack of surgeon input and intraoperative adjustment, and technical complications [37].

Semi-autonomous systems are another group of robotic systems requiring the involvement of the human surgeon to a greater extent compared to the fully-autonomous systems explained above. In such systems, a feedback loop is proved to the surgeon with the main objective of augmenting the surgeon's control as well as safety of the operation. We note, however, that in semi-autonomous systems, the surgeon cannot deviate from the pre-planned level of resection. The feedback can be provided via audio (i.e., beeping), visual (i.e., change of color), and/or haptic (i.e., vibration) signals. These alerts prevent over-resection and malposition during the operation, thus resulting in an increased accuracy and reduced errors in component placement. Semi-autonomous systems are often categorized as (i) image-based and (ii) image-free systems. Examples of semi-autonomous systems include MAKO robotic arm (Stryker, Mahwah, NJ, USA), Navio PFS (Smith & Nephew, Memphis, TN, USA) freehand sculpting robot, OMNIBOT (OMNIlife Science, Inc., Raynham, MA) robotic guide positioner.

Image-free systems do not require any preoperative imaging. Practical examples of image-free semi-autonomous systems are Navio PFS (Smith & Nephew, Memphis, TN, USA) freehand sculpting robot and OMNIBOT. Navio PFS is a handheld smart system, which is image-free. Being approved by FDA in 2012, it allows for freehand sculpting for unicondylar and patellofemoral knee arthroplasty. To be more specific, Navio exploits optical based navigation to provide 3D views of the operation. The main advantages of the Navio PFS, which come from being image-less, are: (i) eliminating the risk of radiation exposure and (ii) reduced cost of preoperative imaging. Also, it has a fairly rapid learning curve. We note, however, that Navio is only approved for UKA, which limits its applicability significantly. Given that the semi-autonomous systems are directly manipulated by the surgeons, the main advantage of such systems is minimizing the learning curve as well as the potential for inadvertent tissue injury.

Unlike image-free semi-autonomous systems, image-based systems rely on various imaging techniques (e.g., CT-scan, X-ray) to guide the surgeon through surgery. A practical example

of such systems is MAKO robotic arm (Stryker, Mahwah, NJ, USA), where a prospective CT-scan is used. MAKO robotic arm is an image-based haptic system, which is used for uni-compartmental knee arthroplasty, THA, and TKA. MAKO system was designed to help the surgeons obtain precision in partial knee arthroplasties. The robotic system provides the surgeon with haptic feedback during the operation, which can help avoid any deviation from the resection plan [41]. MAKO system is mostly used in UKA and THA operations. The MAKO system recreates the posterior tibial slope and coronal tibial alignment [39]. Further, MAKO also provide patient specific planning to the surgeons. MAKO system allows the surgeon to visualize the joint to identify any misalignment and deformity before the surgery. Before an incision is made, the MAKO system generates a virtual projected outcome of the surgery, which can be modified by the surgeon until the desired outcome is reached.

A group of image-based techniques derived from semi-autonomous systems is the so-called patient specific instrumentation (PSI), which has been around since 2000s. In 2006, PSI emerged as a new technology for TKA, which takes into account any slight deformities or osteophytes and applies preoperative planning for bone resection, using the predetermined implant size, position, and rotation [42]. The rate of using this method is greater than the use rate of computer navigation systems. This is because the surgical flow of PSI is simple compared to its counterparts [43]. As the name of this technology describes, PSIs are customized cutting blocks tailored for a given patient considering the unique features of his/her anatomy. These blocks are 3D models that are made regarding the pre-operative CT image or magnetic resonance imaging (MRI).

Unlike autonomous and semi-autonomous systems that inherently keep surgeons out of the loop, passive robotic systems rely on human's full intervention during the surgery. According to the commonly known concept of human-in-the-loop (HITL) systems, keeping humans in their jobs is a very important value. In the context of robotic surgery, passive systems (also known as computer assisted systems) are such systems that operate the task by integration of humans. Therefore, such systems can form an interesting group of HITL-based surgical robotic systems, which tend to keep humans in the loop and augment the humans by extending their capabilities rather than substituting them by robots [44]. Unlike fully- and semi-autonomous systems (where a great portion of the task is done by robots), passive systems use patient- and/or instrument-based reference points to provide the surgeon with preoperative recommendations and guide positioning of the surgical tools [45]. Surgeons can benefit from passive systems, commonly known as computer-assisted systems (CAS) or computer navigation surgery systems, which monitor the progress and provide the surgeon with data and guidance on precise placement of the prostheses. Computer-assisted systems are therefore suitable for minimally invasive surgeries in orthopedic surgery. In par-

ticular, navigation-assisted surgery has been used in TKA to address the major conventional shortcomings related to component malposition. In the following, we focus on the key components of computer-assisted systems namely, object tracking component and elaborate on different objective tracking systems, including mechanical, electromagnetic, optical, acoustic, fluoroscopic, and inertial tracking systems.

Object Tracking System for Passive Robotic Systems

An essential part of a computer-assisted medical intervention is the object tracking module [31]. The object tracking module enables us to continuously localize the medical instruments as well as the patient anatomy, which is key for guiding a surgeon through an operation [31]. The tracking procedure can be defined as determining the position and orientation of a moving object in a given 3D space with respect to a known coordinate system [31]. There exist various technologies of racking systems with different methods in order to define the position and trajectory of the used instruments during the surgery. Some examples include mechanical tracking systems, diverse kinds of optical cameras, electromagnetic systems, global positioning system (GPS)-based devices and ultrasonic sensors [32]. In the following section, we review these tracking systems in more detail.

Mechanical Tracking Systems

Mechanical Tracking Systems are operated by considering some points in a 3D volume as fixed references and then determining the physical links and connections between the points and the subject of tracking. The application of this method is in some of the newest generation of image-guided interventions (IGI) and also in measuring the position of the joints in the biomechanical field [46].

Electromagnetic Tracking Systems

A relatively new tracking technology in the medical field is the electromagnetic tracking (EMT) system. The key advantage of this technology is that unlike optical tracking systems, EMT systems track objects in real-time without needing a line-of-sight. For this reason, they are mostly used in minimally invasive surgery, where the tracking takes place inside the human body.

Optical Tracking Systems

Optical tracking system is a monitoring-based technology for 3D localization of objects in a work volume (measurement space) defined by using two or more cameras. Such a camera

is made by a lens bounded with infrared (IR) LEDs and lens are behind an infrared pass filter. LEDs around the lens illuminate the work volume periodically. The retro-reflective markers or navitrackers are small devices which are placed on the object that need to be tracked. This equipment operated by reflecting the income infrared light and sending it back to the camera. Camera detect reflecting IR and with internally processed procedure define the position of the object [47]. Basically there are two major types of optical tracking systems: (i) active systems and (ii) passive systems. In active systems, the desired object for tracking operation is equipped with a tool, which is equipped with diodes with the capability of emitting infra-red light. The emitted light is tracked by the camera. In contrast, in passive systems the equipment tool consists of infra-red reflecting balls. In such a system the emitted infra-red light by camera will be reflected by the camera so the camera will track the reflected light [48].

Acoustic Tracking Systems

The main idea behind acoustic tracking systems is to determine the location and position by the flighting time of the signals. An acoustic tracking system consists of two main components, a generating wave device and a receiver device. The generator device is responsible for generating the waves with a proper frequency (which can vary depending on the desired performance) and emit the waves through the work volume. The transmitted signals will then be sensed by the receiver. In this particular form of system, the receiver and the emitter should be separated and one of them should be placed on the object, which normally is the emitter on the object to be tracked and the other one on a fixed reference [46].

There is another major form of this technology, where the transmitter and the receiver are integrated. The operation of this specific system is based on the radiation and reflection of the waves. The second type of acoustic tracking system is known as a sound-based tracking system since the sound waves are playing a role as emitted signals. A common sound-based tracking system in the medical field are ultrasound systems [46] [49]. Despite the common properties, these two technologies have a slightly different point, which is the used signal. The used signal in ultrasonic systems is limited to the signals with the frequency greater than 20,000 Hz. In the medical field, this amount is around 10 MHz. An ultrasonic tracking system (UTS) can be viewed as a type of acoustic tracking system (ATS), which is due to the fact that the operation of both technologies is based on signals in various ranges of frequency. The application of ATS is very wide and diverse. They are widely being used in military, underwater research, air-space, meteorology, maritime, and aviation [46].

Fluoroscopic Tracking Systems

“Fluoroscopic navigation systems allow localisation of the position of a surgical instrument relative to the anatomy of the patient. By superimposing the instrument’s geometry onto fluoroscopic images, the surgeon can follow live the progression of the intervention" [48]. Basically, fluoroscopic images can be translated into an X-ray movie because the fluoroscopic image is a series of continual X-ray images. In other words, these systems are based on the combination of X-ray images and the human eye’s functionality. The first generation of these systems were 2D images, which suffered from the lack of depth [50]. Another downside of X-ray images is that the contrast of soft tissue in such an image is poor [51]. In recent computer assisted systems, geometric depth plays an important role regarding the navigation. The idea of creating a 3D image by combining two 2D X-ray images (anteroposterior and lateral images) appeared in the latest fluoroscopic tracking systems [50].

Inertial Tracking Systems (ITS)

Inertial navigation is not a new technology, dating back to the 1950s [52]. In inertial tracking systems, two main devices, accelerometer and gyroscope take action to define the orientation and position of objects and subjects. While accelerometers, also known as motion sensors, are in charge of defining the positions, gyroscopes play a role as the rotation sensors to determine the orientation. These systems follow the basic physical phenomena of a spring-mass system [53]. In the architecture of both gyroscope and accelerometer, there are two planes, namely a fixed plane and a mobile plane with a property to act as a capacitor. By changing the distance between two planes, the capacity of the capacitor will change, which can lead to creation of an electrical pulse. This pulse with the help of dead reckoning method and some built-in devices will be translated to the position and orientation of the object. Since such a system uses the dead reckoning technique, the output location will be continually without any need for external references [54].

Radio tracking systems

Most radio navigation systems operate on the principle of time-of-flight range finding, similar to the acoustic systems we described earlier. Radio tracking systems offer a number of benefits. First, electromagnetic wave-based tracking techniques can provide vastly greater range than quasi-static magnetic fields due to smaller amount of propagation loss. Second, absorption loss of radio waves is negligible in air. In fact, they are virtually unaffected by wind and air temperature. In the downside, radio waves are rapidly attenuated in water, so

the human body is opaque to all radio frequencies useful for precision ranging. Moreover, larger speed of light compared to sound makes the task of measuring time of flight with sufficient precision much more difficult and prone to measurement errors [52].

For completeness, we have summarized the merits and shortcomings of various motion tracking systems in Table 2.1.

Practical State-of-the-Art: iAssist Knee System

Among the variety of methods and techniques that navigate surgeons during a TKA procedure, the passive systems are of particular interest, especially due to the HITL nature of such systems. Despite all this diversity, the portion of surgeries done with this technology is about 5%. This small rate is due to the two major weaknesses of such systems, namely, the complexity of use and the requirement of extra time. Lack of accuracy in the conventional methods was a motivation for development of total knee arthroplasty navigation systems, but the previously mentioned inconvenience points do not exist in conventional systems. Relying on an inertial tracking system, iAssist system is a contemporary attempt to combine the accuracy associated with large console computer-assisted systems and convenience of conventional systems without the need for large computers to assist [55]. iAssist navigation system consists of two components, conventional instruments and miniaturely disposable electric pods, as shown in Fig. 2.2 [56]. The pods are made by the accelerometers and gyroscope. Therefore, the iAssist system falls in the class of inertial navigation systems, thus offering the advantages of using the inertial electronic component, which facilitates the tracking operation. By attaching the electrical pods on the tibial or femoral instrument, the iAssist system gives the proper angle, which guides the surgeon on the execution of femoral and tibial resections. Determining the resection angle is coming from the mechanical axis of the bone. Basically, iAssist determines the cut angle by defining the mechanical axis of the bone and calculation of the perpendicular plane of the mechanical axis. In other words, the proximal cut (i.e., tibial resection) and distal cut (i.e., femoral resection) should be perpendicular to the mechanical axis of the bone. Besides, an accurate component replacement femorotibial alignment is another key factor in a successful TKA. Depending on the preference of the surgeon, the pods are able to navigate him/her to have a neutral angle between the tibia and femur. iAssist is able to provide guidance in all alignment techniques such as anatomical alignment, mechanical alignment, and kinematic alignment [43].

III. Results of Accuracy, Invasiveness, and Ease-of-use

Semi-autonomous Systems

PSIs are considered as blood sparing surgery, which decreases the amount of hidden blood loss. However, this method suffers from a number of drawbacks. First, the requirement of a CT image or an MRI to arrange a preoperative plan and also to manufacture the resection guides can make a gap between the time a patient is listed for surgery until the real-time surgery takes place. Although these personalized instruments are attractive, they have intraoperative obstacles that are not infrequently encountered, and therefore deviations from the preoperative plan may be necessary. Second, once the bone is resected, there is no ability to validate the bone cuts [42]. The main advantages of PSI are: (1) improved accuracy (it is shown in [57] that a statistically significant improvement in neutral mechanical axis reproduction can be achieved using patient-specific instrumentation (1.7 vs 2.8; P 5 .03)), (2) shorter surgery time, (3) reduced intraoperative blood loss [58], (4) reduced pain, (5) elimination of fat emboli because there is no need to violate the femoral canal, (6) fewer required instruments could lead to a reduced potential for intraoperative contamination [42] [58]. In the downside, PSIs suffer from the following disadvantages: (1) lack of verification tool, (2) high cost, and (3) incurring an additional waiting time for surgery [57].

Passive Systems

In passive surgical systems, the computer provides the surgeon with recommendations, though it does not limit the surgeon to pre-determined cutting zones (contrary to semi-autonomous systems). The main advantages of passive surgical systems are: (i) superior accuracy of navigation for achieving femorotibial mechanical axis and component alignment on postoperative radiographs compared to conventional techniques and (ii) reduced outliers compared to jig-based techniques, and (iii) improved safety due to full involvement of human surgeon. In the downside, these systems suffer from relatively long surgery time, complexity of use, and high cost. Table 2.2 summarizes the comparison between different robotic surgery systems in terms of our three evaluation criteria: accuracy (C1), invasiveness (C2), and ease of use (C3). In the following, we evaluate the performance of different motion tracking systems in terms of the aforementioned criteria.

Mechanical Tracking Systems

Coordinate measuring machines (CMM) are one of the most popular techniques which operate based on mechanical tracking. The operation of CMMs is based on probing. Probing can be defined as moving gradually the measuring probe and finding the coordinate system of the points on the work surface. The advantages of this method are as follows: (i) high accuracy, (ii) robustness against error accumulation and external forces, (iii) repeatability. Despite all these strengths, this technology is suffering from some drawbacks such as high-

cost, complexity of use, and lack of standardization [59].

Electromagnetic Tracking Systems

The term “electromagnetic tracking" is self-descriptive, which means electromagnets are in charge of the tracking operation [60]. On the downside, there are a number of drawbacks concerning the medical application as follows. Nearby medical devices such as computerized tomography (CT) scan or magnetic resonance imaging (MRI) scanners or simply ferromagnetic objects, which are used for diagnosis and taking actions during surgeries by making a magnetic field distortion, have negative impact on the accuracy of such systems [61]. Also, they require extra equipment, such as the EM field generator, which should be set near to the patient or be attached to them. Further, fragile EM sensors must be deployed at the medical devices such as instruments and imaging devices [62].

Optical Tracking Systems

Optical tracking technology has been shown to be an interesting alternative to other methods such as electromagnetic, acoustic, mechanical and gyroscopic. Some benefits of optical tracking systems are as follows:

- Less sensitivity to the environment-related noise
- Drift problem is no longer an issue for optical system (which happens in other motion tracking systems)
- Many objects can be tracked at the same time by optical technology
- Facilitated tracking process thanks to wireless and lightweight interaction device

Despite all these advantages, optical methods suffer from an important drawback, which is the need for an available line-of-sight to the retro-reflective markers. This requirement can be an issue in many medical applications such as minimally invasive surgeries, catheter and needle biopsies, and flexible endoscopes [63].

Acoustic Tracking Systems

Acoustic systems can offer a number of benefits to the medical field, such as lack of exposure to X-rays compared to the CT-scans and radiology procedure, compatibility with the hospital and surgical environment (unlike the electromagnetic system the surgical instruments and

metal devices has no impact on it), the line-of-sight (LoS) is not needed thus being suitable for the minimally invasive surgery. Despite all these benefits, the weakness of these systems is that the accuracy of such systems is highly dependent on the sound speed [46] [64].

Fluoroscopic Tracking Systems

Fluoroscopic navigation systems are known as non-invasive procedures having the following benefits: (i) providing a clearer view of the internal anatomy such as the bones, organ, and vessels and (ii) an accurate guidance in joint replacements. Given that these systems use fluoroscopy images during the surgical procedure, both patient and operation team will be exposed to the radiation, which is a major drawback of this kind of system. Another downside for this technology is the dependency of the navigation to the position of the patient during the scan execution. The movement of the patient will affect the accuracy.

Inertial Tracking Systems

Not only does the ITS give the information about the location of objects, but it also gives useful information on the velocity which is the direction and the speed of movements. The inertial sensors can offer a number of benefits such as, commonly availability, small size, high reliability and low cost [53]. An important strength of Inertial systems is the very small range latency, which is on the order of milliseconds or even less [52]. This factor can give a very good opportunity to the inertial system to become the gold standard, especially in applications requiring short delay, such as medical field, virtual reality field, and computer graphics systems [52]. We note, however, that the drift issue does not allow the inertial tracking systems to become a silver bullet for the problems related to the tracking and navigation [52] [53]. Drift issue prevents the use of inertial navigation system in the task with a longer time of procedure. The idea behind the combination of accelerometers and gyroscopes is to solve the outcoming drift. This method is limited to the medical field and it is not applicable in other domains. Therefore, there are some other techniques to solve this shortcoming, which is related to the calibration and compensation steps. The outcome of resounding this drawback will not only improve the stability, but it also will improve the accuracy of the system. These two points are the principle key for reaching the ultimate goal, which is better and ideal performance of the entire system [65].

Table 2.3 compares the aforementioned tracking systems in terms of the three criteria of accuracy, ease of use, and suitability for minimally invasive surgery (MIS).

The discussion above provides us with means, with which we can evaluate the state-of-

the-art iAssist Knee System, which was introduced above in Section 2.2. In the following, we evaluate the performance of iAssist by assessing precisely its drawbacks and benefits. In particular, iAssist has the following important benefits:

- Reducing the cost, which is a direct consequence of lack of the need for a consul setup
- Minimizing the utilization of tracking pins
- Avoiding extra incisions to place more pins
- Reducing the complications coming from the pins placement
- No need for line-of-sight
- Reducing the time of surgery in comparison with large console CAS systems [66].

Despite all these advantages, there are some weakness elements of using iAssist, which are listed as follows:

- “Heavily depends on the surgeon to position and input accurate data to determine the mechanical axis" [66]
- “Soft tissue balancing and implant size information is not provided to the surgeon" [66]
- “Possibility of occurring connection failure of a pod" [66].

IV. Discussion

The scope of this survey covers a wide range of aspects of TKA, including relevant problems, principle of need for such a surgery, statistical reports, repeatability of TKA, taxonomy of surgical assistant robots, various navigation systems, and merits and shortcomings of each technique. Given that the scope of this topic is somehow wide, explanations of some of the less pertinent methods and technologies such as impedance-based tracking systems were excluded from this survey due to space constraints. In a short look, this work aimed to compile the research work on the following objects:

- The growth of TKA rate in the past decades
- A survey of classification of surgical robots for TKA

- The importance of keeping the human in the loop
- Explaining different techniques for object tracking
- Identifying the key advantages and drawbacks of each method
- A brief survey on iAssist navigation system, as an interesting example of a HITL system

This study is designated to the medical robotics and their enhancement of the accuracy in TKA. Although there are some excellent review papers on both subjects of medical robots in the TKA field and drawbacks/advantages of MTS, our study offers a review of the medical robots based on their deployed navigation systems. Since the accuracy of the medical robots was one of the most important criteria and knowing that the accuracy of such robots is highly dependant on their motion tracking system, we reviewed the two in conjunction with each other.

Since the research of this study is not following the pattern of any research strategy, and this study is based on the studying the references of articles and the citation of them, we may have missed a number of related works. Another drawback of this study is lack of quantitative results for the accuracy to better explanation which is due to not be used the all tracking systems in the TKA field. Although we found out the accuracy of some techniques is high, further measurements and evaluations are still needed to validate their performance during a TKA surgical procedure.

V. Conclusions and Future Works

In this work, we presented a comprehensive survey on the application of robotic systems in total knee arthroplasty. After briefly explaining the different types of surgical robotic systems, they were classified in three categories of (i) fully-autonomous systems, (ii) semi-autonomous systems, and (iii) passive systems. Key advantages and disadvantages of each group of robotic systems were identified. We then turned our attention to an interesting group of human-in-the-loop (HITL) systems, namely the passive robotic systems. Such systems augment the capability of human surgeons rather than substitute them. Next, different navigation systems, key components of passive systems, were studies and the advantages and drawbacks of each method were identified. Further, we assessed one of the commonly adopted HITL systems, namely, iAssist knee system, a novel state-of-the-art passive robotic system.

Understanding the concept of TKA and getting familiar with various aspects of this surgery can suggest a number of interesting and promising new ideas for the future works. A few possible directions for the upcoming studies and researches are suggested as follows:

- Leveraging on a hybrid approach, combining different techniques in order benefit from the advantages of each method.
- Redesigning and/or making necessary adjustments to some instruments/robotics systems with the purpose of eliminating the shortcomings.
- Collecting comprehensive feedback from both patients and surgeons to evaluate the efficiency of the CAS in general and iAssis system in particular.
- To examine the feasibility of combining the PSI and iAssist, where the instrument can be customized based on a preoperative image followed by the use the tracking of the pods intraoperatively.
- To investigate the possibility of feeding in the 3D model of the knee based on preoperative image to the iAssist system to enhance the accuracy of the position/orientation of the pods.

Declaration of Interest

The authors declare no competing interest.

List of Tables

Table 2.1 Summary of the advantages and drawbacks of different tracking systems under consideration.

Method	**Pros.**	**Cons.**
Mechanical tracking systems	• High accuracy • Robustness against error accumulation and external forces • Repeatability	• High cost • Complexity of use • Lack of standardization
Electromagnetic tracking systems	• No need for a line-of-sight • Suitable for MIS	• Interference from nearby medical devices • Requires extra equipment
Optical tracking systems	• Less sensitivity to the environmental noise • Drift problem is no longer an issue • Capability of detecting multiple objects • Facilitated tracking process	• Line-of-sight requirement • Cannot be used in MIS
Acoustic tracking systems	• Lack of exposure to X-rays • Compatibility with hospital and surgical environment • Suitable for MIS • No need for line-of-sight	• Reduced accuracy due to high dependency on the the sound speed
Fluoroscopic tracking systems	• Suitable for MIS • Clear view of the internal anatomy • An accurate guidance in joint replacement	• Exposure to radiation • Dependency to the position of the patient during the execution
Inertial tracking systems	• A very small range of latency on the order of ms or even less	• Drift issue especially in tasks with long execution time
Radio tracking systems	• Low propagation loss • Small absorbtion loss	• Rapid attenuation in water • Prone to measurement errors

Table 2.2 Comparison between different robotic systems in terms of our three evaluation criteria: accuracy (C1), invasiveness (C2), and ease-of-use (C3).

Method	**Accuracy**	**Invasiveness**	**Ease-of-use**
Fully-autonomous systems	High	High	Low
Semi-autonomous systems	Medium	Medium	Medium
Passive Systems	Medium	Low	High

Table 2.3 Comparison between different tracking systems in terms of accuracy (C1), applicability in minimally invasive surgery (MIS) (C1), and ease of use (C3).

Method	**Accuracy**	Applicability in MIS	**Ease of use**
Mechanical tracking systems	High	No	Low
Electromagnetic tracking systems	Medium	Yes	High
Optical tracking systems	High	No	High
Acoustic tracking systems	Medium	Yes	Medium
Fluoroscopic tracking systems	High	Yes	Medium
Inertial tracking systems	High	Yes	High
Radio tracking systems	Medium	No	Medium

List of Figures

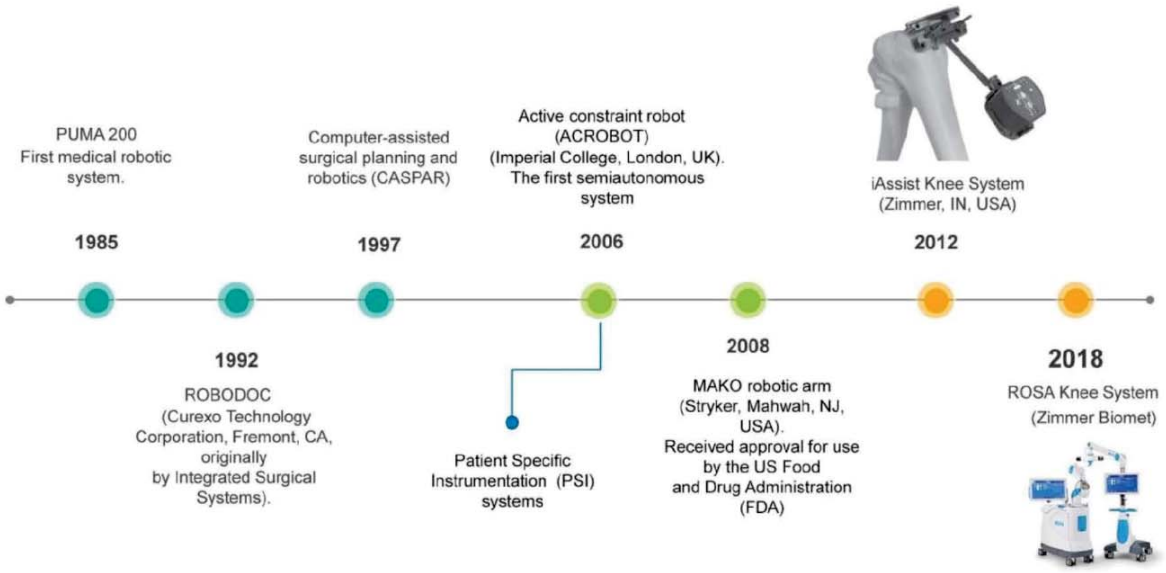

Figure 2.1 Timeline of surgical robotic systems

Figure 2.2 iAssist Knee System [56]

CHAPTER 3 METHODOLOGY

This chapter elaborates on all the requirements in order to achieve the main objective of this thesis, which is designing a system able to validate the accuracy of the femoral workflow of a TKA procedure using the iAssist knee system.

The terms of "requirements" and "needs" in this study are given based on the required features of the specimen and the surgical procedure. The objective of validating the accuracy can be further divided into the following sub-objectives:

1. To characterize the resultant error of iAssist knee system for the femoral distal cut angle (error characterization). The outcome of iAssist consists in two values, the varus-valgus angle and flexion-extension angle of the cut plane regarding to the mechanical axis of the femur.

2. To validate whether the error falls within the acceptable range or not (i.e., error validation). The acceptance range has taken from the conventional TKA (see table 3.1).

Table 3.1 Specification limits for each parameter [67]

Parameter	Accepted range	% of population
Femoral cut F/E angle	±3°	65.7%
Femoral cut V/V angle	±3°	83.6%

3.1 Defining Accuracy Measuring Method

3.1.1 Error Characterization

There are two important requirements to achieve the first sub-objective of our research, as follows:

1. **Measuring Tool**: First, based on rule ten to one to validate and measure the accuracy of a system, having a system ten times more accurate, than the estimated accuracy of to be measured system in our case iAssist knee system is needed [23].

2. **Research Model (specimen)**: The other important requirement is to simulate and perform the entire surgery using iAssist knee system, therefore a specimen is needed.

Measuring Tool

In order to satisfy the first requirement a literature review has been conducted. Since the accuracy of iAssist is coming from the embedded inertial motion tracking system of its electrical pod, we had a comprehensive literature review on different Motion Tracking Systems (MTS) which was discussed in the second chapter.

After assessing different Motion Tracking Systems (MTS) and realizing that the most accurate system is the mechanical tracking system, we opted for the FaroArm, a portable Coordinate Measuring Machine (CMM).

FaroArm falls in the category of mechanical object tracking systems and it is widely used in industry for 3D measurements, imaging and realization [23]. The main idea behind its underlying method is forming a direct physical link between the target object and environment. Normally, the link is an articulated arm, and the position and orientation of the object can be obtained by calculating the direct kinematics of the joints of the arm. The system is known to be very accurate (a single point repeatability of ± 0.02 mm and volumetric performance of ± 0.03 mm [5]) and robust against error accumulation, the procedure is repeatable, and it is easy to use [68].

Research Model (Specimen)

Simulation of the surgical procedure with the iAssist knee system requires the specimens with special properties. The terms of "requirements" and "needs" are given based on the necessary properties of the specimens and test procedure regarding the involvement of FaroArm and the iAssist knee system, such as having bony landmarks and bony shape and structure. The FaroArm also has specific requirements for its proper use, for instance, FaroArm is not compatible with the bone structure and requires other properties to work with.

As a result, the requirements of both systems do not overlap. Therefore we decided to design a specimen with specific features in order to be compatible with both systems.

Here we will assess all the needs and their solutions in order to design a proper specimen for our project. The determination of the requirements has been done following Zimmer Biomet mechanical and system designers requirements and inputs. The design and production of the parts of the specimen has been done in partnership with them.

A. iAssist Requirements

First, we will gather all the requirements coming from the iAssist knee system. As we are focusing on the accuracy of femoral workflow, so the requirements apply only for the femur part of the surgical procedure with the iAssist knee system. The three important steps of a typical femoral surgical procedure with iAssist are as follows:

A.1. Registration

Registration is the key step in surgical navigation systems. Basically, it allows the electrical pod to determine the Mechanical Axis (MA) of the femur. This step first requires a bony shape and bony material which provide the anatomical landmark of the femur (the patellar surface, on the top of the intercondyloid fossa). As shown in figure 3.1, the femoral spike should be placed into the specimen, from the previously mentioned landmark (on the patellar surface, on the top of the intercondyloid fossa). As we have to fix the femoral spike on the bone with two screw, the spongy material is needed to simulate the bone marrow (spongy tissue inside the bone). The Second requirement is 3 Degree Of Freedom with specified angles (Roll 0° to 360°, Yaw $-170°$ to 170° and Pitch $-170°$ to 170°). In order to achieve this requirement a ball-and-socket type joint (black joint) with 3 DOF has been proposed. The proposed joint makes us able to make a star pattern with the required movement during the femur registration 3.2. From these properties we will design the specimen from two essential parts: lower femur (distal femur) by using off the shelf sawebone (artificial distal femur with 15mm canal, SKU:1120-6) and the upper femur (proximal femur) which is the ball-and-socket will be off the shelf part made of metal.

A.2. Navigation and Cut

In the navigation/cut step, in addition to what we saw previously, in order to execute the cut, we have to consider two important points. First, we must be able to cut the sawbone, not all sawbone products are possible to be cut, some could be made of glass, very hard plastic or even steel. Second, the specimen should be stable at an angle more than 45° with respect to the ground. To achieve this, we will need a stopper that can provide a position of 45° for the femur regarding the ground (figure 3.2). For the stopper, we need a revolute joint as well as a lock to easily use it or remove it, when needed (figure 3.2). Before the cut, an important step for the surgeon is to remove the spike from the specimen. This step takes uses a surgical Slap-hammer and applies a large force. "A surgical Slap-hammer including an adjustable striking member and a releasable retaining mechanism for releasably retaining a sliding weight is disclosed" (Patent: USOO84.86084B2). This will create an important need: the specimen and workspace should be heavy and stable enough to resist the presence of the

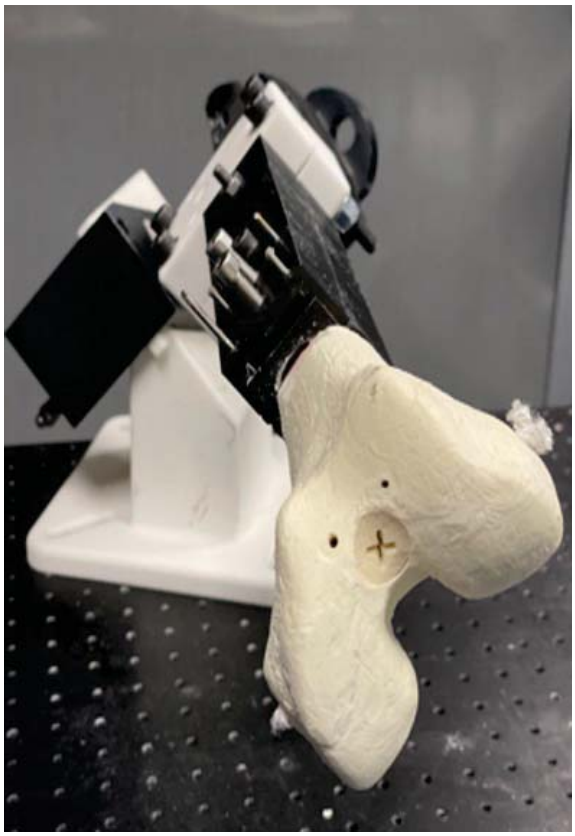

Figure 3.1 An illustration of the anatomical landmark of the distal femur bone (sawbone)

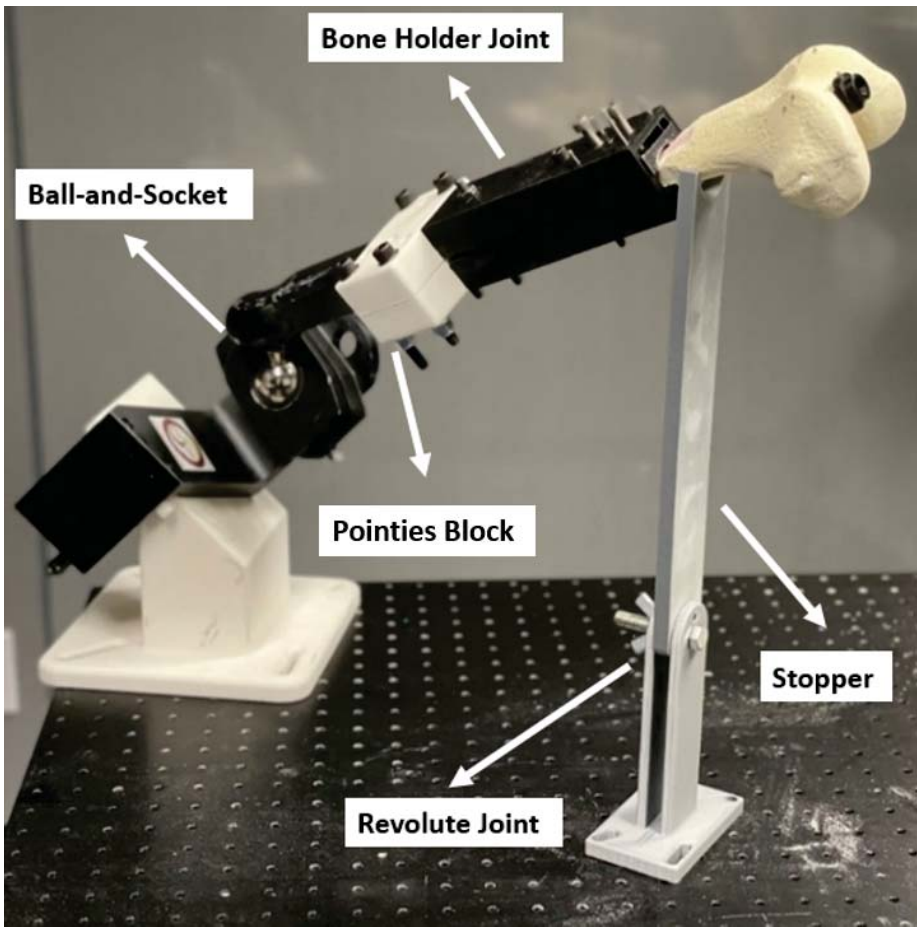

Figure 3.2 An illustration of the designed artificial femur with a ball-and-socket type joint

excessive force coming from this step. We note that this issue will be largely solved with a fixture plate and clamping kits, which will be assembled on the workbench of the FaroArm (figure 3.2). In fact, the specimen will be fixed on the workbench with some screws. We have to make sure that, the specimen has a clearance with the navigated and cut instruments, to prevent any interference during the test execution.

A.3. Validation and Cut

All the requirements for each step in the validation workflow such as placing the validation tool with the screws and being able to make the required movements of the femur have been met with the solutions in the registration and navigation phase mentioned above (since there are the same acts as in the previous steps).

B. FaroArm Requirements

Since we already assessed all the needs and their solutions from the involvement of iAssist knee system, now is the time to add up the requirements of the involvement of FaroArm to the previous needs.

As mentioned previously the inertial pods of the iAssist knee system determine the position and orientation of the objects by the linear acceleration (accelerometer) and angular velocity (gyroscope) of the movements of the objects [69]. On the contrary, FaroArm defines the location of objects by a direct physical link between the target object and FaroArm (probing) [70]. In fact by probing the object FaroArm collects number of points from the object. Next, FaroArm not only reconstruct the shape of the object in the help of best fitting algorithm but also define the position of the object.

Therefore, by directly probing the spongy surface of the femoral distal cut we would not be able to obtain the cut plane accurately. We will have the same challenge for in probing the anatomical landmark of the distal femur (the center of the knee joint).

To cope with this challenge, we designed two special parts. The first part is a flat and rigid part (Resection Plate) for the femoral distal cut surface (figure 3.3) and the second part is a cone shape component named Mechanical Axis Entry Point (MAEP) for the anatomical landmark of the center of the knee joint (figure 3.4).

In order to take into account the biomechanical properties of the hip joint, a ball-and-socket joint has been added in the proximal part of the artificial femur. The sphere of the femoral head of the hip joint has been manufactured with steel material which has two advantages. First, the rotation of the femur around the hip joint will be smoother to simulate the gliding of the articular cartilage of the joint. Second, the probing outcome of FaroArm is more precise thanks to the smooth and hard surface obtained by steel material (figure 3.2).

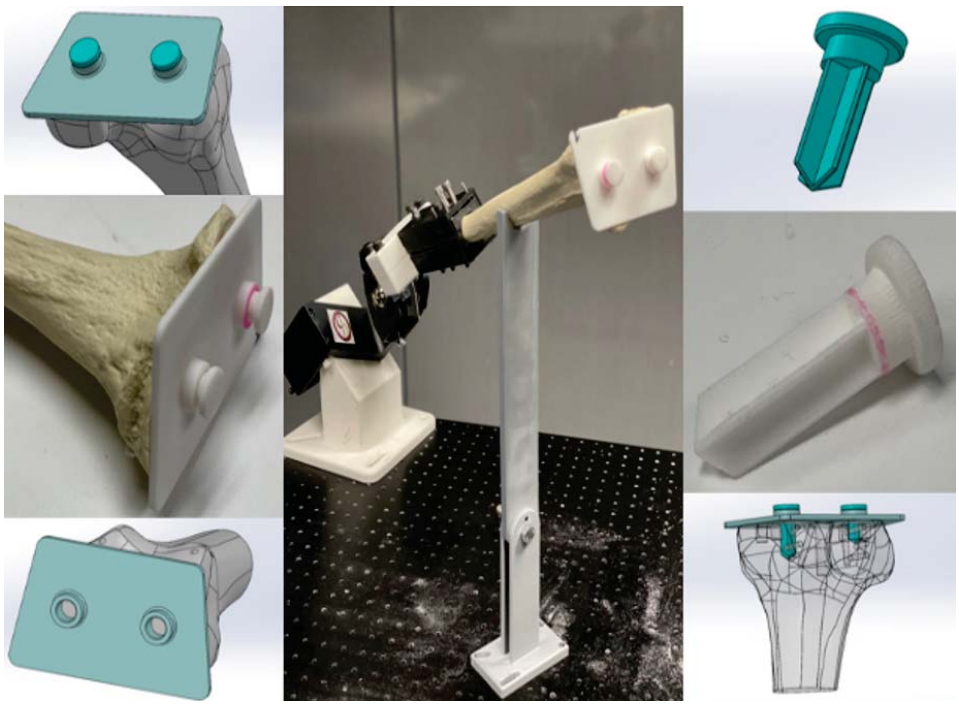

Figure 3.3 An illustration of the resection plate on the cut surface of the sawbone

Figure 3.4 An illustration of the placement of the MAEP on the distal femur bone (anatomical landmark of the sawbone)

Additional Requirement because of the Sample Size:

Apart from the technical features of the specimen, it is also important to determine the number of experiments, as it will have a huge impact on the resultant statistical analysis that needs to be carried out. In order to have meaningful results we have to define a sample size for our test.

Since this test procedure is a characterization study, the minimum number of samples to determine normality is 20. This sample size is based on Anderson-Darling test which says, to obtain a normal distributed dataset from a characterisation study, a minimum sample size of 20 is required.

In order to add more reliability, we have increased the sample size up to 30, and we have performed the test procedure with multiple operators.

As the sawbone will not be reusable because we have to cut it, we bought a number of replaceable sawbones sufficient to meet our sample size requirement (figure 3.2).

In order to attach the proximal femur (ball and socket joint) and the distal femur (sawbone) together, a bone holder joint has to be designed. Its properties must be as follow:

1. It should be designed in such a way that it allows for an easily replacement of the distal femur.

2. The bone holder joint should be compatible with the cross section of the sawbones as well as the cross section of the proximal femur jig (figure 3.5).

3. It should be resistant to the forces coming from the execution of the different steps of working with the iAssist knee system, especially the removal of the femoral spike with the slap hammer.

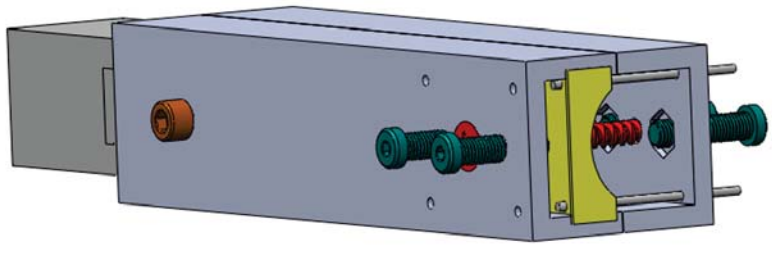

Figure 3.5 An illustration of the bone holder joint in the proximal part. The cross section of the part is in square shape and on the distal part has a circle cross section.

Establishing the test procedure

This test method will be executed on the artificial femur. The central part of this test method is the involvement of FaroArm. As a summary, acquisition of the mechanical axis of the femur with FaroArm must be performed before the execution of the femoral workflow of iAssist, which will be explained in greater detail later, in the appendix regarding the test protocol.

In the next step, the surgeon will be asked to execute the femur workflow using the iAssist knee system.

Once the resection has been done on the distal femur, we have to retrieve the initial obtained MA (obtained by FaroArm) because the specimen has moved due to execution of surgical procedure with iAssist knee system. A specific command (move device command) will be used in order to retrieve the initial MA.

This command is able to retrieve the entire device (in our case the MA) with 3 reproducible points. The requirement of three reproducible points is coming from the software of FaroArm (Farocam2). In order to answer the requirement of three reproducible points, a block with two conical holes, called pointies block has been used. The pointies block has been designed in such a way, to be embedded on the artificial femur 3.6. The third reproducible point of the artificial femur will be the center of the femoral head on the proximal femur.

Once the new position of the femoral mechanical axis is obtained, by placing the resection plate on the surface of the femoral distal cut and probing its surface, the plane of the cut will be obtained in the FaroArm. The plane of the cut is needed in order to evaluate the angle of the femoral distal cut relatively to the mechanical axis of the femur. As previously mentioned in the introduction chapter, based on the literature review, the best femoral distal cut is perpendicular to the mechanical axis of the bone [71]

3.1.2 Error Validation

As mentioned previously (first section of this chapter), after designing the femoral specimen and defining the test procedure, in order to achieve the first objective of our study, it is important to validate the resultant error of the surgical procedure with iAssist. Thus, we have to create a dataset and characterize the accuracy of iAssist with statistical analysis.

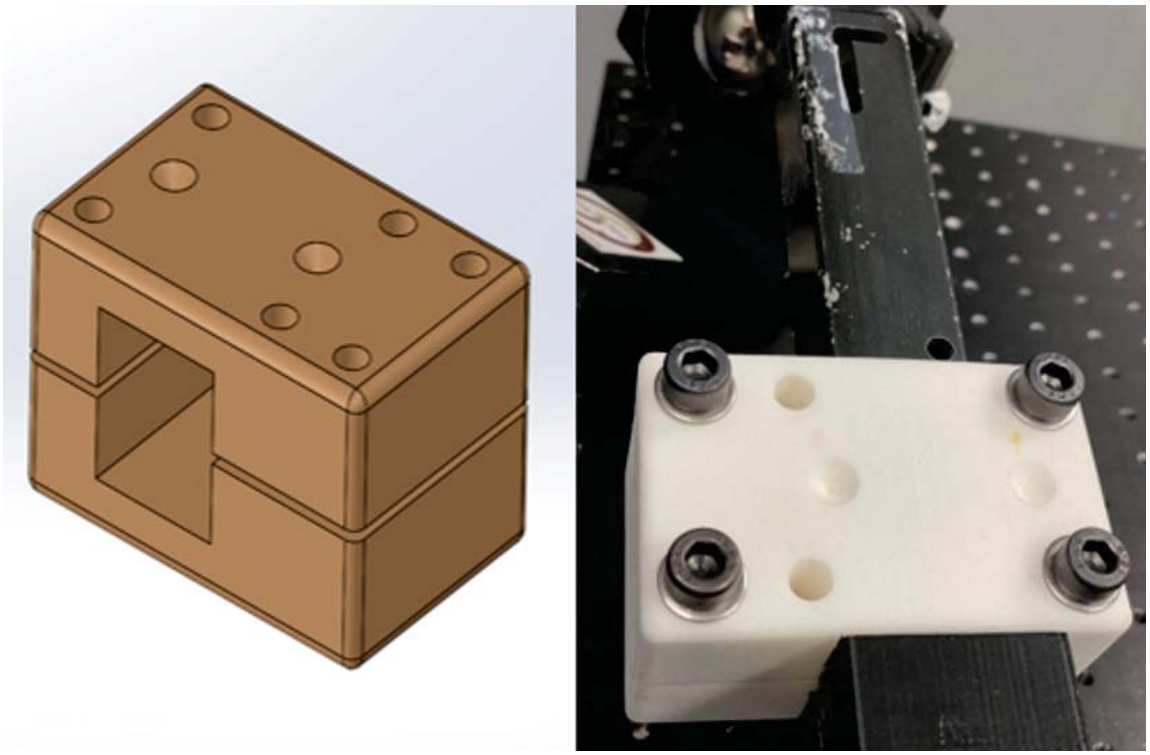

Figure 3.6 An illustration of the pointies block.

DataSet Creation

The outcome of the iAssist knee system is a set of angles (two angles per cut), which shows the relation of the femoral distal cut and the identified femoral MA by the iAssist system. Varus/ Valgus (V/V) angle and Flexion/Extension (F/E) angle of the femoral distal cut relatively to the femoral MA are the resultant value of iAssist.

The resultant outcome of the FaroArm, should be obtained in the form of Varus/ Valgus angle and Flexion/Extension angle between the plane of the resection plate and the MA obtained by FaroArm. This is required in order to characterize the outcomes from both technique and the accuracy of iAssist Knee System.

The created dataset will consist of cut angles value from the iASSIST Knee System and the resultant obtained values of the FaroArm for the following parameters used to validate the accuracy acceptance criteria for the femoral workflow:

1. Femoral cut F/Extension angle
2. Femoral cut V/V angle

For each parameter, the following calculation should be done in order to validate the

accuracy of the system:

$\Delta_{FaroArm-iAssist}$: Difference between the value obtained by the FaroArm and the iAssist value.

A. The resultant value of iAssist

The data of iAssist will be collected from the values obtained in the validation step. These values will be considered as the result of iAssist. In order to distinguish the orientation of the cut (varus/valgus and flexion/extension) from its value on the log of the tablet, we ran an entire femoral workflow with iAssist. F/E angle of the cut has been selected at 5° flexion and the V/V angle of the cut has been selected at 7° varus. After performing the cut and validation step with iAssist, the value of the cut has been appeared as 3° for flexion and 7° for varus on the tablet. At the end we checked the value of the validated cut of iAssist. As a conclusion, a positive angle of F/E angle represent a flexion cut and a negative value represent an extension cut. In addition a positive angle of V/V angle represent a varus cut and a negative value represent a valgus cut.

B. The resultant value of FaroArm

The error contribution from FaroArm will be obtained doing the sum of three values for both V/V and F/E of the cut.

1. The resultant value from the mechanical stack-up for all the possible source of errors of using the designed artificial femur as specimen and FaroArm as measuring tool (mechanical stack up will be explained in detail in the next chapter).
2. The resultant error from the step of using move device command of FaroArm.
3. The resultant value of the measurement of the specimen with FaroArm.

B.1. The resultant value from the mechanical stack-up

The result and the way of performing the mechanical stack-up (Validation of the Proposed Test Method) will be detailed later in section 3.2.

B.2. The resultant error from the step of using move device command

The error from the FaroArm "Move Device" command step will be obtained from the angular momentum.

Angular momentum is the quantity of rotation of a body (the artificial femur in our case) which is the product of its moment of inertia and its angular velocity.

The mechanical idea of angular momentum, considers a rigid body which rotates with an angular velocity around its specific rotation axis. Since we assume such system consist of N particles, its specifications are as follows:

m_i: The mass of the particle i

r_i: The position vector of the particle i

v_i: The velocity vector of particle i

Therefore the angular momentum of the assumed rigid body is equal to the sum of the part the impulses of each particle of the system.

$\omega = \sum_{i=1}^{N} (m_i \; r_i \; X \; v_i)$

According to the hypotheses the linear velocity of each particle of the body is equal to:

$v_i = \omega \; X \; r_i$

In our calculation, as position vector we will use the length of two specific particle, which is the center of the femoral sphere and the point 1 of the pointies block. The velocity vector in our case, will be considered as the offset of the FaroArm in the measurement and calculation of the new position of the device.

The length of the line which passes from the center of the femoral sphere and the point 1 of pointies block has been obtained by FaroArm which is 227.098 mm. The offset for calculating error of move device command will be obtained after each trial. After performing "Move Device" command (the steps from 16-21 on the appendixe B), as result of this displacement a "Results portion" window will appear which has the resultant error from using the "Move Device" command and the direction of the offsets in all the three axes.

Here there are two possibilities

i) the offset of the femoral sphere and the point 1 of pointies block in different directions (figure. 3.7)

or

ii) the offset of the femoral sphere and the point 1 of pointies block are in same direction (figure. 3.8).

For the first possibility the formula for the calculation is as follows:

$\omega = \frac{V_1}{l_1} = \frac{V_2}{l_2} = \frac{V_1'}{l_1'} = \frac{V_2'}{l_2'}$

For the second possibility the formula for the calculation is as follows:

$\omega = \frac{V_1}{l_1} = \frac{V_2}{l_2} = \frac{V_3}{l_3} = \frac{V_4}{l_4}$

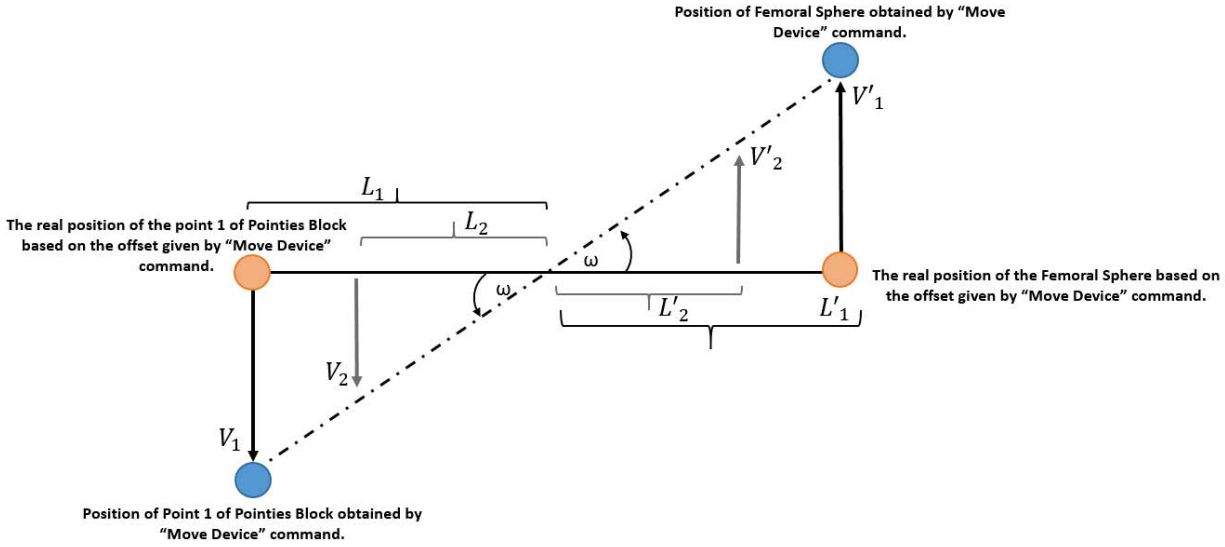

Figure 3.7 An illustration of the offset of measured features of move device command in different direction

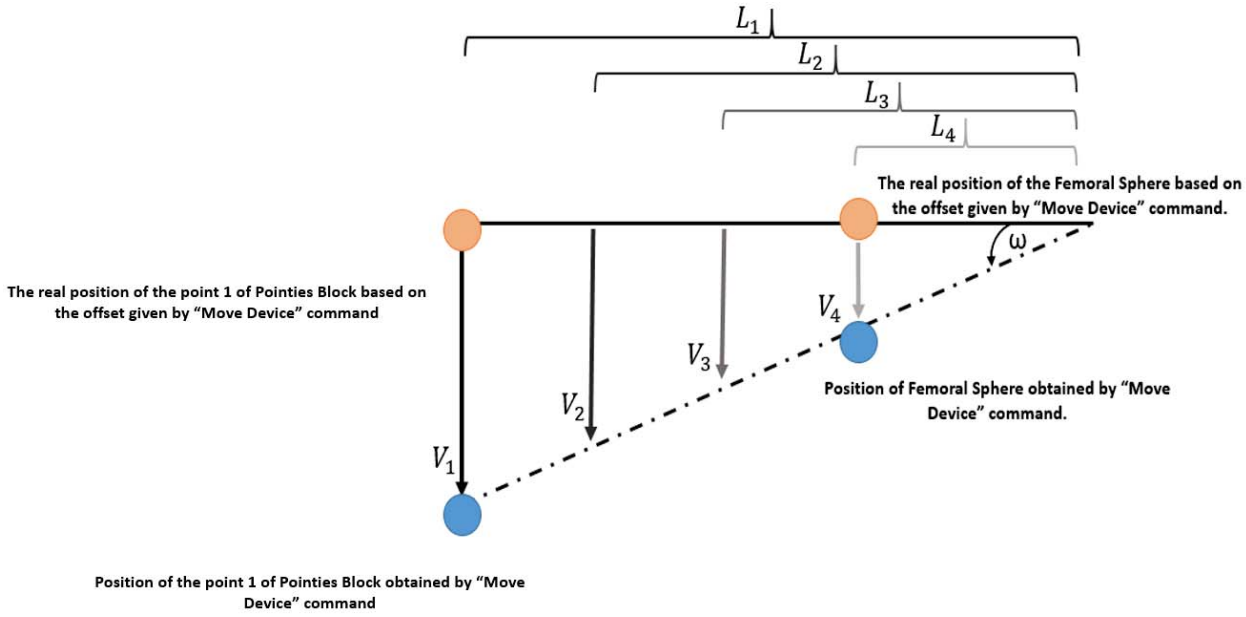

Figure 3.8 An illustration of the offset of measured features of move device command in same direction

The results of the above calculations, will be used as the contribution error from the step of using move device command during the test procedure.

The details of how we will obtain and use these values will be explained in the results chapter.

B.3. The resultant value of the measurement of the specimen with FaroArm

During the measuring of the previously mentioned features (see the test method description) with FaroArm, we have defined two coordinate systems. One of the coordinate systems consist of the normal of the plane of the Resection Plate as Z axis. The other one consist of the MA of the artificial femur as Z axis of it. The X axis of both coordinate systems has been defined as the line which passes from the two points of the pointies block. The origin of both coordinate system will be defined as the point 1 of pointies block.

In fact the V/V angle between the MA of the artificial femur and the Femoral Distal Cut is the angle between the Z axis of the two coordinate systems in the coronal plane. Moreover, the F/E angle is the angle between the Z axis of the previously mentioned coordinate systems in the sagittal plane (figure. 3.9).

The anatomical coronal plane in our coordinate system is the plane which is created by the Y axis and the Z axis and the sagittal plane is the plane which is created by the X axis and the Z axis.

In order to calculate the value of V/V and F/E angle we have used the principles of the rotation matrix. A rotation matrix for a 3D coordinate system is a 4X4 matrix. Rotation matrix consists of the rotate angles each axes of the base coordinate system and the transferred coordinate system. In another word, the rotation matrix is used to transfer a coordinate system in a new position in the Euclidean Space.

In the result chapter the outcome values will be presented.

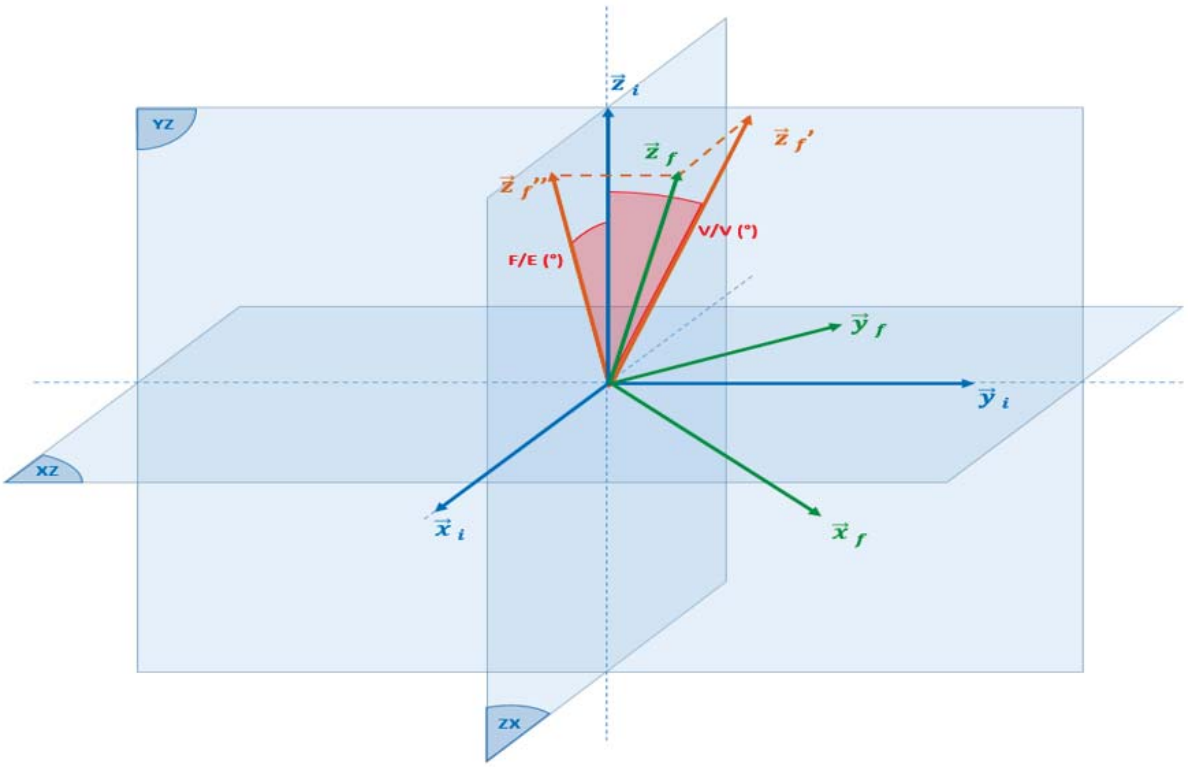

Figure 3.9 An illustration of V/V and F/E angle in coronal plane (Y-Z) and sagittal plane (X-Z) (From An Internal documents of Zimmer Biomet).

The varus/valgus angle is the angle between the projection of the z vector (Mechanical Axis) of the sawbone coordinate system on the YZ plane, defined by the coordinate system of the resection plane. That correspond to take the arctangent of the second and third value of the third column of the rotation matrix.

As shown in figure. 3.10 and based on the right-handed rule, a positive value of the calculation represent a varus cut whereas a negative value represent a valgus cut.

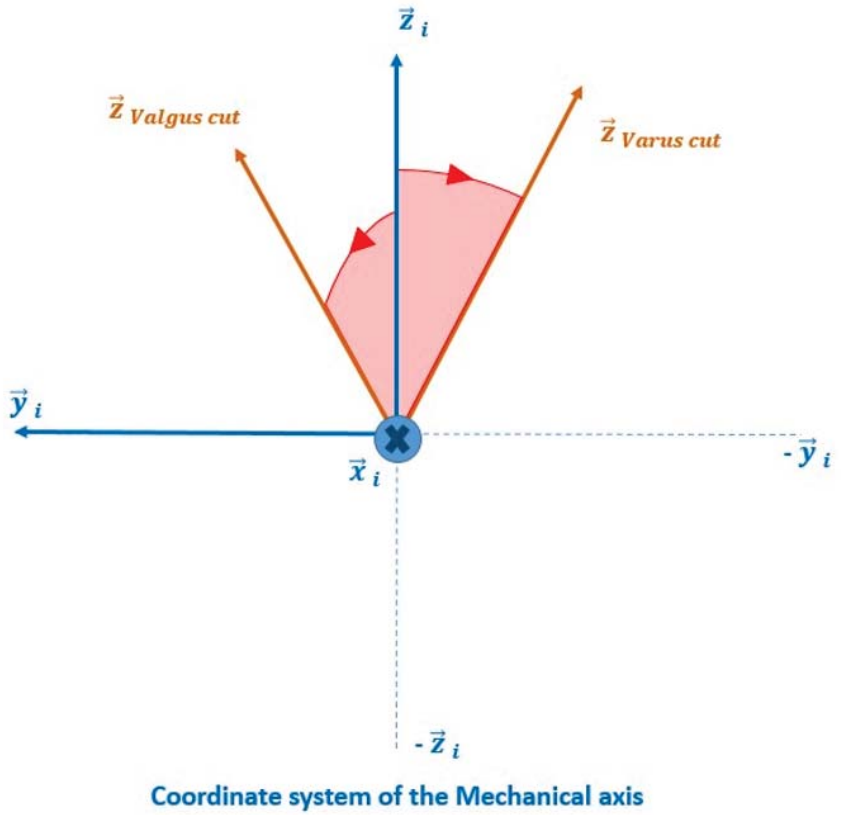

Figure 3.10 An illustration of cross product between the normal of the resection plate and the mechanical axis of the femur in the coronal plane.

The flexion/extension angle is the angle between the projection of the z vector (Mechanical Axis) of the sawbone coordinate system on the ZX plane, defined by the coordinate system of the resection plane. That corresponds to take the arctangent of the first and third value of the third column of the rotation matrix.

As shown in fig. 3.11 and based on the right-handed rule a positive value of calculation represent a flexion cut whereas a negative value represent an extension cut. These values will be the resultant value of the measurement of the specimen with FaroArm.

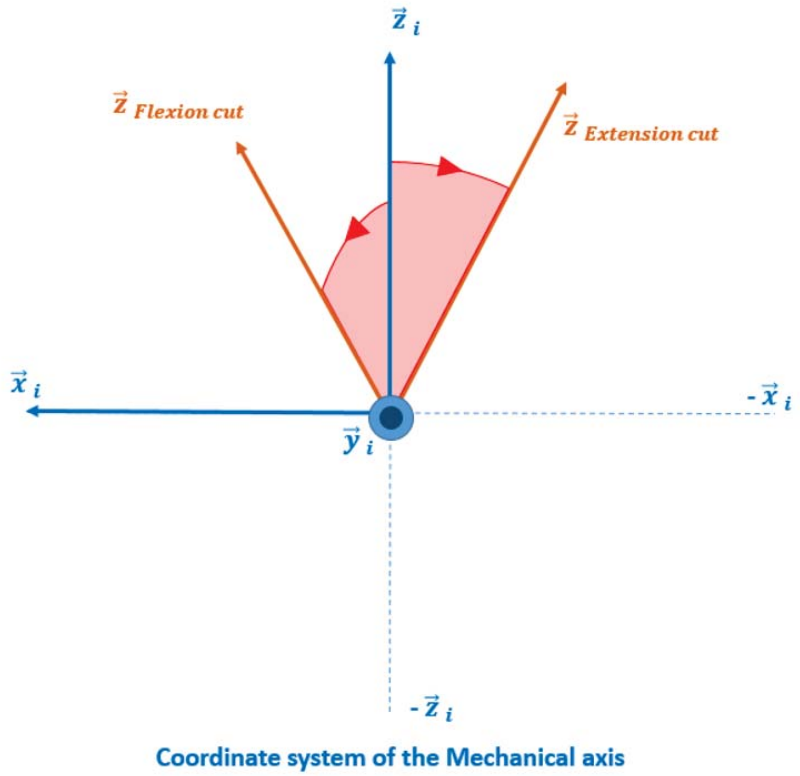

Figure 3.11 An illustration of cross product between the normal of the resection plate and the mechanical axis of the femur in the sagittal plane.

Comparing the outcome with the acceptance criteria

a. Normality testing of the data

The distribution of each parameter will be tested for normality using Minitab statistical software.

If a sample fails the normality test, other statistical tests such as one way ANOVA and Kruskal-Wallis will be executed on the dataset.

b. Analysis of parameters following a normal distribution

For any given parameter, the error ($\Delta_{FaroArm-iAssist}$) and proportion of the population (%) will be computed. Therefore, we would be able to verify if the acceptance criteria (see table. 3.1) are met or not.

For each parameter, i) if the error ($\Delta_{FaroArm-iAssist}$) is within the acceptance interval limits which is $\pm 3^{\circ}$ and ii) proportion of the population is equal or greater than the specific percentages (V/V 83.6% and F/E 65.7%) hence the acceptance criteria are met and the accuracy of the femoral workflow is validated.

A Brief Summary

The figure. 3.11 is a block diagram, showing the summary of calculation of the resultant value for both F/E and V/V angles.

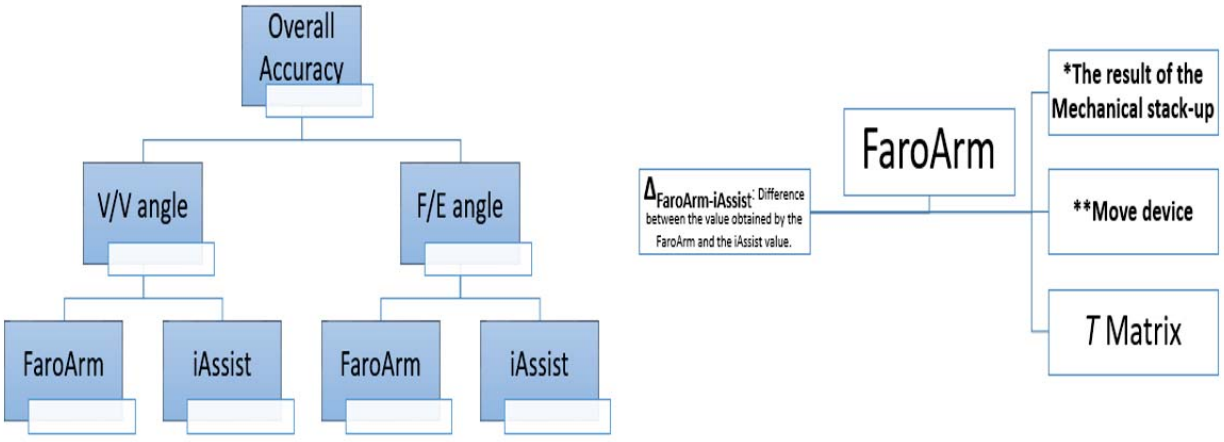

Figure 3.12 A block diagram of calculation of the resultant value for F/E and V/V angles.

$$
\begin{aligned}
&Final\ Value\ of\ FaroArm\ for\ F/E\ angle^{\circ} = \\
&The\ resultant\ value\ of\ Mechanical\ stack\ up\ for\ F/E\ angle^{\circ} \\
&+ The\ calculated\ offset\ from\ MoveDevice\ command\ step^{\circ} \\
&+ The\ obtained\ F/E\ angle\ from\ transformation\ matrix\ of\ the\ proposed\ test\ procedure^{\circ}
\end{aligned}
$$

$$
\begin{aligned}
&Final\ Value\ of\ FaroArm\ for\ V/V\ angle^{\circ} = \\
&The\ resultant\ value\ of\ Mechanical\ stack\ up\ for\ V/V\ angle^{\circ} \\
&+ The\ calculated\ offset\ from\ MoveDevice\ command\ step^{\circ} \\
&+ The\ obtained\ V/V\ angle\ from\ transformation\ matrix\ of\ the\ proposed\ test\ procedure^{\circ}
\end{aligned}
$$

3.2 Validation of the Proposed Method

This section is dedicated to the characterization of the accuracy and the efficiency of the proposed method. An error study was conducted to evaluate the performance of the proposed test protocol as well as the efficiency of the artificial femur as specimen. In this section, we will characterise, not only the sources of errors due to the involvement of the artificial femur, but also the sources of errors related to FaroArm.

The source of errors of this proposed method are as follows:

1. Probing process (operator and calibration of the system).
2. Fitting algorithm (accuracy of the software and FaroArm).
3. Stability and the design of the parts.

Finally, after evaluating all the possible errors from the different steps of the protocol, we will be able to assess, if the test protocol is accurate enough to measure the accuracy of iAssist.

The objective of characterizing the possible contributing errors during the execution of the proposed test protocol can be formulated as follows:

1. To characterize the error contribution of FaroArm during the measurement steps.
2. To evaluate and characterize the offset created during the manufacturing procedure of the resection plate and the mechanical axis entry part.
3. To characterize the repeatability and stability of the measuring procedure with FaroArm, specially the steps of using the Mechanical Axis Entry Point (MAEP) and the Resection Plate.

3.2.1 First Objective: To characterize the resultant offset from the accuracy of FaroArm in measurements

In the proposed method, we have decided to use FaroArm. It has a single point repeatability of 0.020mm and volumetric performance of 0.030mm (see appendix C).

Since it is desirable to have the resultant offset in the form of angle, therefore the accuracy of FaroArm will be converted into angle in the help of tangent formula.

As shown in the figure. 3.13, in order to obtain the accuracy of FaroArm in angles we used the dimention of Resection Plate. The shortest length, which has to be probed during

the performing of our test procedure belongs to Resection Plate (the shortest length of the Resection Plate). We assume the offset of the probed point on the Z axis remains constant as shown in figure. 3.13 and figure 3.14 (0.02mm + 0.03 mm).

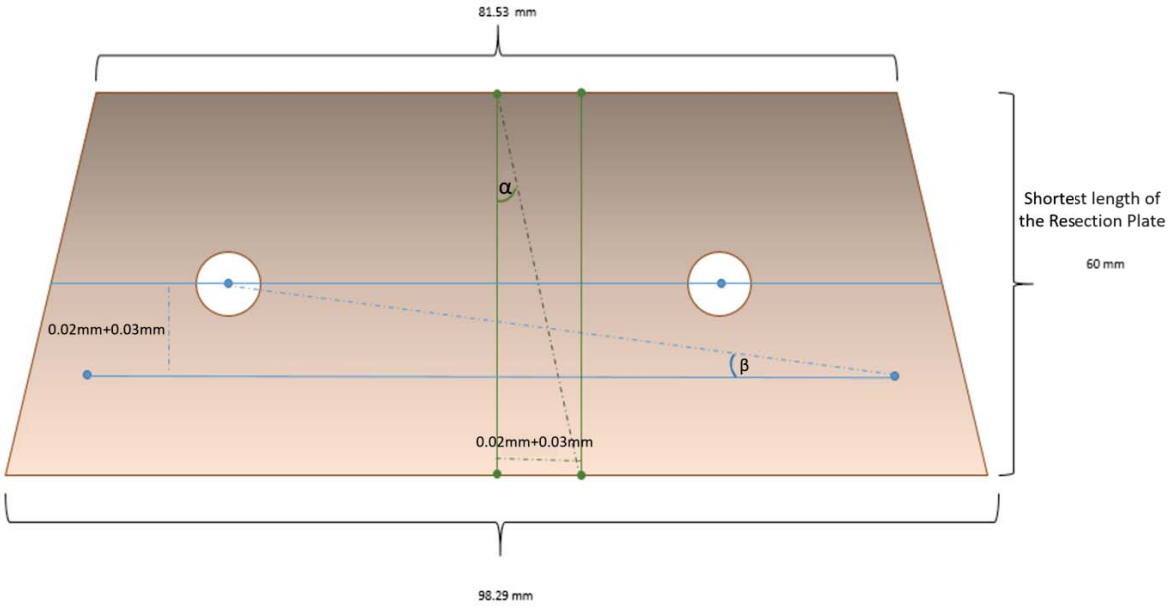

Figure 3.13 An illustration of Resection Plate with the shortest length.

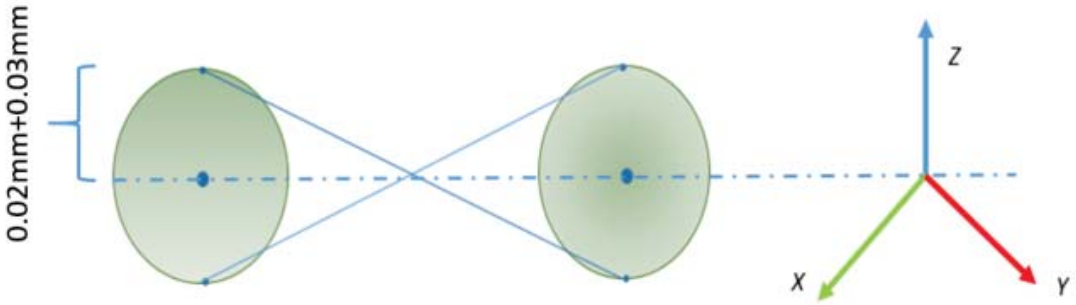

Figure 3.14 An illustration of direction of the offset on Z axis.

Hypothesis:

The resultant offset angle due to inaccuracy of probing the shortest length of the Resection Plate is the biggest obtained offset angle among all other to be probed features (e.g. mechanical axis of the femur).

Figure 3.15 shows the tangent relation of trigonometric functions. The adjacent side of the triangle (length between two probed point), has an inverse relation with the tan a (the resultant angle due to the uncertainty of the measurements with FaroArm). Thus the shortest length of the Resection Plate has the largest resultant offset angle. Therefore, the resultant offset of any other features such as, MA and the longer lengths of the Resection Plate will be smaller. This means in the calculation of the overall distributed error, the inaccuracy of the obtained angles is overestimated. In another word, the inaccuracy of the obtained angles is less than the uncertainty of the measurements with FaroArm.

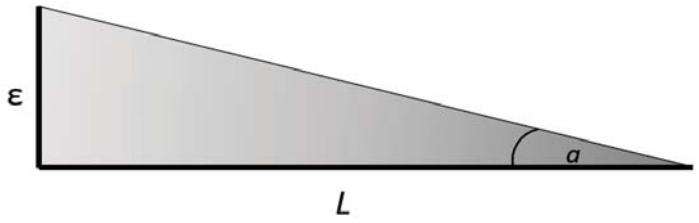

$$Tan\ a = \frac{\varepsilon}{L}$$

Figure 3.15 An illustration of the tangent relation of trigonometric functions.

$$\tan\alpha \ = \ \frac{\epsilon \ = \ The\ offset\ of\ the\ probed\ point\ (mm)}{L \ = \ The\ shortest\ length\ of\ the\ Resection\ Plate\ (mm)}$$

Accuracy of single point repeatability in angle $\tan\alpha \ = \ Arc\ tan\ (\frac{\epsilon \ = \ 0.02mm}{L \ = \ 60mm})$

Accuracy of volumetric performance in angle $\tan\alpha \ = \ Arc\ tan\ (\frac{\epsilon \ = \ 0.03mm}{L \ = \ 60mm})$

The obtained angle of single point repeatability is 0.0191° and the angle of volumetric performance is 0.0286°. Since in this test protocol, repeatability and measurement accuracy are involved therefore the sum of both errors will be considered as the error contribution of faroarm. The final accuracy of FaroArm in angle is 0.0477° which is way smaller than the estimated accuracy of iAssist Knee system (±3°).

This value will be used in the result chapter.

3.2.2 Second Objective: To evaluate and characterize the offset created during the manufacturing procedure of the resection plate and the mechanical axis entry part

Mechanical Axis Entry Part

The Mechanical Axis Entry Part has been 3D printed by Ultimaker S5 3D printers. In order to characterize the error of the manufacturing process of the MAEP we did a comparative assessment between the accuracy of the 3D printer and the FaroArm.

The accuracy of the 3D printer on the X axis is 0.0069mm, on the Y axis 0.0069mm and on the Z axis 0.0025mm (see appendix D) and the accuracy of the measurements of FaroArm Quantum S Arm on all axis is 0.030 mm.

The printing of the MAEP is done with a system, which is 4.35 times more accurate than the probing procedure of the MAEP. As shown in the figure. 3.16. FaroArm with the accuracy of 0.030 mm is not able to detect the small offset that may have been created during the printing procedure of the MAEP due to the accuracy of 3D printer (0.0069mm). Therefore, the contributed error from the offset of the center point of the MAEP will be negligible.

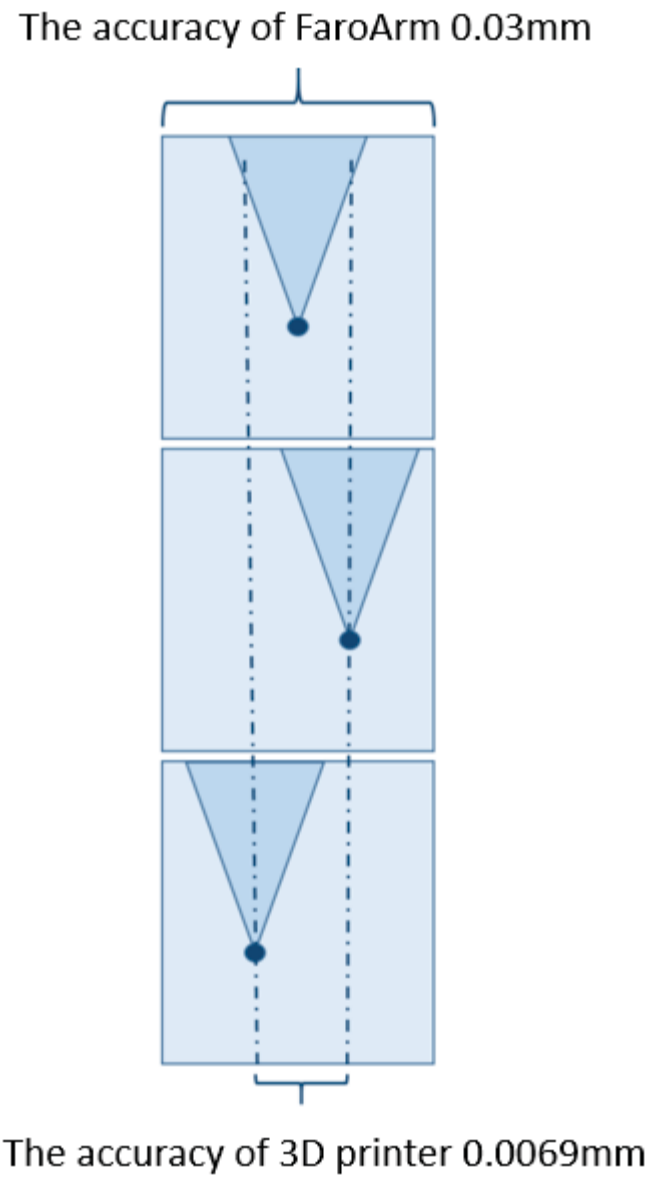

Figure 3.16 An illustration of the created offset in the manufacturing procedure of the MAEP with the 3D printer.

Resection Plate

In order to validate the efficiency of resection plate we passed the part through a production procedure with CMM. In the production procedure the flatness of the bottom surface and profile of the of the top surface of the Resection Plate (figure. 3.17) has been assessed and characterized.

RP1.png RP1.png RP1.png RP1.png

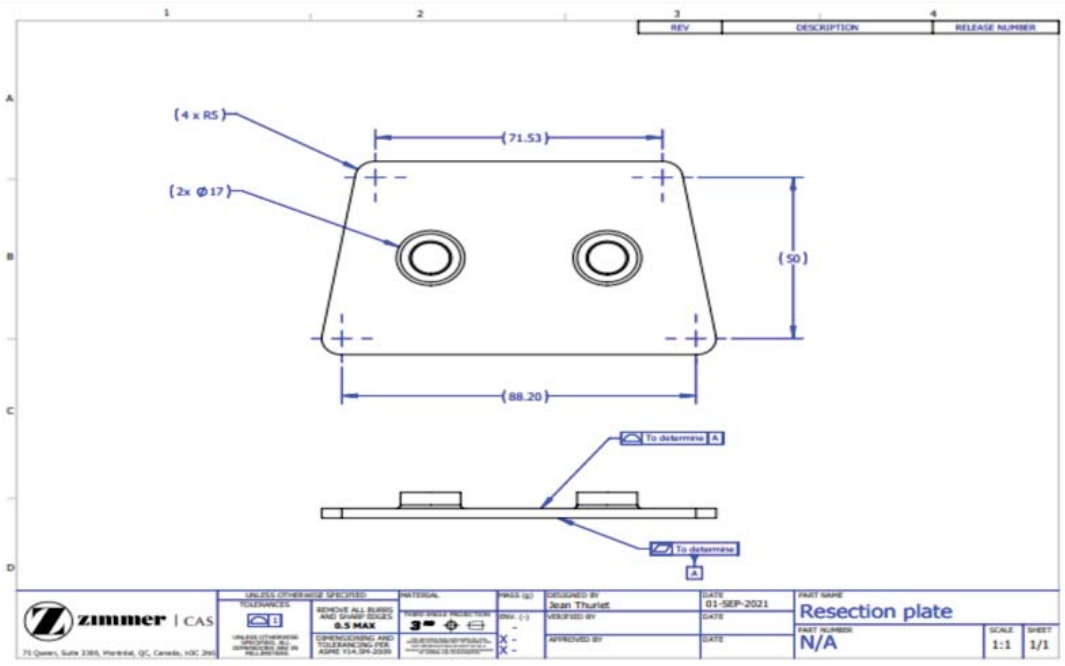

Figure 3.17 2D illustration of the Resection Plate for the production procedure

The figure 3.18 shows the results of the production procedure on the resection plate.

As per ASME Y 14.5 standard, a flatness of 0.283mm (figure. 3.18 and figure. 3.19) for a surface means, if we assume 2 lines with a distance of 0.283mm from each other, all the points of the surface are within these two lines.

A Profile of 0.176mm (figure. 3.18 and figure 3.19) means, if we assume a line which passes from the highest point of a surface and a line which passes from the lowest point of the surface, the distance of these two lines, is 0.176mm. All the point of the surface are within these two lines.

A datum is a plane which passes from the 3 highest points of the surface (figure. 3.19).

RP2.png RP2.png RP2.png RP2.png

FCFFLAT1	MM	0.01				
Feature	MEAS	NOMINAL	+TOL	-TOL	DEV	OUTTOL
PLN3	0.283	0.000	0.010		0.283	0.273
FCFPROF1	MM	0.01 A ASME_Y14_5				
Feature	MEAS	NOMINAL	+TOL	-TOL	DEV	OUTTOL
Set	0.176	0.000	0.005	0.005	0.176	0.171

FCFPROF1 Datum Shift						
Segment	Shift X	Shift Y	Shift Z	Rotation X	Rotation Y	Rotation Z
Segment 1	0.000	0.000	Fixed	Fixed	Fixed	-0.302

Figure 3.18 The result of the CMM for the Resection Plate

RP3.png RP3.png RP3.png RP3.png

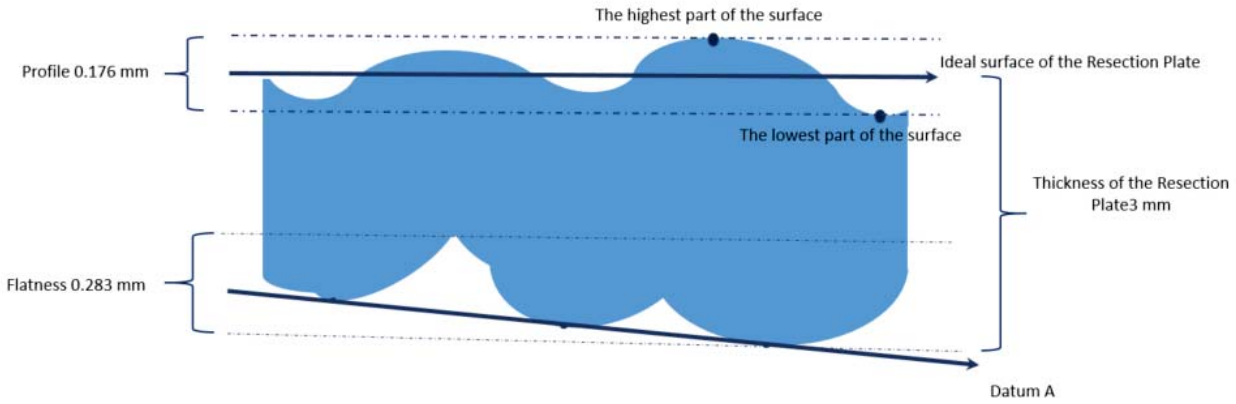

Figure 3.19 An illustration of defining the flatness of the bottom surface of the Resection plate and the profile of the top surface of the resection plate.

Hypothesis:

The resultant offset angle due to the profile of the top surface of the RP for the smallest measured length of the resection plate during the production procedure, is the biggest obtained offset angle .

As discussed in section 3.2.1 and shown in figure 3.15, the resultant offset angle due to the profile of the RP has been calculated with the tangent relation.

As demonstrated in the section 3.2.1 the adjacent side of the triangle (the smallest measured length), has an inverse relation with the tan a (the resultant angle due to the profile of the top surface of the RP). Thus the smallest measured length of the resection plate during the production procedure, has the largest resultant offset angle due to the profile of the top surface of the RP.

In order to obtain the smallest measured length on the resection plate we checked the trajectory of the CMM probe on the Resection Plate as shown in the figure 3.20. As shown in the figure 3.17 and based on the trajectory of the probing step with CMM, the smallest measured length is 50mm.

RP4.jpeg RP4.jpeg RP4.jpeg RP4.jpeg

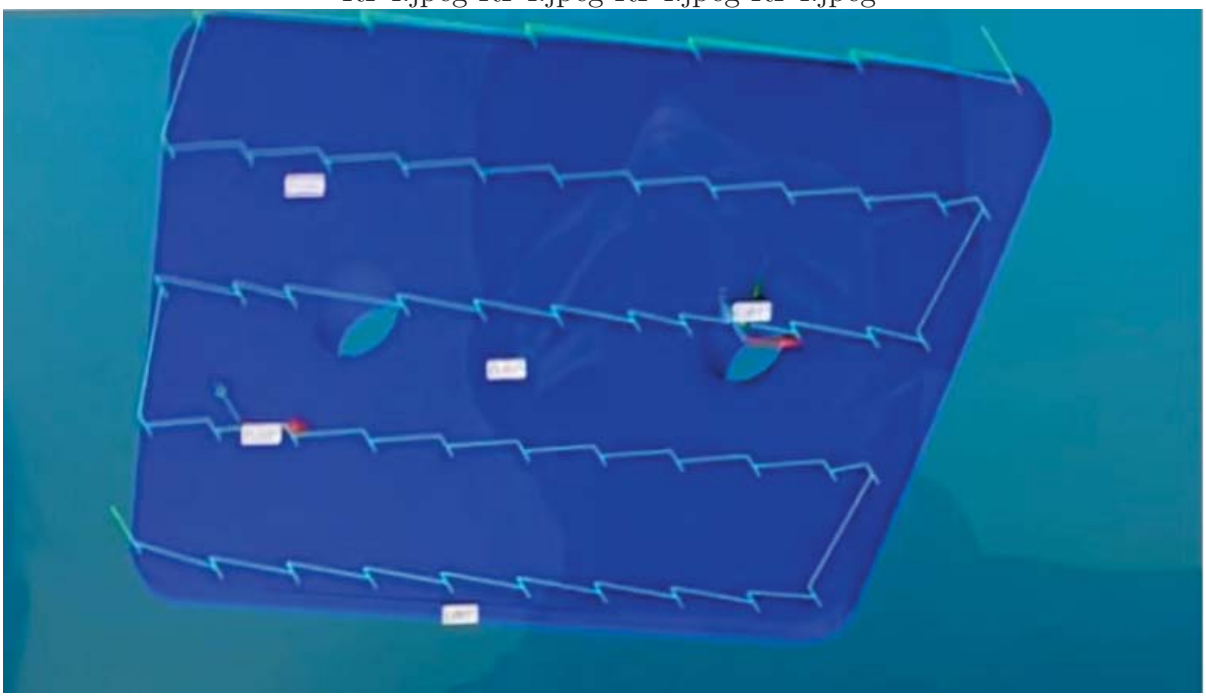

Figure 3.20 An illustration of the trajectory of the CMM probing

$$\tan\alpha \;=\; \frac{\epsilon = The\ profile\ of\ the\ top\ surface\ of\ the\ RP\ (mm)}{L = The\ smallest\ measured\ length\ of\ the\ RP\ (mm)}$$

The resultant offset angle from the profile of the RP $\tan\alpha \;=\; Arc\ tan\ (\frac{\epsilon\ =\ 0.176mm}{L\ =\ 50mm})$

The resultant offset angle from the profile of the top surface of the resection plate has been calculated 0.2017°. This value will be used in the result chapter.

The resultant offset angle from the flatness of bottom surface of the resection plate has been neglected. The reasons of neglecting the offset angle from the flatness of the RP are as follows:

1. The probing process has been executed all over the surface of the RP, in the zone which has the most contact with the cut surface of the sawbone.
2. The probing process has been executed with a high density (55 points from the bottom surface of the RP which has 40cm area).
3. Based on the definition of the flatness for datum A (figure. 3.17 and figure 3.19, a plane which passes, from the three highest points of the bottom surface of RP identifies the bottom surface of the RP.

As a conclusion, we can confidently assume that all the three highest points are in contact with the cut surface of the sawbone. Therefore the plane of the femoral distal cut, is the datum plane of the bottom surface of the RP.

3.2.3 Third Objective: To characterize the repeatability and stability of the outcome value for the measuring procedure with FaroArm specially the steps of using the Mechanical Axis Entry Part (MAEP) and the Resection Plate

Mechanical Axis Entry Part (MAEP)

The uncertainty of the outcome values in measuring the MAEP and the Resection Plate are coming from the following source of errors:

1. Probing step (Operator, Calibration, fitting algorithm and the accuracy of the surface).
2. Loosening of the placement of the parts (MAEP and the Resection Plate) on the bone.

The probing of the parts (figure. 3.3 and figure 3.4) may causes some errors due to the instability of the parts on the sawbone, and to the probing technique of the operator. Therefore the repeatability and reproducibility of the outcome value of this step is an important feature to be evaluated

Repeatability in our case is related to the probing technique of the operator, whereas reproducibility is related to the setup of the artificial femur specimen specially the sawbone of the specimen.

In the appendix E (test procedure for validation of the MAEP) and appendix F (Test procedure for validation of the Resection Plate) we will explain how to run the test protocols to validate the obtained values from measuring the MAEP and the Resection Plate.

This test method validation has been dedicated to evaluate the proposed test method. Thus, the resultant dataset should be compatible with obtained dataset from the proposed test method. As explained in section 3.1.2, the dataset of contributed error of this test method validation should be in the form of V/V and F/E angles.

In order to evaluate the F/E and V/V angle in the test procedure of the MAEP and Resection Plate we have defined two coordinate systems. For the MAEP, the Mechanical Axis of the jig has been set as Z axis of the coordinate system. The X axis of the coordinate systems has been defined as the line which passes from the two points of the pointies block. For the Resection Plate, the normal of the plane of the Resection Plate has been set as Z axis of the coordinate system. The X axis of the coordinate systems has been defined as the line which passes from the two points of the pointies block (figure. 3.21).

The anatomical coronal plane in our coordinate system is the plane which is created by the Y axis and the Z axis and the sagittal plane is the plane which is created by the X axis and the Z axis. In fact the V/V angle of Mechanical Axis is the angle between the Z axis of the coordinate system 1 and the Z axis of the virtual coordinate system in the coronal plane which is a plane that passes from Y axis and Z axis (figure. 3.9 and 3.21). The F/E angle of Mechanical Axis is the angle between the Z axis of the coordinate system 1 and the Z axis of the virtual coordinate system in the sagittal plane which is a plane that passes from X axis and Z axis (figure. 3.9 and figure 3.21).

Sample Size of Test procedure for validating the probing step of the MAEP and Resection Plate

Since this test procedure is a characterization test and does not have an acceptance criteria, it is not possible to define a confidence and reliability level. However, according to Anderson Darling test, the minimum number of samples to determine normality is 20.

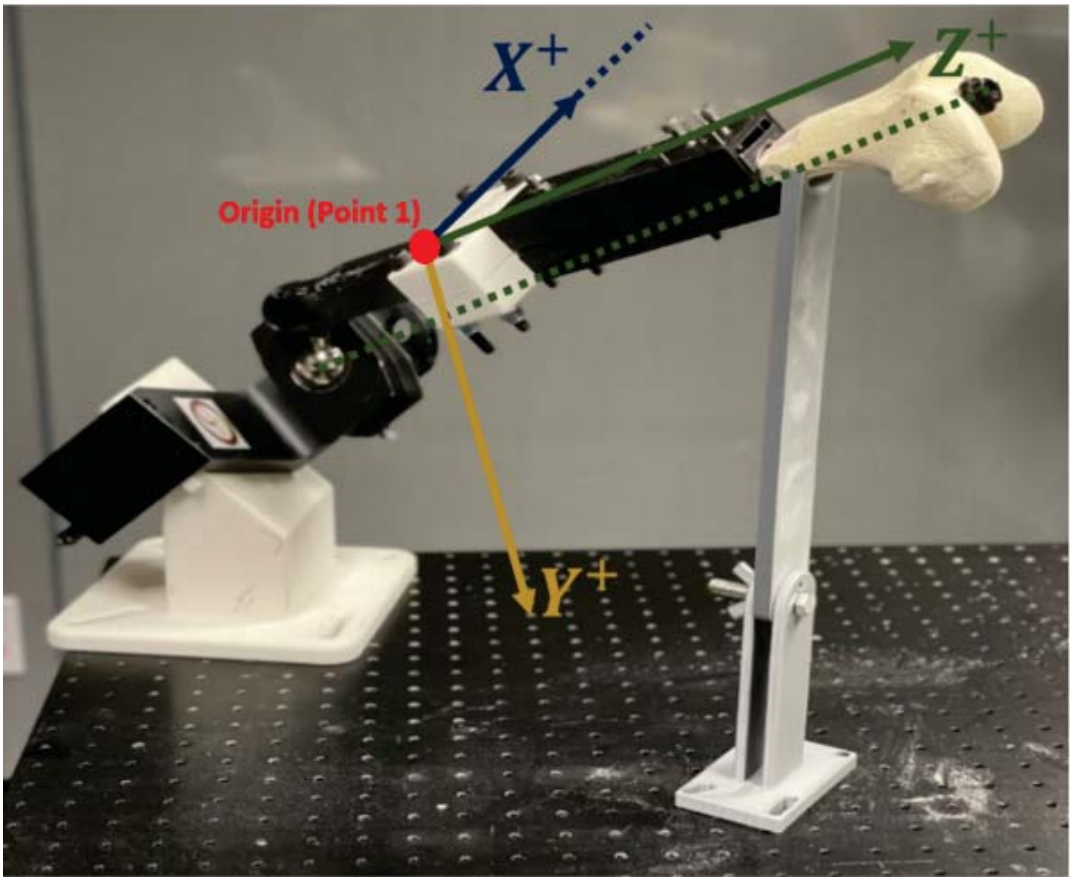

Figure 3.21 An illustration of the created offset in the manufacturing procedure of the MAEP with the 3D printer.

Moreover, when characterizing an error with CMM measurements, it is important to characterize the user variability. Thus we have involved three different operators for execution of the test procedure.

In parallel with user variability, the probing act can vary in different trial for the same operator. As an example the pressure of the operator's hand can change in different experiments. Therefore we have decided to perform ten measurements with each operators.

In addition, the set-up variability should be assessed as well. For instance, the density of the cancellous bone texture, is not the same for different sawbones. Hence, we have decided to involve three different sawbones in executing the test procedure.

As result each operator had executed 10 probing procedure (measurement) on 3 different setups. Therefore, the sample size for these two test procedures became 90.

In the result chapter the outcome values has been explained in detail.

CHAPTER 4 RESULTS

In this chapter all the results from the execution of the proposed test method as well as the results of the validation of the proposed test method has been documented.

In the first section, the results has been gathered from different parts of the validation of the proposed test method (see section 3.2). The second section has been dedicated to the results of the proposed test method. In the last section by comparing the resultant value for the accuracy of the iAssist to the accuracy of the conventional method, we will be able to validate the accuracy of iAssist knee system (see table 3.1).

4.1 The validation of the proposed test method

The resultant error contribution of the proposed test method and efficiency of the designed artificial femur consist of following offset values:

1. Offset resultant of the accuracy of FaroArm for Single Point Repeatability (Error of SPR).
2. Offset resultant of the accuracy of FaroArm for Volumetric Performance (Error of VP).
3. Offset resultant of the profile of the Resection Plate (Error of the profile of the RP).
4. Offset resultant of the measuring the Mechanical Axis Entry Part (Error of the MAEP).
5. Offset resultant of the measuring the resection Plate (Error of the RP).

$$Overall\ Error\ Contribution = E_{SPR} + E_{VP} + E_{Profile of RP} + E_{RP} + E_{MAEP}$$

4.1.1 The Calculated Contributed Errors from Method Chapter

The contributed error due to accuracy of Single Point Repeatability and accuracy of the Volumetric Performance of the FaroArm has been calculated in section 3.2.1. The contributed error from the profile of the Resection Plate has been calculated in section 3.2.2.

The resultant offset due to measuring the MAEP and RP will be explained in section 4.1.2 and 4.1.3 respectively.

The table 4.1 presents the results of the value for the error caused by the accuracy of FaroArm (the accuracy of Single Point Repeatability plus the accuracy of Volumetric Performance of the FaroArm) and the error value from the profile of the RP. These values will be used for the calculation of the overall contributed error of the proposed test method.

Table 4.1 Resultant contributed error due to the profile of the Resection Plate, accuracy of Single Point Repeatability and accuracy of Volumetric Performance of the FaroArm.

Source of Error	**Accuracy of FaroArm**	**Profile of the RP**
Contributed Error	0.0477°	0.2017°

4.1.2 Contributed Errors of measuring the MAEP

After execution of the test procedure for validation of the MAEP (see appendix E) we obtained two datasets. One dataset with 90 values for V/V angles and one dataset with 90 values for F/E angles from the exported transformation matrices.

As we observed the obtained values for both V/V and F/E angle (see appendix G) are smaller than the accuracy of FaroArm which is 0.0477°. Thus we assume that the offset from this step is noise and we are able to neglect it.

4.1.3 Contributed Errors of measuring the RP

After execution of the test procedure for validation of the RP (see appendix F) we obtained two datasets. One dataset with 90 values for V/V angles and one dataset with 90 values for F/E angles, from the exported transformation matrices (see appendix H).

We have executed Anderson-Darling normality test on the dataset for both V/V angle and F/E angle in Minitab 17 statistical software (figure. 4.1). We observed that both datasets are not normally distributed. Since the datasets are not normally distributed in our case, parametric features such as standard deviation and mean of datasets are not reliable to characterise the offset of the measurements with FaroArm.

We have tried normality test within the groups (for the 10 measurements of each operators on all the 3 set-ups) in order to use one-way anova test on the datasets. We observed that the datasets are not normally distributed for any of the groups.

The Idea of executing of Pearson Correlation test has been rejected, due to the presence of the outlier in the datasets. Thus we observed that, we were not able to use parametric methods.

R1.png R1.png R1.png R1.png

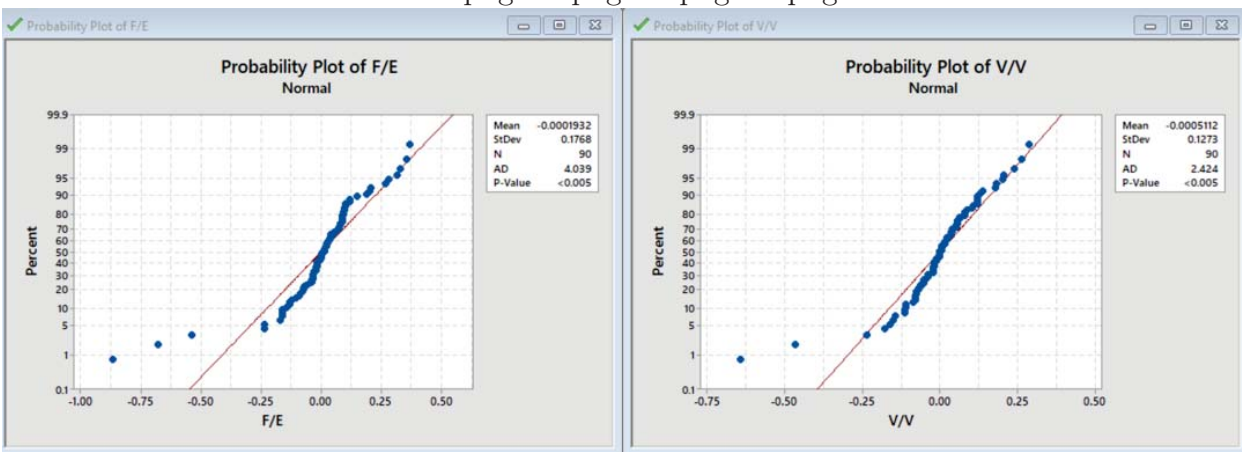

Figure 4.1 A figure of Anderson-Darling test on the datasets of V/V and F/E angles.

Among the nonparametric tests, A Kruskal-Wallis test has been suggested. Basically this test is the equivalent of the parametric one-way ANOVA test when the normality assumption of the dataset is violated [72].

A Kruskal-Wallis, determines whether or not exist a statistically significant difference among the medians of different independent groups (three and more groups). As the Kruskal-Wallis test is not based on normality assumption of the data therefore is much less sensitive to outliers compare to the one-way ANOVA [72].

The assumptions to conduct a Kruskal-Wallis test which should be met are as follows:

1. The response variable should be continuous [73].
2. Each group should have an independent observations from other groups [73].
3. Each group should have a similar shapes of distributions [73].

Since all the assumptions has been met, then we proceed with conducting the test.

We have run Kruskal-Wallis test on both V/V and F/E data sets in Minitab 17 software. First we have conducted the test versus the set-ups (S-up) to verify the reproducibility of the proposed test method. Next, we have conducted the test versus the operators (Op) to verify the repeatability of the proposed test method (see appendix K).

The null hypothesis and alternative hypothesis for the first test has been set as follows:

- The null hypothesis (H0): The median of the set-up impact on the measurement across all the three groups are equal.

- The alternative hypothesis: (Ha): At least one of the median of the set-up impact on the measurement is different from the others groups.

The null hypothesis and alternative hypothesis for the second test has been set as follows:

- The null hypothesis (H0): The median of the operator impact on the measurement across all the three groups are equal.
- The alternative hypothesis: (Ha): At least one of the median of the operator impact on the measurement is different from the others groups.

The results of both ran Kruskal-Wallis test has been gathered in the table. 4.2.

Table 4.2 The results of the Kruskal-Wallis tests

Test	V/V versus S-up	V/V versus Op	F/E versus S-up	F/E versus Op
P-Value	0.968	0.528	0.976	0.289

As we observed from the results of the tests, the p-value of all the for tests are greater than 0.05, thus the rejection of null hypothesis has failed.

As result, we did not have sufficient evidence to say that there is a statistically significant difference between the median of the operator impact and the set-up impact across these three groups.

In addition, as the p-value for the tests on the impact of the operators are less than the p-value for the tests on the impact of the set-ups we have conclude, the measuring procedure of the operators had more impact on the obtained data.

The main goal of executing this test was to characterize the uncertainty of measuring the resection plate with the FaroArm. In order to characterize the uncertainty in measurements, guard-banding technique has been proposed.

Guard-Banding Technique

"Guard-banding is one technique to protect against in-correct conformity decisions caused by measurement uncertainty or entity dispersion, where the region of permissible values of the entity's quality characteristic is reduced in proportion to the actual measurement uncertainty or dispersion" based on ISO 14253-1:1998.

Basically a guard band will be set, by applying an uncertainty around the measured value. In another word, we are characterizing the uncertainty of measurements by creating

a boundary (confidence interval) around the measured value. Applying guard-banding technique in our measurements will make us to be definitely sure that the contributed error due to measuring the RP is not higher than the obtained upper guard band [74].

One of the methods of defining the guard-band on the measurements is generating a confidence interval (guard-band) in the help of bootstrapping.

Bootstrapping

In order to generate confidence interval (uncertainty of measurements) and increase the accuracy of guard-banding technique bootstrapping method has been used.

In statistics, bootstrapping is a computer-based method for better understanding and analyzing the complicated data sets. This technique heavily depends to the computer calculations.

This method can be used to assign measures of accuracy for statistical estimates. Bootstrapping is an inferential statistical method, which considered as a re-sampling technique. Almost any statistic of data distribution can be estimated with bootstrapping [75].

This technique has a very simple procedure but should be repeated so many times. The main steps of a bootstrapping procedure are as follows:

1. Re-sampling a population.
2. Measuring a statistic of this sample (e.g. variance, standard deviation, mean and ...).
3. Analyzing the corresponding parameter of the dataset in the help of using this statistic.

As we can see from the steps, Bootstrapping provides a technique other than confidence intervals (typically used method in research and studies) to estimate statistical parameters of a population (dataset).

With the bootstrapping code in Matlab, we resampled the data set for 1000 times and we generated 1000 datasets with the same size of our main dataset which was 90. We calculate the standard deviation of each resampled datasets. Therefore we created a new dataset with the size of 1000 from standard deviation of all the resamples datasets (see appendix. I).

The standard deviation was chosen as statistical parameter. As general definition of standard deviation, the distance of each member of dataset from the mean value of the dataset is the standard deviation (σ). Since we attempted to characterize the uncertainty of the measurement of each trial, thus standard deviation was the best parameter for our calculations.

In order to determine the number of re-samples of the bootstrapping we took an increasing numbers (e.g. 100, 1000, 10,000, 100,0000). We observed the distribution of the sample mean gets narrower and narrower by increasing the number of re-sampling. In other words, we are arbitrarily making the standard deviation of the bootstrap smaller by increasing the number of re-samples. Standard deviation of the dataset is the uncertainty of measurements which is the most critical feature of our study. Therefor, decreasing the standard deviation of the bootstrap, in our case, is not desirable. In order to avoid missing information 1000 re-sampling has been performed on the datasets.

We have executed Anderson-Darling normality test on the previously mentioned new dataset for both V/V angle and F/E angle in Minitab 17 software (figure. 4.2 and figure. 4.3). We observed that, the both datasets are normally distributed.

R2.png R2.png R2.png R2.png

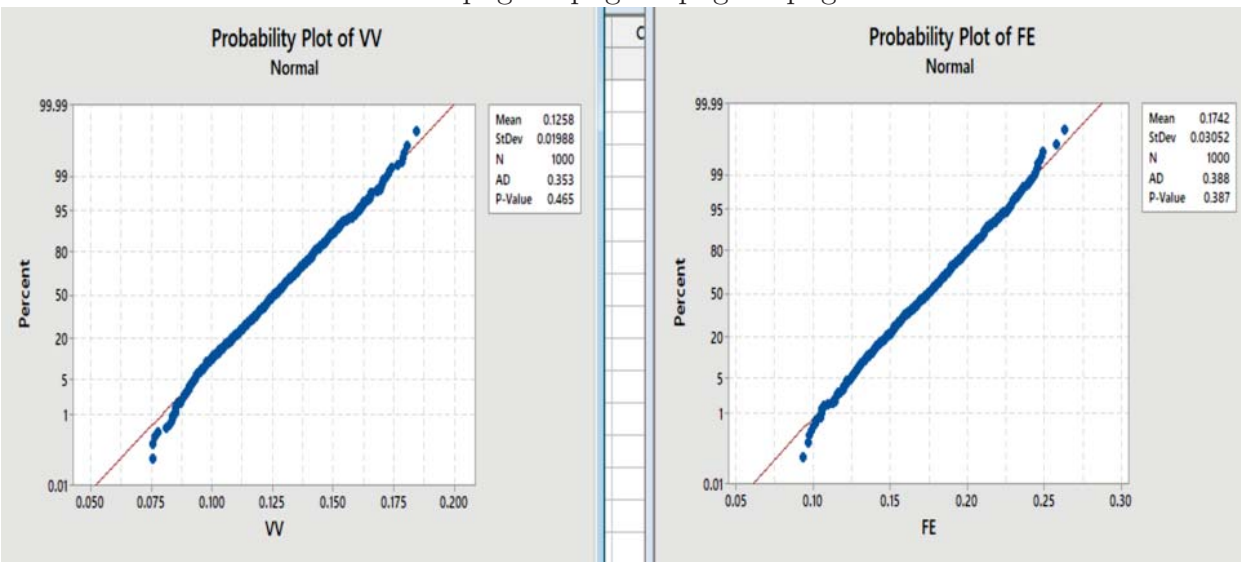

Figure 4.2 A figure of Anderson-Darling test on the both bootstrap datasets of V/V and F/E angles.

In order to calculate the uncertainty of the measurements we will follow the normal distribution law. As shown in fig. 4.4. based on the normal distribution law, 68.26% of values are within 1 standard deviation from the mean, 95.44% of values are within 2 standard deviations from the mean and 99.73% of values are within 3 standard deviations from the mean for the entire population (ref).

In general to achieve a confidence level of 95.44% for the entire population we have to add up the mean value of the dataset with two times of the standard deviation of the data set.

R3.png R3.png R3.png R3.png

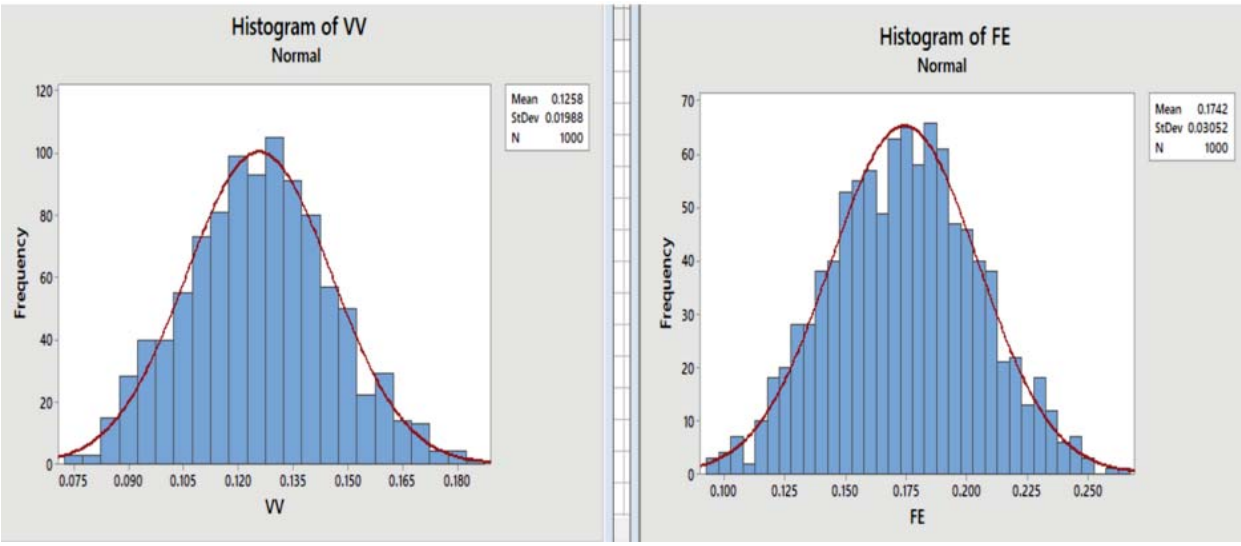

Figure 4.3 An illustration of histograms of the both datasets (V/V and F/E angles).

$$\text{Tolerance Interval } (X_{Upper}/X_{Lower}) = \bar{x}_{dataset} \pm Z_{Score} \times \sigma_{dataset}$$

$\bar{x}_{dataset}$ = The mean value of the dataset.

$\sigma_{dataset}$ = The mean value of the dataset.

Z_{Score} = Determines the confidence level for the entire population of the dataset.

Since our goal is to achieve a confidence level of 95% for a specific percentage of the population (based on table 3.1), therefore we are not able to use two times of the standard deviation of the dataset in our calculations. Thus in order to define the upper limit of the offset, we have updated the calculation formula as follows:

$$\text{Tolerance Interval } (X_{Upper}/X_{Lower}) = \bar{x}_{bootstrapdataset} \pm K_4 \times \sigma_{bootstrapdataset}$$

$\bar{x}_{test}$ = The mean value of the bootstrap dataset.

σ_{test} = The mean value of the bootstrap dataset.

K_4 = equivalent of the Z_{Score} with specific confidence level and specific percentage of the population.

The k4 factor, for calculating the guard-bands, lower limit (X_{Lower}) and the upper limit (X_{Upper}) were computed using Minitab 17 software (see appendix J) for both V/V and F/E based on the user need criteria (see table 3.1). The k4 factor for the F/E angle has been

R4.png R4.png R4.png R4.png

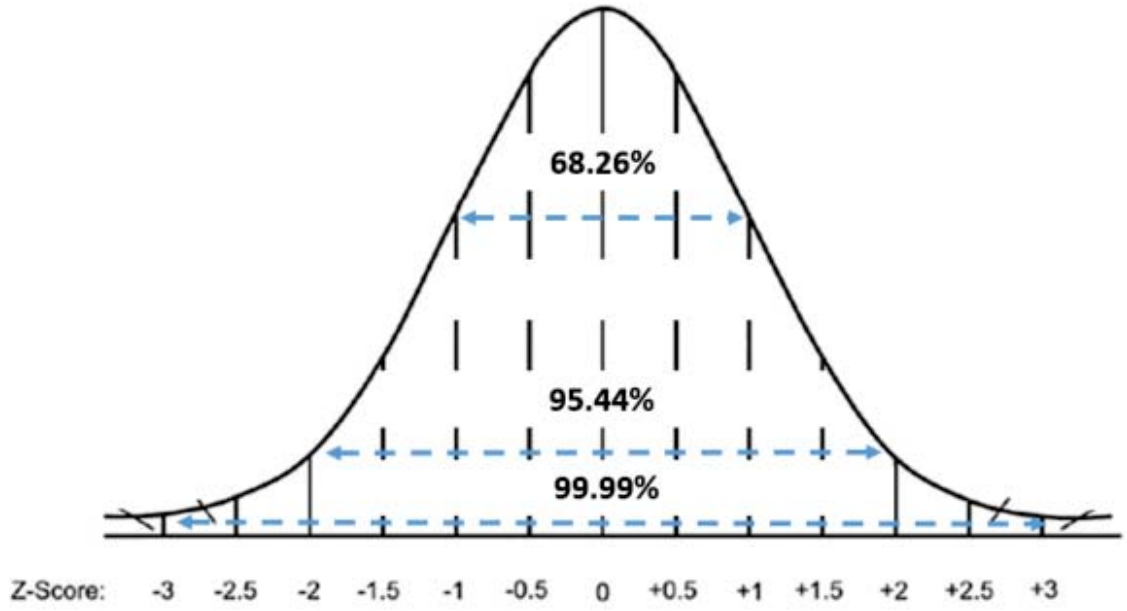

Figure 4.4 An illustration of the law of normal distribution on a normally distributed dataset [76]

calculated 1.2377 with confidence level of 95% and for the V/V angle 1.8156 with confidence level of 95%. In the calculation of k factor the sample size was set to 30, the percentage of population per table. 3.1 and the mean and standard deviation per table.4.3 from previous performed studies by Zimmer Biomet engineers. The table.4.3 has been taken from an internal investigative test document of the Zimmer Biomet company.

Table 4.3 The standard deviation and the mean from an internal investigative test document

Feature / Dataset	Dataset of F/E	Dataset of V/V
Mean $\bar{x}$	0.23	0.15
Standard Deviation σ	0.88	0.82

The upper limit (upper guard band) and the lower limit (lower guard band) for both V/V and F/E angles has been calculated by using the values of the table. 4.4 and the following fomulas:

$$X_{Upper} = \bar{x}_{bootstrapdataset} + K_4 \times \sigma_{bootstrapdataset}$$
$$X_{Lower} = \bar{x}_{bootstrapdataset} - K_4 \times \sigma_{bootstrapdataset}$$

The upper limit (upper guard band) and the lower limit (lower guard band) for V/V

Table 4.4 The standard deviation and the mean from bootstrap data sets

Feature / Dataset	Dataset of F/E	Dataset of V/V
Mean $\bar{x}$	0.1742	0.1258
Standard Deviation σ	0.0305	0.0199
K4 Factor	1.2377	1.8156

angle has been calculated 0.1619 and 0.0897 respectively. The upper limit (upper guard band) and the lower limit (lower guard band) for F/E angle has been calculated 0.2119 and 0.1364 respectively.

As these values has been considered as the offset of measuring the resection plate and has been added to the overall contributed error of FaroArm, therefore the worst case has been selected among these values (see the table. 4.5).

Table 4.5 The values of the overall contributed errors for the proposed test method.

Overall Contributed Error V/V	Upper limit of V/V	Accuracy of Faro	Profile of RP
0.4113	0.1619	0.0477	0.2017
Overall Contributed Error F/E	Upper limit of F/E	Accuracy of Faro	Profile of RP
0.4614	0.2120	0.0477	0.2017

As the results of the overall contributed error demonstrate, the proposed test protocol for V/V angle is 7.3 and for F/E angle is 6.5 times more accurate than the accuracy of iAssist knee system respectively.

4.2 iAssist Validation

In this section, the results from execution of the proposed test has been gathered and assessed. The results are from both iAssist as target system and FaroArm as measuring tool or the gold-standard.

The dataset of executing the test method has been created as explained previously in section 3.1.2.

Figure. 4.5 and figure. 4.6 show the different contributed values in the overall value of V/V angle and F/E angle (angle between MA of the artificial femur and the Femoral Distal Cut) from FaroArm respectively. The explanation of the contributed values are in the section 3.1.2.

R5.png R5.png R5.png R5.png

No	Op No of execution	B.3	B.2	B.1	Overall value of Faro V/V
1	A.Z 1	0.756335993	-0.005550499	0.411302812	1.162088306
2	A.Z 2	-1.23999961	-0.007064271	0.411302812	-0.835761069
3	A.Z 3	-0.418502854	-0.004036726	0.411302812	-0.011236768
4	A.Z 4	-0.727690044	-0.008578043	0.411302812	-0.324965275
5	B.A 1	-0.745101185	-0.015642314	0.411302812	-0.349440687
6	B.A 2	0.126151432	-0.014633133	0.411302812	0.522821112
7	B.A 3	-0.911108327	-0.01311936	0.411302812	-0.512924875
8	B.A 4	-0.315344346	-0.015642314	0.411302812	0.080316151
9	B.A 5	0.120357067	-0.010596406	0.411302812	0.521063473
10	C.O 1	-0.022918311	-0.024220356	0.411302812	0.364164145
11	C.O 2	-0.968593868	-0.022706584	0.411302812	-0.57999764
12	C.O 3	-0.56726641	-0.0433948	0.411302812	-0.199358397
13	C.O 4	0.200534409	-0.019174449	0.411302812	0.592662772
14	C.O 5	0.298054588	-0.022201994	0.411302812	0.687155406
15	J.T 1	-0.779330412	-0.023211175	0.411302812	-0.391238775
16	J.T 2	0.807897739	0.017156086	0.411302812	1.236356637
17	J.T 3	-2.430071275	-0.00983952	0.411302812	-2.028607983
18	J.T 4	-2.650156999	-0.019426745	0.411302812	-2.258280931
19	J.T 5	-0.34748859	0.014633133	0.411302812	0.078447354
20	N.G 1	-0.395374141	-0.020183631	0.411302812	-0.00425496
21	N.G 2	0.257906638	0.005298203	0.411302812	0.674507654
22	N.G 3	0.446898017	0.005045908	0.411302812	0.863246737
23	N.G 4	-0.017188733	0.01311936	0.411302812	0.407233439
24	N.G 5	-0.704773021	-0.011605588	0.411302812	-0.305075797
25	N.G 6	-1.994483829	-0.011605588	0.411302812	-1.594786605
26	R.P 1	-1.128806577	-0.010091816	0.411302812	-0.727595581
27	R.P 2	0.951307932	0.013623951	0.411302812	1.376234695
28	R.P 3	1.329422358	0.005550499	0.411302812	1.746275669
29	R.P 4	0.739370276	-0.008578043	0.411302812	1.142095045
30	R.P 5	-1.444269955	-0.010091816	0.411302812	-1.043058958

Figure 4.5 An illustration of the Excel sheet of the contributed values in the overall value of V/V from FaroArm (raw data).

R6.png R6.png R6.png R6.png

No	Op No of execution	B.3	B.2	B.1	Overall value of Faro F/E
1	A.Z 1	0.091682337	-0.005550499	0.461382904	0.547514743
2	A.Z 2	-3.526645324	-0.007064271	0.461382904	-3.072326691
3	A.Z 3	1.919842122	0.004036726	0.461382904	2.385261752
4	A.Z 4	0.297965164	-0.008578043	0.461382904	0.750770025
5	B.A 1	-1.449853747	-0.015642314	0.461382904	-1.004113157
6	B.A 2	2.252365992	0.014633133	0.461382904	2.728382029
7	B.A 3	-0.807978534	-0.01311936	0.461382904	-0.359714991
8	B.A 4	2.131911602	0.015642314	0.461382904	2.60893682
9	B.A 5	1.409614674	0.010596406	0.461382904	1.881593984
10	C.O 1	0.338041177	0.024220356	0.461382904	0.823644437
11	C.O 2	1.220703727	0.022706584	0.461382904	1.704793215
12	C.O 3	-0.303695157	-0.0433948	0.461382904	0.114292947
13	C.O 4	-0.085943605	-0.019174449	0.461382904	0.35626485
14	C.O 5	1.661776383	0.022201994	0.461382904	2.145361281
15	J.T 1	-0.636084241	0.023211175	0.461382904	-0.151490162
16	J.T 2	0.469861846	-0.017156086	0.461382904	0.914088664
17	J.T 3	0	-0.00983952	0.461382904	0.451543384
18	J.T 4	5.84299348	-0.019426745	0.461382904	6.284949639
19	J.T 5	8.366719791	0.014633133	0.461382904	8.842735828
20	N.G 1	-0.670397068	-0.020183631	0.461382904	-0.229197795
21	N.G 2	1.443981136	0.005298203	0.461382904	1.910662243
22	N.G 3	0.28647651	-0.005045908	0.461382904	0.742813506
23	N.G 4	0.017188733	-0.01311936	0.461382904	0.465452277
24	N.G 5	-0.481321358	-0.011605588	0.461382904	-0.031544042
25	N.G 6	-0.699463409	-0.011605588	0.461382904	-0.249686093
26	R.P 1	-0.481369498	-0.010091816	0.461382904	-0.03007841
27	R.P 2	-1.014333648	-0.013623951	0.461382904	-0.566574695
28	R.P 3	-0.578841338	-0.005550499	0.461382904	-0.123008932
29	R.P 4	1.386841805	-0.008578043	0.461382904	1.839646666
30	R.P 5	1.100493931	-0.010091816	0.461382904	1.551785019

Figure 4.6 An illustration of the Excel sheet of the contributed values in the overall value of F/E from FaroArm (raw data).

Since the obtained offset angle from the using the “Move Device” command of FaroArm is a 3D angle we decided to add it to both V/V and F/E angle and over estimate the offset of this step. Thus we are definitely sure that the offset for V/V and F/E angle is less than the obtained 3D angle.

In order to consider the worst case scenario for the Resultant Offset Move Device we had a comparison between the obtained value from the log of iAssist and the obtained value of FaroArm. If the value of iAssist is greater that the value of the FaroArm we consider the Resultant Offset Move Device as negative value. In the other case, where the value of iAssist is smaller than the value of the FaroArm, we consider it as positive value (figure. 4.7). We did these steps for both V/V and F/E angles.

R7.png R7.png R7.png R7.png

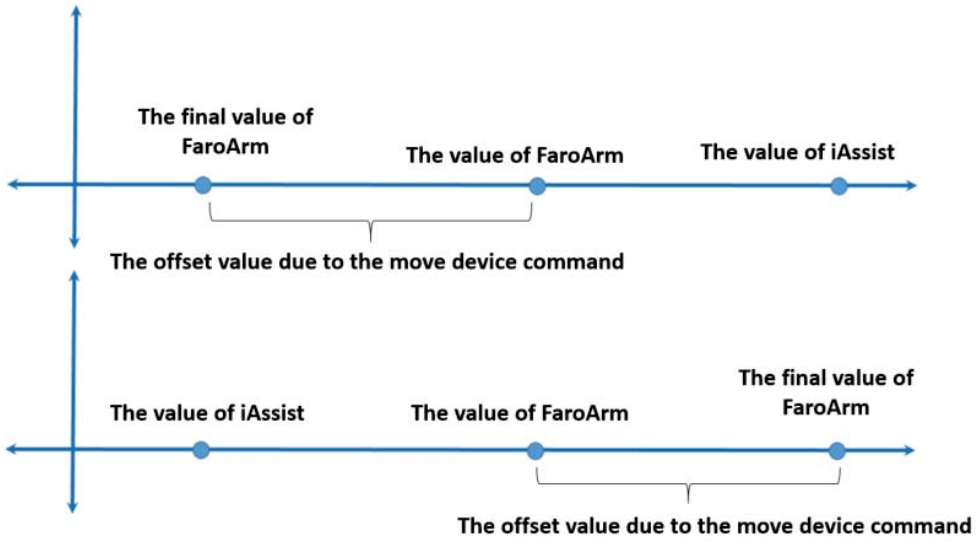

Figure 4.7 An illustration of defining the worst case scenario for the resultant offset of move device.

Figure. 4.8 shows the recognised V/V angle from both iAssist system and FaroArm system, and the figure. 4.8 shows the recognised F/E angle from both iAssist system and FaroArm system.

The raw data for iAssist was taken directly from the data recordings of the iAssist Tablet. In order to assess the accuracy of iAssist, the difference between iAssist and the FaroArm data obtained was calculated for both V/V angle and F/E angle (see section 3.1.2).

R8.png R8.png R8.png R8.png

No	Op No of execution	The value of iAssist for V/V	Overall value of Faro V/V	Difference OF iAssist and FaroArm
1	A.Z 1	0.855976028	1.162088306	-0.306112279
2	A.Z 2	-0.009260717	-0.835761069	0.826500352
3	A.Z 3	2.345144903	-0.011236768	2.356381671
4	A.Z 4	0.393698209	-0.324965275	0.718663484
5	B.A 1	0.10928597	-0.349440687	0.458726657
6	B.A 2	0.476188661	0.522821112	-0.046632451
7	B.A 3	0.643202421	-0.512924875	1.156127296
8	B.A 4	1.521111273	0.080316151	1.440795121
9	B.A 5	0.211829945	0.521063473	-0.309233527
10	C.O 1	1.075350108	0.364164145	0.711185963
11	C.O 2	-0.026569715	-0.57999764	0.553427926
12	C.O 3	0.166348556	-0.199358397	0.365706953
13	C.O 4	0.236095854	0.592662772	-0.356566918
14	C.O 5	0.628947231	0.687155406	-0.058208175
15	J.T 1	0.032516845	-0.391238775	0.423755619
16	J.T 2	-1.42638989	1.236356637	-2.662746527
17	J.T 3	-1.016484424	-2.028607983	1.012123559
18	J.T 4	-0.328856575	-2.258280931	1.929424356
19	J.T 5	-1.735678238	0.078447354	-1.814125592
20	N.G 1	0.552993081	-0.00425496	0.55724804
21	N.G 2	0.03920607	0.674507654	-0.635301584
22	N.G 3	-0.115893319	0.863246737	-0.979140056
23	N.G 4	-0.270741466	0.407233439	-0.677974905
24	N.G 5	-0.591527357	-0.305075797	-0.28645156
25	N.G 6	0.635685215	-1.594786605	2.230471819
26	R.P 1	0.596460524	-0.727595581	1.324056105
27	R.P 2	0.381687867	1.376234695	-0.994546827
28	R.P 3	-0.078519855	1.746275669	-1.824795524
29	R.P 4	1.230707614	1.142095045	0.088612569
30	R.P 5	3.30905472	-1.043058958	4.352113679

Figure 4.8 An illustration of the Excel sheet of difference between iAssist and FaroArm for V/V angle (raw data).

R9.png R9.png R9.png R9.png

No	Op No of execution	The value of iAssist for F/E	Overall value of Faro F/E	Difference OF iAssist and FaroArm
1	A.Z 1	1.671014221	0.547514743	1.123499478
2	A.Z 2	1.080277545	-3.072326691	4.152604237
3	A.Z 3	1.040554381	2.385261752	-1.344707371
4	A.Z 4	2.648629188	0.750770025	1.897859164
5	B.A 1	1.622977439	-1.004113157	2.627090596
6	B.A 2	-1.83773348	2.728382029	-4.566115509
7	B.A 3	1.384294681	-0.359714991	1.744009671
8	B.A 4	-1.966929733	2.60893682	-4.575866554
9	B.A 5	-0.475909058	1.881593984	-2.357503042
10	C.O 1	-0.226375625	0.823644437	-1.050020062
11	C.O 2	0.200299743	1.704793215	-1.504493472
12	C.O 3	0.929423487	0.114292947	0.81513054
13	C.O 4	0.560082288	0.35626485	0.203817438
14	C.O 5	1.268201972	2.145361281	-0.877159308
15	J.T 1	-0.691307957	-0.151490162	-0.539817795
16	J.T 2	2.001364497	0.914088664	1.087275833
17	J.T 3	4.389761984	0.451543384	3.9382186
18	J.T 4	7.701240316	6.284949639	1.416290677
19	J.T 5	8.355500822	8.842735828	-0.487235006
20	N.G 1	0.824600859	-0.229197795	1.053798653
21	N.G 2	1.134674158	1.910662243	-0.775988085
22	N.G 3	1.081194278	0.742813506	0.338380771
23	N.G 4	1.153484363	0.465452277	0.688032086
24	N.G 5	1.492388899	-0.031544042	1.523932941
25	N.G 6	1.355732735	-0.249686093	1.605418828
26	R.P 1	1.504209018	-0.03007841	1.534287427
27	R.P 2	1.557786301	-0.566574695	2.124360996
28	R.P 3	1.704772894	-0.123008932	1.827781826
29	R.P 4	2.707683948	1.839646666	0.868037283
30	R.P 5	2.094189389	1.551785019	0.54240437

Figure 4.9 An illustration of the Excel sheet of difference between iAssist and FaroArm for F/E angle (raw data).

We have executed Anderson darling normality test on both datasets (V/V and F/E) in the Minitab 17 software. Figure 4.10 shows the data distribution of the V/V angle and Figure 4.11 shows the data distribution of the F/E angle.

R10.png R10.png R10.png R10.png

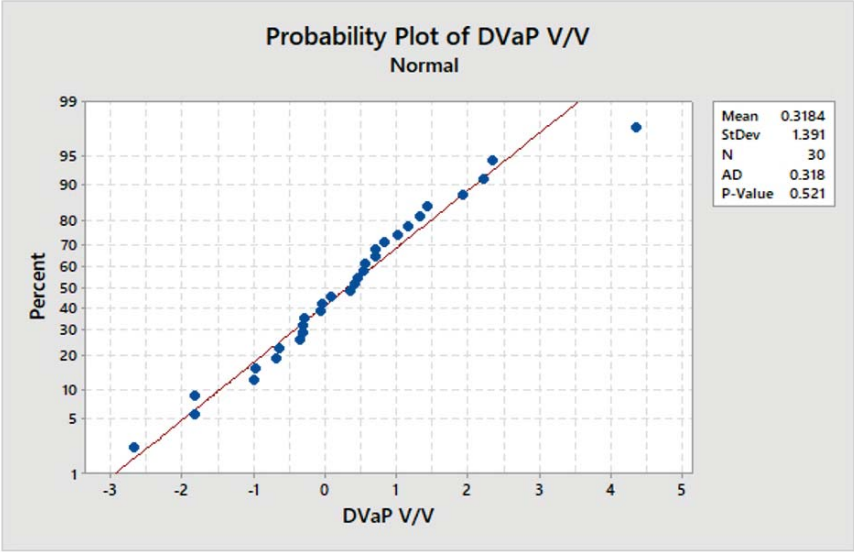

Figure 4.10 An illustration of normality test on dataset of V/V angle.

We observed the p.value for the V/V dataset was 0.521 and the p.value for F/E dataset was 0.080. Since both p.values are greater than 0.05, therefore both datasets are normally distributed per Anderson darling test.

In order to obtain the overall accuracy of iAssist, the two-sided tolerance interval method per normal distribution law, has been used (see section 4.1.3 fig. 4.4).

$$X_{Upper} = \bar{x}_{dataset} + K_4 \times \sigma_{dataset}$$
$$X_{Lower} = \bar{x}_{dataset} - K_4 \times \sigma_{dataset}$$

The k4 factor, for calculating the lower limit (X_U) and the upper limit (X_L) were extracted from table. 4.4. In the calculation of the tolerance interval, the mean and standard deviation values has been taken from table. 4.6.

The tolerance interval has been calculated for both V/V and the F/E angles as follows:

$$V/V_{Upper} = 0.3184 + (1.8156 \times 1.391)$$
$$V/V_{Lower} = 0.3184 - (1.8156 \times 1.391)$$

R11.png R11.png R11.png R11.png

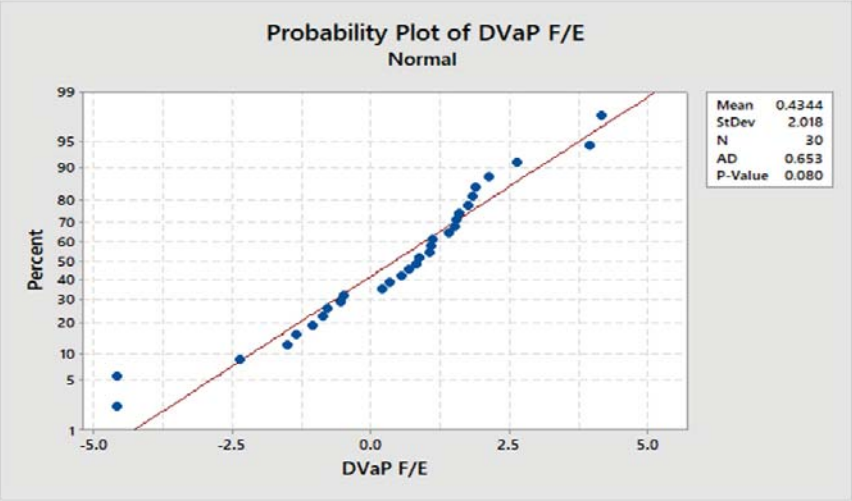

Figure 4.11 An illustration of normality test on dataset of F/E angle.

Table 4.6 The standard deviation and the mean values from the normality test on F/E and V/V datasets

Feature / Dataset	Dataset of F/E	Dataset of V/V
Mean $\bar{x}$	0.4344	0.3184
Standard Deviation σ	2.018	1.391

$$F/E_{\ Upper} = 0.4344 + (1.2377 \times 2.018)$$

$$F/E_{\ Lower} = 0.4344 - (1.2377 \times 2.018)$$

The overall accuracy of iAssist for V/V angle is [-2.21, +2.84] in 96.6% of the cases, and for F/E angle is [-2.06, +2.93] in 86.6%.

CHAPTER 5 GENERAL DISCUSSION

This chapter summarizes challenges and limitations of our study.

5.1 Limits and discussion of validating the proposed method

In this section, we will explain the challenges that we faced during the validation of the proposed method.

5.1.1 Repeatability, Reproducibility and Accuracy

The accuracy of the previous version of iAssist has been obtained ±3° in 65.7% of cases for the F/E angle of the femoral distal cut and ±3° in 83.6% of cases for the V/V angle of the femoral distal cut. We expected that the accuracy of the new version will be almost the same. We have set the tolerance of our measurement at ±3°. Based on the rule ten to one, we need a measuring system with discrimination of ±0.3° (ten times more accurate than iAssist) [23].

This value (10 times more accurate) is coming from the acceptance ranges for total Gage Repeatability and Reproducibility (Gage R & R) percentage. Gage R & R is a technique used for defining the amount of variation in measurement data due to the measuring system. This technique after comparing the measurement variation with the final observed variability, defines the capability of the measuring system. As shown in figure 5.1, the acceptable percentage for validating the measuring system is 10% which is equivalent to an accuracy of 10 times higher [23].

Figure 5.1, shows the criteria for determining whether the measuring system is adequate or not.

The results of validating the proposed method, demonstrate that, the measuring method is 6.5 to 7.3 time more accurate than iAssist. These values can be justified based on the three following reason:

- This value has been obtained from the parts, which are not fully developed and quite optimized therefore, it can be considered as an adequate accuracy for a prototype. As an example, the resection plate and the mechanical axis entry point have been manufactured with high density plastic. If these parts will be manufactured with controlled precision and higher density material, we guess the inaccuracy of measurement with FaroArm will decrease. Thus, we know the accuracy of the proposed test method will

D1.png D1.png D1.png D1.png

Figure 5.1 An illustration of Gage R&R tolerance rang [23]

be higher than the obtained accuracy.

- Based on the Gage repeatability and reproducibility tolerance rang, the obtained accuracy is almost in the marginal level, which means that the measuring method is not excellent but it can be acceptable [23].

5.1.2 Move Device Command and The Accuracy of FaroArm

The main inaccuracy and uncertainty through the calculation procedure of the final value of the contributed error of FaroArm for both F/E and V/V angle, is the resultant offset from the move-device command and the accuracy of FaroArm. The main challenge through calculating this values were the lack of ability of decomposing the resultant offset angle to F/E and V/V angles in sagittal and coronal planes. In order to overcome this challenge we have obtained the offset as a 3D angle for both move device command and the accuracy of FaroArm. We have overestimated this offset by adding it to both F/E and V/V angles.

Based on the experimental observations the resultant offset from this step is small. If the resultant offset obtained is a big value, we have to recheck the some physical features during the execution such as, the temperature and humidity of the measuring room, the assembly

of the artificial femur.

In one of the experiments we had a big offset from the move device command (0.2°), we rechecked the assembly of the artificial femur and we realized that, one of the screws of the bone-holder was missed.

5.2 Limits and discussion of validating iAssist

In this section we will explain the challenges and limitations that we faced during the execution of the test procedure on iAssist knee system.

5.2.1 Specimen

The average length of femur for an adult male is 48 centimeters [77] whereas, the length of our specimen was 61 to 63 centimeters. iAssist uses the length of the femur as a feature to determine the MA of the femur. Since this gap is out of the known range for iAssist, hence determination of the plane of the distal cut might have been affected. In another word there is a doubt, that the recognized angle of the femoral distal cut by iAssist is not perpendicular to the MA of the femur.

During the execution of the test procedure we have used our designed specimen. The lack of physiological features such as cartilage tissues, blood of specimen may affect the accuracy of iAssist. As observed, in a TKA with iAssist the range of the movement of the leg is limited. This fact demonstrate that, the results of our test might be diffident than the results of iAssist for a TKA procedure on human leg.

5.2.2 Operators

The operators, which performed the test procedure on iAssist were not surgeons. As the knowledge of the surgeons can improve the surgical procedure with iAssist thus, we can consider the obtained value as worst case. The surgeons known well the anatomical land marks of the femur. One of the steps during a TKA procedure with iAssist depends on correctly placing the parts of iAssist into the bone trough anatomical landmark of the femur. The anatomical knowledge of the surgeons will improve the accuracy.

5.2.3 Results of the accuracy of iAssist

The overall accuracy of iAssist for V/V angle has been obtained as [-2.21, +2.84] in 96.6% of the cases, and for F/E angle has been obtained as [-2.06, +2.93] in 86.6% of the cases.

Previously, a similar study has been done in Zimmer Biomet company on the accuracy of TKA surgical procedure with iAssist knee system. In this study, which is referred to as the gold standard, they have used the optical system, which has been explained in Section 2.2. These two studies are different from a number of aspects. First, they have used cadavers as research model. In contrast, in our study, we have designed a research model with sawbones (artificial femur). Second, the operators for executing the test procedure were surgeons. In contrary, our study relies on system engineers at Zimmer Biomet to execute the proposed test method on the designed research model. Third, in the previous study, they have executed TKA procedure with both systems on the cadavers. They have considered the difference between the resultant angle of the femoral distal cut of the gold standard system (optical system) and iAssist as the accuracy of iAssist. Whereas, in our accuracy test method, we basically define the mechanical axis of the femur and the plane of the femoral distal cut by measuring the special anatomical landmark and test equipment. We calculated the accuracy of iAssist from the resultant angle of the femoral distal cut and the measured values using FaroArm. The accuracy of iAssist knee system from the optical system for V/V angle has been obtained as [-3, +3] in 100% of the cases, and for F/E angle has been obtained as [-3, +3] in 95.24% of the cases. We observe that there is a difference between the results of our study and those of the previous study. Since the obtained tolerance interval in our study is narrower than the tolerance interval obtained by the cadaveric study with optical system, it is obvious to see the decrease of the covered population. By comparing the results of our study to those of the optical study , we observe that both results are very close, meaning that the results of our study are realistic and reliable. The advantages of our study are summarized as follows:

- Given that our proposed method relies on using sawbones (i.e., artificial bones), preparation of surgical room is more convenient compared to the study with cadavers.
- Our proposed method does not involve cadavers. Thus it is not subject to compliance with any health related standards which add some complexities and administration works.
- The proposed method serves as a less time consuming method of validating the accuracy of the iAssist system compared to using cadavers.

CHAPTER 6 CONCLUSION

This chapter concludes the outcome of this thesis. In addition, some possible future works has been proposed in this chapter.

6.1 Summary of Results

This thesis aimed to develop a test protocol to measure the accuracy of iAssist knee system. After a detailed literature review, we have decided to use a mechanical tracking system as measuring tool or gold standard. In order to perform the test protocol, we have designed an artificial specimen with anatomical and bio mechanical properties of a human femur, to use it as research model for the test procedure. We have performed a detail study on the contributed and possible source of errors of the proposed test method. The results of this study has shown that, the proposed method is accurate enough to measure the accuracy of iAssist knee system. Finally after executing the test procedure on the iAssist knee system, the accuracy of iAssist has been measured. Thus, we achieved the main objective of this thesis.

6.2 Future Work

In the following, we lay down a few future research directions that can be built on this study.

- An interesting future research is to improve the artificial femur with the purpose of being more realistic and adding additional anatomical and physiological properties of the femur (e.g. adding some weights to simulate the muscles of the leg). Adding weights and tendons on the artificial femur will restrict the range of motions for the registration step of the iAssist surgical procedure. As observed in the TKA procedure on patients, the range of the motion is restricted due to the weight of the muscles.

- Another research avenue is to combine different tracking system to improve the accuracy of the proposed method and further reduce the possible contributed error. By Using two tracking systems (e.g., Mechanical Tracking System (FaroArm) and Optical Tracking System), we will be able to define the femoral distal cut more accurately.

- Last but not least, trained surgeons can serve as operators for executing the involved steps with iAssist to improve the accuracy of the femoral distal cut. Recognizing the

femoral distal cut by iAssist highly depends on placing the femoral spike of the iAssist on the anatomical landmark of the femur; therefore, the knowledge of the surgeons will improve the performance of our proposed method.

REFERENCES

[1] M. Sloan, A. Premkumar, and N. P. Sheth, "Projected volume of primary total joint arthroplasty in the us, 2014 to 2030," *JBJS*, vol. 100, no. 17, pp. 1455–1460, 2018.

[2] L. March *et al.*, "Osteoarthritis: A serious disease: Submitted to the us food and drug administration," 2016.

[3] S. A. Ofa *et al.*, "Robotic total knee arthroplasty vs conventional total knee arthroplasty: A nationwide database study," *Arthroplasty today*, vol. 6, no. 4, pp. 1001–1008, 2020.

[4] A. V. Lombardi Jr and K. R. Berend, "Patient-specific approach in total knee arthroplasty," *Orthopedics (Online)*, vol. 31, no. 9, p. 927, 2008.

[5] M. T. Hirschmann and H. Behrend, "Functional knee phenotypes: a call for a more personalised and individualised approach to total knee arthroplasty?" 2018.

[6] J. Bellemans *et al.*, "Is neutral mechanical alignment normal for all patients?" *Clinical Orthopaedics and Related Research*, 2001.

[7] C. Rivière *et al.*, "Alignment options for total knee arthroplasty: a systematic review," *Orthopaedics & Traumatology: Surgery & Research*, vol. 103, no. 7, pp. 1047–1056, 2017.

[8] Y. Ma *et al.*, "Effects of tibial baseplate shape on rotational alignment in total knee arthroplasty: three-dimensional surgical simulation using osteoarthritis knees," *Archives of orthopaedic and trauma surgery*, vol. 138, no. 1, pp. 105–114, 2018.

[9] A. Desseaux *et al.*, "Radiographic outcomes in the coronal plane with iassist^{TM} versus optical navigation for total knee arthroplasty: a preliminary case-control study," *Orthopaedics & Traumatology: Surgery & Research*, vol. 102, no. 3, pp. 363–368, 2016.

[10] M. Fosco *et al.*, "Concepts in computer assisted total knee replacement surgery," *Orthopaedic Surgery, University of Bologna*, pp. 397–420, 2012.

[11] B. Parcells, "Patient risk factors."

[12] G. R. Scuderi *et al.*, "Total knee arthroplasty with a novel navigation system within the surgical field." *The Orthopedic Clinics of North America*, vol. 45, no. 2, pp. 167–173, 2014.

[13] K. T. Kim *et al.*, "Causes of failure after total knee arthroplasty in osteoarthritis patients 55 years of age or younger," *Knee surgery & related research*, vol. 26, no. 1, p. 13, 2014.

[14] K. Kawaguchi *et al.*, "Comparison of an accelerometer-based portable navigation system, patient-specific instrumentation, and conventional instrumentation for femoral alignment in total knee arthroplasty," *Knee surgery & related research*, vol. 29, no. 4, p. 269, 2017.

[15] S. R. Knight, R. Aujla, and S. P. Biswas, "Total hip arthroplasty-over 100 years of operative history," *Orthopedic reviews*, vol. 3, no. 2, 2011.

[16] D. K. Bae and S. J. Song, "Computer assisted navigation in knee arthroplasty," *Clinics in orthopedic surgery*, vol. 3, no. 4, pp. 259–267, 2011.

[17] G. Welch and E. Foxlin, "Motion tracking: No silver bullet, but a respectable arsenal," *IEEE Computer graphics and Applications*, vol. 22, no. 6, pp. 24–38, 2002.

[18] B. A. Rebal *et al.*, "Imageless computer navigation in total knee arthroplasty provides superior short term functional outcomes: a meta-analysis," *The Journal of arthroplasty*, vol. 29, no. 5, pp. 938–944, 2014.

[19] J.-Y. Jenny, R. K. Miehlke, and A. Giurea, "Learning curve in navigated total knee replacement. a multi-centre study comparing experienced and beginner centres," *The Knee*, vol. 15, no. 2, pp. 80–84, 2008.

[20] J. Bové, "Computer-assisted total-knee arthroplasty. comparison of two successive systems. learning curve," *Revue de chirurgie orthopedique et reparatrice de l'appareil moteur*, vol. 94, no. 3, pp. 252–260, 2008.

[21] J.-t. Li, X. Gao, and X. Li, "Comparison of iassist navigation system with conventional techniques in total knee arthroplasty: A systematic review and meta-analysis of radiographic and clinical outcomes," *Orthopaedic Surgery*, vol. 11, no. 6, pp. 985–993, 2019.

[22] L. van den Haak *et al.*, "Human cadavers to evaluate prototypes of minimally invasive surgical instruments: A feasibility study," *Technology and Health Care*, vol. 25, no. 6, pp. 1139–1146, 2017.

[23] M. A. Durivage, *Practical Attribute and Variable Measurement Systems Analysis (MSA): A Guide for Conducting Gage R&R Studies and Test Method Validations.* Quality Press, 2015.

[24] Y. Ma *et al.*, "Effects of tibial baseplate shape on rotational alignment in total knee arthroplasty: three-dimensional surgical simulation using osteoarthritis knees," *Archives of orthopaedic and trauma surgery*, vol. 138, no. 1, pp. 105–114, 2018.

[25] M. Hadi *et al.*, "Does malalignment affect revision rate in total knee replacements: a systematic review of the literature," *Springerplus*, vol. 4, no. 1, p. 835, 2015.

[26] J. L. Boakes, P. M. Stevens, and R. F. Moseley, "Treatment of genu valgus deformity in congenital absence of the fibula," *Journal of Pediatric Orthopaedics*, vol. 11, no. 6, pp. 721–724, 1991.

[27] L. March *et al.*, "Osteoarthritis: a serious disease," *OARSI. org*, 2016.

[28] C. I. for Health Information, "Hip and knee replacements in canada, 2016–2017: Canadian joint replacement registry annual report," 2018.

[29] L. K. George, D. Ruiz Jr, and F. A. Sloan, "The effects of total knee arthroplasty on physical functioning in the older population," *Arthritis & Rheumatism: Official Journal of the American College of Rheumatology*, vol. 58, no. 10, pp. 3166–3171, 2008.

[30] R. B. Bourne *et al.*, "Patient satisfaction after total knee arthroplasty: who is satisfied and who is not?" *Clinical Orthopaedics and Related Research®*, vol. 468, no. 1, pp. 57–63, 2010.

[31] C. Rivière *et al.*, "Alignment options for total knee arthroplasty: a systematic review," *Orthopaedics & Traumatology: Surgery & Research*, vol. 103, no. 7, pp. 1047–1056, 2017.

[32] L. Sheehy *et al.*, "Does measurement of the anatomic axis consistently predict hip-knee-ankle angle (HKA) for knee alignment studies in osteoarthritis? analysis of long limb radiographs from the multicenter osteoarthritis (most) study," *Osteoarthritis and cartilage*, vol. 19, no. 1, pp. 58–64, 2011.

[33] Y. S. Kwoh *et al.*, "A robot with improved absolute positioning accuracy for ct guided stereotactic brain surgery," *IEEE Transactions on Biomedical Engineering*, vol. 35, no. 2, pp. 153–160, 1988.

[34] H. A. Paul *et al.*, "Development of a surgical robot for cementless total hip arthroplasty," *Clinical Orthopaedics and Related Research®*, vol. 285, pp. 57–66, 1992.

[35] A. P. Schulz *et al.*, "Results of total hip replacement using the robodoc surgical assistant system: clinical outcome and evaluation of complications for 97 procedures," *The*

International Journal of Medical Robotics and Computer Assisted Surgery, vol. 3, no. 4, pp. 301–306, 2007.

[36] J. Cobb *et al.*, "Hands-on robotic unicompartmental knee replacement: a prospective, randomised controlled study of the acrobot system," *The Journal of bone and joint surgery. British volume*, vol. 88, no. 2, pp. 188–197, 2006.

[37] A. H. Jinnah *et al.*, "General concepts in robotics in orthopedics," in *Robotics in Knee and Hip Arthroplasty*. Springer, 2019, pp. 27–35.

[38] S. E. Park and C. T. Lee, "Comparison of robotic-assisted and conventional manual implantation of a primary total knee arthroplasty," *The Journal of arthroplasty*, vol. 22, no. 7, pp. 1054–1059, 2007.

[39] D. J. Jacofsky and M. Allen, "Robotics in arthroplasty: A comprehensive review," *The Journal of Arthroplasty*, vol. 31, no. 10, pp. 2353 – 2363, 2016.

[40] "Technique and first clinical results of robot-assisted total knee replacement," *The Knee*, vol. 9, no. 3, pp. 173 – 180, 2002.

[41] J. Lang *et al.*, "Robotic systems in orthopaedic surgery," *The Journal of bone and joint surgery. British volume*, vol. 93, no. 10, pp. 1296–1299, 2011.

[42] L. Mattei *et al.*, "Patient specific instrumentation in total knee arthroplasty: a state of the art," *Annals of translational medicine*, vol. 4, no. 7, 2016.

[43] G. R. Scuderi *et al.*, "Total knee arthroplasty with a novel navigation system within the surgical field," *Orthopedic Clinics*, vol. 45, no. 2, pp. 167–173, 2014.

[44] M. Maier, A. Ebrahimzadeh, and M. Chowdhury, "The tactile internet: Automation or augmentation of the human?" *IEEE Access*, vol. 6, pp. 41 607–41 618, 2018.

[45] J. Lang *et al.*, "Robotic systems in orthopaedic surgery," *The Journal of bone and joint surgery. British volume*, vol. 93, no. 10, pp. 1296–1299, 2011.

[46] N. Glossop, "Localization and tracking technologies for medical robotics," in *Medical Robotics*. Elsevier, 2012, pp. 41–58.

[47] T. Peters and K. Cleary, *Image-guided interventions: technology and applications*. Springer Science & Business Media, 2008.

[48] A. Sarvestani, "Basic principles of fluoro-navigation," in *Practice of Intramedullary Locked Nails*. Springer, 2006, pp. 243–247.

[49] J. D. Sieber, J. S. Sieber, and W. K. Stewart, "Smart tracking system," Jul. 27 1993, uS Patent 5,231,483.

[50] R. Hofstetter *et al.*, "Fluoroscopy as an imaging means for computer-assisted surgical navigation," *Computer Aided Surgery*, vol. 4, no. 2, pp. 65–76, 1999.

[51] Y. Ma *et al.*, "Real-time x-ray fluoroscopy-based catheter detection and tracking for cardiac electrophysiology interventions," *Medical physics*, vol. 40, no. 7, p. 071902, 2013.

[52] G. Welch and E. Foxlin, "Motion tracking: No silver bullet, but a respectable arsenal," *IEEE Computer graphics and Applications*, vol. 22, no. 6, pp. 24–38, 2002.

[53] Y. Wu *et al.*, "Strapdown inertial navigation system algorithms based on dual quaternions," *IEEE transactions on aerospace and electronic systems*, vol. 41, no. 1, pp. 110–132, 2005.

[54] J. Clark, "Self-calibration and performance control of MEMS with applications for iot," *Sensors*, vol. 18, no. 12, p. 4411, 2018.

[55] V. S. Rajendren *et al.*, "An experimental study of iAssist total knee arthroplasty technique," *Science Letters*, vol. 6, no. 2, pp. 46–53, 2018.

[56] G. R. Scuderi *et al.*, "Total knee arthroplasty with a novel navigation system within the surgical field," *Orthopedic Clinics of North America*, vol. 45, no. 2, pp. 167–173, 2014. [Online]. Available: https://www.sciencedirect.com/science/article/pii/S0030589813001818

[57] J. W. Noble Jr, C. A. Moore, and N. Liu, "The value of patient-matched instrumentation in total knee arthroplasty," *The Journal of arthroplasty*, vol. 27, no. 1, pp. 153–155, 2012.

[58] M. P. Ast, D. Nam, and S. B. Haas, "Patient-specific instrumentation for total knee arthroplasty: a review," *Orthopedic Clinics*, vol. 43, no. 5, pp. e17–e22, 2012.

[59] R. Leach, *Fundamental principles of engineering nanometrology*. Elsevier, 2014.

[60] M. Feuerstein *et al.*, "Magneto-optical tracking of flexible laparoscopic ultrasound: model-based online detection and correction of magnetic tracking errors," *IEEE Transactions on Medical Imaging*, vol. 28, no. 6, pp. 951–967, 2009.

[61] Z. Yaniv *et al.*, "Electromagnetic tracking in the clinical environment," *Medical physics*, vol. 36, no. 3, pp. 876–892, 2009.

[62] A. M. Franz *et al.*, "Electromagnetic tracking in medicinea review of technology, validation, and applications," *IEEE transactions on medical imaging*, vol. 33, no. 8, pp. 1702–1725, 2014.

[63] T. Koivukangas, J. P. Katisko, and J. P. Koivukangas, "Technical accuracy of optical and the electromagnetic tracking systems," *SpringerPlus*, vol. 2, no. 1, pp. 1–7, 2013.

[64] M. K. Chmarra, C. Grimbergen, and J. Dankelman, "Systems for tracking minimally invasive surgical instruments," *Minimally Invasive Therapy & Allied Technologies*, vol. 16, no. 6, pp. 328–340, 2007.

[65] S. Li *et al.*, "Accelerometer-based gyroscope drift compensation approach in a dual-axial stabilization platform," *Electronics*, vol. 8, no. 5, p. 594, 2019.

[66] G. S.-H. Goh *et al.*, "Accelerometer-based navigation is as accurate as optical computer navigation in restoring the joint line and mechanical axis after total knee arthroplasty: a prospective matched study," *The Journal of arthroplasty*, vol. 31, no. 1, pp. 92–97, 2016.

[67] B. M. Hetaimish *et al.*, "Meta-analysis of navigation vs conventional total knee arthroplasty," *The Journal of arthroplasty*, vol. 27, no. 6, pp. 1177–1182, 2012.

[68] A. Tofil and I. Usydus, "The use of a 3d scanner and measuring faro arm for measuring of bend angle bars on a three-roller bending machine." in *2019 IEEE 5th International Workshop on Metrology for AeroSpace (MetroAeroSpace)*. IEEE, 2019, pp. 633–637.

[69] M. C. Kinney *et al.*, "Comparison of the iassist handheld guidance system to conventional instruments for mechanical axis restoration in total knee arthroplasty," *The Journal of arthroplasty*, vol. 33, no. 1, pp. 61–66, 2018.

[70] A. Wozniak and M. Dobosz, "Factors influencing probing accuracy of a coordinate measuring machine," *IEEE Transactions on Instrumentation and Measurement*, vol. 54, no. 6, pp. 2540–2548, 2005.

[71] R. Nagamine *et al.*, "Distal femoral cut perpendicular to the mechanical axis may induce varus instability in flexion in medial osteoarthritic knees with varus deformity in total knee arthroplasty: a pitfall of the navigation system," *Journal of Orthopaedic Science*, vol. 9, no. 6, pp. 555–559, 2004.

[72] E. Ostertagova, O. Ostertag, and J. Kováč, "Methodology and application of the kruskal-wallis test," in *Applied Mechanics and Materials*, vol. 611. Trans Tech Publ, 2014, pp. 115–120.

[73] A. Vargha and H. D. Delaney, "The kruskal-wallis test and stochastic homogeneity," *Journal of Educational and behavioral Statistics*, vol. 23, no. 2, pp. 170–192, 1998.

[74] L. R. Pendrill, "An optimised uncertainty approach to guard-banding in global conformity assessment," in *Advanced Mathematical and Computational Tools in Metrology and Testing: AMCTM VIII*. World Scientific, 2009, pp. 256–261.

[75] B. Efron and R. J. Tibshirani, *An introduction to the bootstrap*. CRC press, 1994.

[76] A. Lyon, "Why are normal distributions normal?" *The British Journal for the Philosophy of Science*, vol. 65, no. 3, pp. 621–649, 2014.

[77] M. R. Feldesman, J. G. Kleckner, and J. K. Lundy, "Femur/stature ratio and estimates of stature in mid-and late-pleistocene fossil hominids," *American Journal of Physical Anthropology*, vol. 83, no. 3, pp. 359–372, 1990.

APPENDIX A ASSEMBLY OF THE ARTIFICIAL FEMUR

This appendix contains the Description of assembling the Artificial Femur:

1. First we have a base part (see the figure. A.1), which has to be fixed on the workbench with 3 screws (M6 screws).

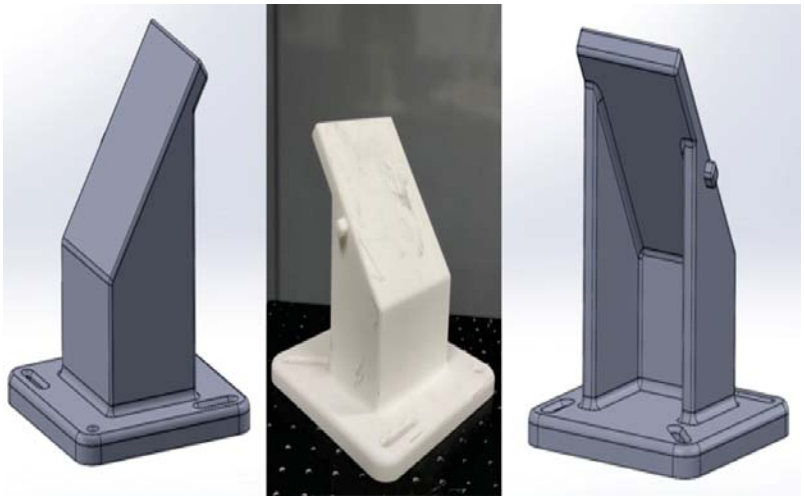

Figure A.1 An illustration of the base part from different angles.

2. Next, add the femoral proximal part (see figure. A.2) joint on the base part.

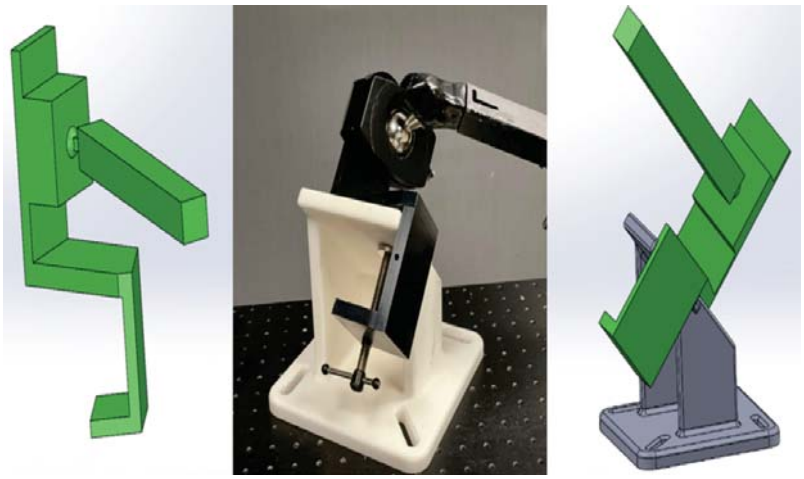

Figure A.2 An illustration of the assembled femoral proximal part on the base.

3. Next we have to assemble the ponties block (see figure. 3.6) on the femoral proximal part (see figure. A.3).

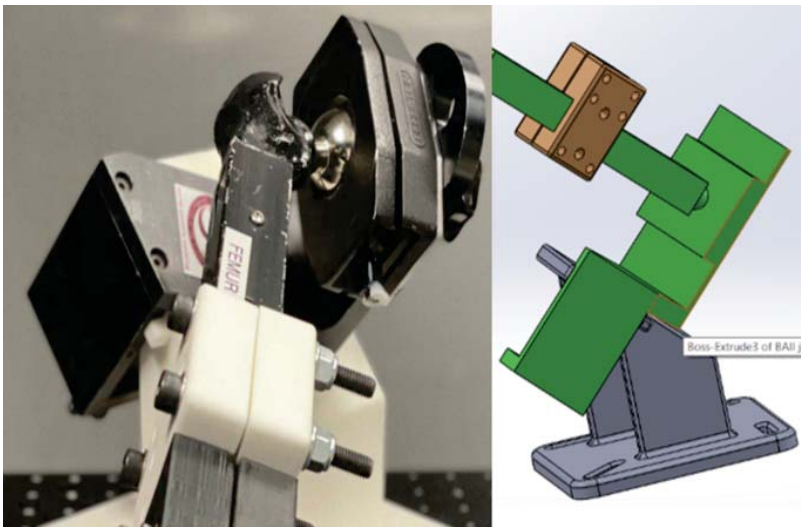

Figure A.3 An illustration of the assembled pointies block on the femoral proximal part.

4. Install the bone holder part on the femoral proximal part below the pointies block (see figure 3.5 and see figure A.4).

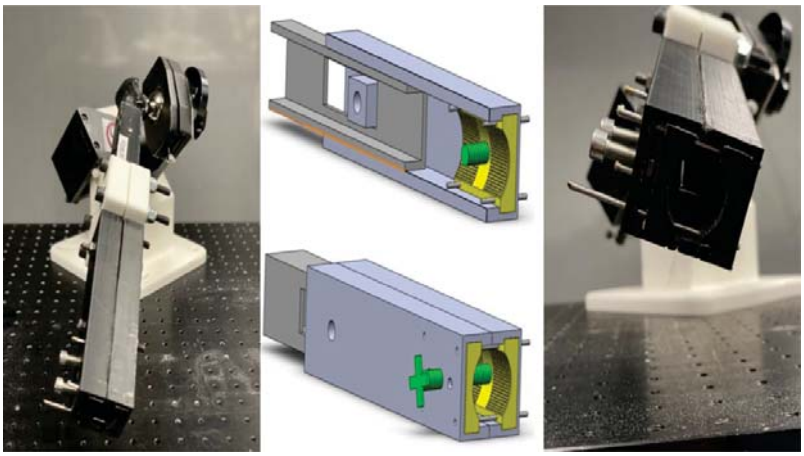

Figure A.4 An illustration of the bone holder part to attach the proximal femur and the distal femur part (sawbone).

5. Place the sawbone into the bone holder part (see figure 3.4) and place the MAEP into the anatomical landmark of the sawbone.

6. Fix the stopper part on the workbench with 3 screws (M6 screws) and put the distal part of the jig (sawbone) of the stopper (see figure 3.2).

7. After execution of the femoral cut, place the resection plate on the surface of the resected bone and fix it with the two captive spikes (see figure 3.3).

APPENDIX B PROPOSED TEST PROCEDURE TO MEASURE THE ACCURACY OF IASSIST

This appendix contains the Test Method Description:

Before the test procedure begins, the specimen (artificial femur) should be assembled and ready (see appendix A).

In addition, there are three important properties for the test environment regarding the requirement for the pods which should be met by setting the test environment before the test begins.

1. First, the temperature of the test environment should be in the acceptance range for the performance of the pods. know that the performance of the pods were designed in such a way to be compatible with the temperature of the operation room, the temperature should be between $15°C$ to $30°C$.

2. Second, since the pods are made by inertial sensors which are sensitive to the vibration and movements the test environment and the surgical table should be stable and immobile (The vibration coming from the cut step with the saw-slot is in the acceptance range of the inertial sensors and the vibration test was executed and the result didn't demonstrate significant impact on the performance of the pods).

3. Third property for the test environment is the absence of the electrical noise of the environment. Electrical noises may affect the pods and the interaction between pods and the tablet.

Different steps of the proposed test procedure are as follows:

1. Fix the FaroArm on the table.

2. Fix the femoral jig with 3 screws on the table at a distance of approximately one meter from FaroArm (make sure that the jig is fixed as per appendix 1 and oriented correctly to execute the surgical flow and to perform the measurements with the Faro Arm).

3. Fix the Stopper part on the table and place the sawbones part of the jig on it.

4. Make sure the jig is rigid without any looseness.

5. Place the MAEP into the center of knee joint landmark of the sawbone by using a hammer.

6. Place the artificial femur on the stopper and make it stable with the help of plastic zip tie.

7. Open “FaroCam2”.

8. Choose “Measure” from the toolbar.

9. Select “Sphere” from toolbar and probe 10 points on the femoral sphere of the jig and name it Femoral Sphere.

10. Select the “Point” from toolbar and probe 5 points of MAEP and name MAEP.

11. Probe 5 points from each cone of the pointies block and name them Pointies 1 and Pointies 2, the number of the points has written next to the cone.

12. Take the MAEP off from the sawbone and open the zip tie.

13. Ask a surgeon to perform all the surgical steps for the femoral workflow with iAssist. The surgeon must execute the validation step of the iAssist knee system on the jig as well.

14. Place the Resection Plate on the cut surface and fix it by using the captive spikes. Use a hammer to make sure, there is no space or gap between the plate and cut surface.

15. Place the artificial femur on the stopper and make it stable with the help of plastic zip tie.

16. Choose “Device” from the toolbar.

17. Select “Move Device” command and select “manual” from the opened window and click on “Next”.

18. Select the Femoral Sphere and the two points of the pointies block (Pointies 1 and Pointies 2) from the features in order to reprobe them, then click on “next”.

19. In this step FaroArm asks to reprobe the selected features.

20. Probe the features asked by FaroArm one after the other, and click on “next”.

21. From the “Results portion” in the opened window, note “Max Error” (or took a screenshot from the results portion table) and click on “Finish”.

22. Once the femoral jig (device) has been retrieved in its new position. Choose “Measure” from the toolbar.

23. Select “Plane” from toolbar and probe 10 points on the Resection Plate and name it Femoral Distal Cut.

24. Open “Alignments” tab and click on “Coordinate System”.

25. Choose “Advanced” from the opened window and click on the Line shape for both

Primary and Secondary features.

26. Choose Femoral Sphere and MAEP (with Z+ as the Axis) as “Primary”.

27. Choose Pointies 1 and Pointies 2 (with X+ as the Axis) as “Secondary” and set the Pointies 1 as the “Origin”.

28. Make sure the option Align with World is not checked and click on “Hold to Primary”.

29. Name the Coordinate System, Coordinate System Mechanical Axis.

30. Open the “Alignments” tab and click on “Coordinate System”.

31. Choose “Advanced” from the opened window and click on the plane shape for Primary and line shape for Secondary feature.

32. Choose Femoral Distal Cut (with Z+ as the Axis) as “Primary”.

33. Choose Pointies 1 and Pointies 2 (with X+ as the Axis) as “Secondary” and set the Pointies 1 as the “Origin”.

34. Make sure the option Align with World is not checked and click on “Hold to Primary”.

35. Name the Coordinate System Coordinate, System Femoral Distal Cut.

36. Click on “Alignment” choose “Manage Alignments”.

37. Click on “Coordinate system”

38. Choose coordinate system Mechanical Axis as “Measured Coordinate System” and World as “Nominal Coordinate System”.

39. In the Existing Alignments delete all the alignments and set the obtained alignment from the step 36 as active alignment.

40. Open the “File” then click on “Import/Export” and then open “Transformation Matrix”.

41. In the opened Window choose the coordinate system Femoral Distal Cut as the “Matrix” and then click the “Use base matrix”.

42. As “Base Matrix” choose Coordinate System Mechanical Axis.

43. Save it as “Euler File” type.

44. Name the file based on the name of surgeons and the number of execution (e.g. first surgeon 1).

45. Prepare a new sawbone and repeat all the steps for couple of sawbones with the first surgeon.

46. Ask the other surgeons to redo all the steps for a total 30 trials (depending on the number of surgeons the trial of each surgeon can vary).

APPENDIX C THE SPEC-SHEET OF FAROARM

A7.png A7.png A7.png A7.png

Quantum^S

Quantum^S Accuracy 6-Axis	ISO 10360-12 Maximum Permissible Error (MPE)
1.5M length	
Volumetric Accuracy (E_{Uni})	0.022 mm (0.0009 in)
Single Point Repeatability (SPAT)	0.012 mm (0.0005 in)
P_{Size}	0.007 mm (0.0003 in)
P_{Form}	0.012 mm (0.0005 in)
L_{Dia}	0.024 mm (0.0009 in)
2.5M length	
Volumetric Accuracy (E_{Uni})	0.026 mm (0.0010 in)
Single Point Repeatability (SPAT)	0.018 mm (0.0007 in)
P_{Size}	0.009 mm (0.0004 in)
P_{Form}	0.018 mm (0.0007 in)
L_{Dia}	0.032 mm (0.0013 in)
3.0 M length	
Volumetric Accuracy (E_{Uni})	0.038 mm (0.0015 in)
Single Point Repeatability (SPAT)	0.027 mm (0.0011 in)
P_{Size}	0.012 mm (0.0005 in)
P_{Form}	0.026 mm (0.0010 in)
L_{Dia}	0.046 mm (0.0018 in)
3.5M length	
Volumetric Accuracy (E_{Uni})	0.052 mm (0.0020 in)
Single Point Repeatability (SPAT)	0.036 mm (0.0014 in)
P_{Size}	0.016 mm (0.0006 in)
P_{Form}	0.034 mm (0.0013 in)
L_{Dia}	0.064 mm (0.0025 in)
4.0M length	
Volumetric Accuracy (E_{Uni})	0.063 mm (0.0025 in)
Single Point Repeatability (SPAT)	0.045 mm (0.0018 in)
P_{Size}	0.020 mm (0.0008 in)
P_{Form}	0.038 mm (0.0015 in)
L_{Dia}	0.078 mm (0.0031 in)

Figure C.1 Spec-sheet of the FaroArm from Faro website

APPENDIX D THE SPEC-SHEET OF 3D PRINTER

Ultimaker S5 specifications

Printer and printing properties	Technology	Fused deposition modeling (FDM)
	Print head	Dual-extrusion print head with an auto-nozzle lifting system and swappable print cores
	Build volume	XYZ: 330 x 240 x 300 mm (left or right nozzle, or dual extrusion)
	Filament diameter	2.85 mm
	Layer resolution	0.25 mm nozzle: 150 - 60 micron 0.4 mm nozzle: 200 - 20 micron 0.8 mm nozzle: 600 - 20 micron
	XYZ accuracy	6.9, 6.9, 2.5 micron
	Build speed	<24 mm^3/s
	Build plate	Heated glass build plate, Heated aluminum build plate
	Build plate temperature	20 - 140 °C
	Build plate leveling	Active leveling
	Supported materials	Optimized for: PLA, Tough PLA, Nylon, ABS, CPE, CPE+, PC, TPU 95A, PP, PVA, Breakaway Also supports third-party materials
	Nozzle diameter	0.25 mm, 0.4 mm, 0.8 mm
	Nozzle temperature	180 - 280 °C
	Nozzle heat up time	<2 min
	Build plate heat up time	<4 min (from 20 to 60 °C)
	Operating sound	50 dBA
	Power rating	500 W
	Material recognition	Auto-recognition with NFC scanner
	Connectivity	Wi-Fi, LAN, USB port
	Display	4.7-inch (11.9 cm) color touchscreen
	Language support	English, Dutch, French, German, Italian, Japanese, Korean, Portugese, Russian, Spanish, Simplified Chinese
	Monitoring	Live camera (view from desktop or app)
Physical dimensions	Dimensions	495 x 457 x 520 mm
	Dimensions (with bowden tubes and spool holder)	495 x 585 x 780 mm
	Net weight	20.6 kg
	Shipping weight	29 kg
	Shipping box dimensions	650 x 600 x 700 mm
Ambient conditions	Operating ambient temperature	15 - 32 °C, 10 - 90% RH non-condensing
	Non-operating temperature	0 - 32 °C
Software	Supplied software	Ultimaker Cura, our free print preparation software Cura Connect, our free printer management solution
	Supported OS	MacOS, Windows and Linux

Figure D.1 Spec-sheet of the 3D printer from Ultimaker website

APPENDIX E TEST PROCEDURE FOR VALIDATION OF THE MAEP

1. Fix the FaroArm on the table.

2. Fix the femoral jig and the pointies block of the jig with 3 screws on the table at a distance of approximately one meter from FaroArm.

3. Fix the Stopper part on the table with 3 Screws and place the sawbones part of the jig on it.

4. Make sure the jig is rigid without any looseness.

5. Place the MAEP with your hand in the center of knee joint landmark, on the sawbone.

6. Open “FaroCam2”.

7. Choose “Measure” from the toolbar.

8. Select “Sphere” from toolbar and probe 10 points on the femoral sphere of the jig and name it Sphere1.

9. Select “Point” from toolbar and probe 5 points of MAEP and name MAEP 1.

10. Probe 5 points from each cone of the pointies block and name them first point 1 and second point 1.

11. Open “Alignments” tab and click on “Coordinate System”.

12. Choose “Advanced” from the opened window and click on the Line shape for both Primary and Secondary features, make sure to click on “Hold to Primary”.

13. Choose Sphere1 and MAEP 1 (with Z+ as the Axis) as “Primary”.

14. Choose first point1 and second point 1 (with X+ as the Axis) as “Secondary” and set the Sphere 1 as the “Origin”.

15. Make sure the option Align with World is not checked.

16. Name the Coordinate System Coordinate System1.

17. Redo the steps from 7-16 for another 9 times and update the names based on the number of the trial.

18. Open “construct” tab and choose point then click on “by best fit”.

19. As feature select all the 10 points of the center of spheres and name it virtual center of the sphere.

20. Construct a new point following the steps 18 and 19 from all the MAEP points and name it virtual MAEP.

21. Redo steps 18 and 19 and construction new points for all the first points and second points and name them virtual first point and virtual second point respectively.

22. Redo the steps from 11 to 16 and as “Primary” choose center of virtual sphere and MAEP virtual (with Z+ as the Axis), choose first point virtual and second point virtual (with X+ as the Axis) as “Secondary” and set the center of virtual sphere as the “Origin”.

23. Make sure to click on “Hold to primary” and name the coordinate system as virtual coordinate system.

24. Click on “Alignment” choose “Manage Alignments”.

25. Click on “Coordinate system”

26. Choose coordinate system virtual as “Measured Coordinate System” and World as “Nominal Coordinate System”.

27. In the Existing Alignments delete all the alignments and set the obtained alignment from the step 26 as active alignment.

28. Open the “File” then click on “Import/Export” and then open “Transformation Matrix”.

29. In the opened Window choose the coordinate system Number 1 as the “Matrix” and then click the “Use base matrix”.

30. As “Base Matrix” choose Virtual Coordinate System.

31. Save it as “Euler File” type.

32. Name the file as name of the operator execution date and the number of coordinate system.

33. Redo the steps from 28 to 32 and update the number of the “Euler File” based on the number of the coordinate system.

34. Ask the second and third operator to redo step from 7-33 each of the operators for 10 times.

35. Prepare the second sawbone and repeat these steps for each three operators.

36. Prepare the third sawbone and repeat these steps for each three operators.

APPENDIX F TEST PROCEDURE FOR VALIDATION OF THE RESECTION PLATE

1. Fix the FaroArm on the table.

2. Fix the femoral jig and the pointies block of the jig with 3 screws on the table at a distance of approximately one meter from FaroArm.

3. Fix the Stopper part on the table with 3 Screws and place the sawbones part of the jig on it.

4. Make sure the jig is rigid without any looseness.

5. Place the resection plate on the cut surface of the sawbone and secure it with the two special screws (the screw can be place in the bone with using your hands).

6. Open “FaroCam2”.

7. Choose the “Measure” from the toolbar.

8. Select “Plane” from toolbar and prob 10 points from the surface of the resection plate and name it Plane1.

9. Select the “Point” from toolbar and probe 5 points of the first cone (has been written on the pointies block) of the Pointies Block of the jig and name it First Point 1.

10. Probe 5 points of the second cone (has been written on the pointies block) of the Pointies Block of the jig and name it Second point 1.

11. Open the “Alignments” tab and click on “Coordinate System”.

12. Choose “Advanced” from the opened window and click on the plane shape in the first tap and make sure to click on “Hold to Primary”.

13. Choose plane 1 (with Z+ as the Axis) as “Primary”.

14. Select the Line shape in the second tab.

15. Choose first point1 and second point 1 (with X+ as the Axis) as “Secondary” and set the first point1 as the “Origin”.

16. Make sure the option Align with World is not checked.

17. Name the Coordinate System Coordinate System 1.

18. Redo the steps from 7-17 for another 9 times and update the names based on the number of the trial.

19. After all the 10 measuring procedure choose the “Measure” from the toolbar and select the “Point” from toolbar and obtain 3 points of the surface of the resection plate and name them projection point 1 to 3.

20. Open “construct” tab and choose “point” and click on “by the best fit” and from features select all the 10 first points and name it first point virtual.

21. Construct another point by choosing all the 10 second points and name it second point virtual.

22. Choose “Construct” click on “Point” and choose “by projection”.

23. Select the projection point1 and project it to all the 10 planes. Redo this step for projection point 2 and projection point 3 on all the 10 planes.

24. Name the points as projected point 1 to 30.

25. Choose “Construct” click on “Plane” and choose “by best fit”.

26. Select all the 30 projected points from features and name the constructed plane as Virtual Plane.

27. Open the “Alignments” tab and click on “Coordinate System”.

28. Choose “Advanced” from the opened window and click on the plane shape in the first tap and make sure to click on “Hold to Primary”.

29. Choose virtual plane (with Z+ as the Axis) as “Primary”.

30. Select the Line shape in the second tab.

31. Choose first point virtual and second point virtual (with X+ as the Axis) as “Secondary” and set the first point virtual as the “Origin”.

32. Make sure the option Align with World is not checked.

33. Name the Coordinate System Coordinate System virtual.

34. Click on “Alignment” choose “Manage Alignments”.

35. Click on “Coordinate system”

36. Choose coordinate system virtual as “Measured Coordinate System” and World as “Nominal Coordinate System”.

37. In the “Existing Alignments” delete all the alignments and set the obtained alignment from the step

36 as active alignment.

38. Open the “File” then click on “Import/Export” and then open “Transformation Matrix”.

39. In the opened Window choose the coordinate system Number 1 as the “Matrix” and then click the “Use base matrix”.

40. As “Base Matrix” choose Virtual Coordinate System.

41. Save it as “Euler File” type.

42. Name the file as name of the operator execution date and the, the number of the coordinate system.

43. Redo the steps from 38 to 42 and update the number of the “Euler File” based on the number of the coordinate system.

44. Ask the second and third operator to redo step from 7 to 43 each of the operators for 10 times

45. Prepare the second sawbone and repeat these steps for each three operators.

46. Prepare the third sawbone and repeat these steps for each three operators.

APPENDIX G RAW DATA FOR THE TEST PROCEDURE OF MAEP

Number of run\ Test features	Operator	Setup	V/V angle	F/E angle
1	N.A	1	-0.0057296	-0.005730
2	N.A	1	0.0000000	0.005730
3	N.A	1	0.0000000	-0.005730
4	N.A	1	0.0057296	0.000000
5	N.A	1	0.0057296	0.005730
6	N.A	1	0.0000000	0.005730
7	N.A	1	0.0000000	0.000000
8	N.A	1	-0.0057296	-0.005730
9	N.A	1	0.0000000	-0.005730
10	N.A	1	0.0000000	-0.005730
11	N.A	2	0.0114592	0.000000
12	N.A	2	0.0000000	-0.005730
13	N.A	2	0.0000000	0.011459
14	N.A	2	-0.0057296	0.005730
15	N.A	2	0.0000000	0.000000
16	N.A	2	-0.0057296	0.000000
17	N.A	2	0.0000000	0.005730
18	N.A	2	-0.0057296	-0.017189
19	N.A	2	0.0000000	0.005730
20	N.A	2	0.0000000	0.000000
21	N.A	3	0.0057296	0.000000
22	N.A	3	-0.0114592	-0.005730
23	N.A	3	0.0057296	0.005730
24	N.A	3	0.0000000	-0.011459
25	N.A	3	0.0057296	0.000000
26	N.A	3	-0.0114592	0.000000
27	N.A	3	-0.0114592	-0.005730
28	N.A	3	0.0000000	0.005730
29	N.A	3	0.0057296	0.011459
30	N.A	3	0.0000000	0.000000

Figure G.1 The V/V and F/E angle resultant from the measuring the MAEP for the First Operator.

Number of run\ Test features	Operator	Setup	V/V angle	F/E angle
1	J.T	1	-0.0057296	-0.005730
2	J.T	1	0.0114592	0.011459
3	J.T	1	-0.0057296	0.000000
4	J.T	1	0.0000000	0.005730
5	J.T	1	0.0057296	0.000000
6	J.T	1	0.0000000	0.005730
7	J.T	1	-0.0057296	-0.011459
8	J.T	1	0.0000000	0.000000
9	J.T	1	0.0000000	0.000000
10	J.T	1	0.0057296	-0.005730
11	J.T	2	0.0114592	0.017189
12	J.T	2	-0.0057296	0.005730
13	J.T	2	-0.0057296	-0.005730
14	J.T	2	-0.0057296	-0.011459
15	J.T	2	0.0000000	0.005730
16	J.T	2	0.0000000	0.005730
17	J.T	2	0.0000000	-0.022918
18	J.T	2	0.0057296	0.011459
19	J.T	2	0.0000000	-0.005730
20	J.T	2	0.0000000	0.000000
21	J.T	3	-0.0114592	-0.017189
22	J.T	3	0.0114592	-0.011459
23	J.T	3	-0.0114592	0.000000
24	J.T	3	-0.0057296	0.005730
25	J.T	3	0.0000000	0.034377
26	J.T	3	0.0057296	0.005730
27	J.T	3	0.0057296	0.005730
28	J.T	3	0.0057296	0.011459
29	J.T	3	0.0000000	-0.017189
30	J.T	3	0.0000000	-0.022918

Figure G.2 The V/V and F/E angle resultant from the measuring the MAEP for the Second Operator.

Number of run\ Test features	Operator	Setup	V/V angle	F/E angle
1	A.Z	1	0.0000000	0.000000
2	A.Z	1	-0.0057296	-0.017189
3	A.Z	1	0.0000000	-0.011459
4	A.Z	1	0.0057296	0.000000
5	A.Z	1	0.0000000	0.000000
6	A.Z	1	0.0000000	0.000000
7	A.Z	1	0.0000000	0.005730
8	A.Z	1	0.0000000	0.017189
9	A.Z	1	0.0000000	0.000000
10	A.Z	1	0.0000000	0.000000
11	A.Z	2	0.0057296	-0.013132
12	A.Z	2	-0.0114592	0.022918
13	A.Z	2	-0.0171887	-0.005730
14	A.Z	2	0.0057296	0.005730
15	A.Z	2	0.0000000	0.011459
16	A.Z	2	0.0057296	-0.011459
17	A.Z	2	0.0000000	0.000000
18	A.Z	2	0.0000000	0.022918
19	A.Z	2	0.0000000	0.022918
20	A.Z	2	0.0000000	0.022918
21	A.Z	3	-0.0057296	0.000000
22	A.Z	3	0.0000000	0.005730
23	A.Z	3	0.0057296	0.017189
24	A.Z	3	0.0057296	-0.005730
25	A.Z	3	-0.0057296	0.005730
26	A.Z	3	-0.0057296	0.000000
27	A.Z	3	-0.0057296	0.000000
28	A.Z	3	0.0057296	-0.017189
29	A.Z	3	0.0000000	-0.005730
30	A.Z	3	0.0057296	0.000000

Figure G.3 The V/V and F/E angle resultant from the measuring the MAEP for the Third Operator.

APPENDIX H RAW DATA FOR THE TEST PROCEDURE OF RP

Number of run\ Test features	Operator	Setup	V/V angle	F/E angle
1	N.A	1	0.05729576	-0.040107
2	N.A	1	-0.017188733	0.103132
3	N.A	1	-0.074484471	0.000000
4	N.A	1	-0.063025332	-0.022918
5	N.A	1	-0.148968691	-0.160428
6	N.A	1	0.040107039	0.051566
7	N.A	1	0.10886185	0.051566
8	N.A	1	0.200534409	0.189075
9	N.A	1	-0.051566188	-0.131780
10	N.A	1	-0.045836614	-0.034377
11	N.A	2	0.028647887	0.017189
12	N.A	2	0.263558727	0.120321
13	N.A	2	-0.051566188	-0.034377
14	N.A	2	0.063025332	-0.022918
15	N.A	2	-0.177616348	-0.022918
16	N.A	2	-0.080214039	-0.068755
17	N.A	2	0.183345869	0.120321
18	N.A	2	-0.074484471	0.000000
19	N.A	2	-0.14323915	-0.103132
20	N.A	2	-0.011459156	-0.005730
21	N.A	3	0.017188733	-0.011459
22	N.A	3	0.080214039	0.080214
23	N.A	3	-0.063025332	0.063025
24	N.A	3	0.022918311	-0.074484
25	N.A	3	-0.040107039	0.085944
26	N.A	3	-0.017188733	0.000000
27	N.A	3	0	0.068755
28	N.A	3	-0.022918311	-0.005730
29	N.A	3	0.063025332	-0.131780
30	N.A	3	-0.040107039	-0.074484

Figure H.1 The V/V and F/E angle resultant from the measuring the RP for the First Operator.

Number of run\ Test features	Operator	Setup	V/V angle	F/E angle
1	J.T	1	0.017188733	0.355229
2	J.T	1	0.080214039	-0.017189
3	J.T	1	0.011459156	0.091673
4	J.T	1	-0.068754902	0.022918
5	J.T	1	-0.051566188	-0.171887
6	J.T	1	-0.005729578	-0.034377
7	J.T	1	0.040107039	-0.234911
8	J.T	1	-0.022918311	-0.120321
9	J.T	1	0	0.040107
10	J.T	1	-0.011459156	0.074484
11	J.T	2	-0.080214039	-0.143239
12	J.T	2	0.034377464	0.022918
13	J.T	2	-0.068754902	-0.085944
14	J.T	2	0.080214039	0.034377
15	J.T	2	0	0.074484
16	J.T	2	0.005729578	0.085944
17	J.T	2	0.051566188	-0.063025
18	J.T	2	-0.040107039	0.011459
19	J.T	2	0	-0.034377
20	J.T	2	0.017188733	0.097403
21	J.T	3	-0.022918311	-0.017189
22	J.T	3	0	-0.091673
23	J.T	3	0.022918311	0.005730
24	J.T	3	0.034377464	0.011459
25	J.T	3	-0.022918311	-0.040107
26	J.T	3	0.005729578	0.022918
27	J.T	3	-0.114591406	-0.017189
28	J.T	3	0.034377464	0.005730
29	J.T	3	0.022918311	0.028648
30	J.T	3	0.045836614	0.085944

Figure H.2 The V/V and F/E angle resultant from the measuring the RP for the Second Operator.

Number of run\ Test features	Operator	Setup	V/V angle	F/E angle
1	A.Z	1	0.240640859	0.040107
2	A.Z	1	0.126050512	0.103132
3	A.Z	1	0.12032096	-0.080214
4	A.Z	1	-0.10886185	-0.045837
5	A.Z	1	0.206263915	0.366688
6	A.Z	1	-0.10886185	-0.017189
7	A.Z	1	0.12032096	0.315124
8	A.Z	1	-0.017188733	0.097403
9	A.Z	1	0.051566188	0.085944
10	A.Z	1	-0.641814253	-0.865274
11	A.Z	2	-0.022918311	0.028648
12	A.Z	2	0.103132292	0.148969
13	A.Z	2	0.28647651	0.269288
14	A.Z	2	0.085943605	0.091673
15	A.Z	2	0.05729576	0.080214
16	A.Z	2	-0.464132076	-0.538618
17	A.Z	2	-0.114591406	-0.160428
18	A.Z	2	-0.080214039	-0.028648
19	A.Z	2	0.005729578	0.034377
20	A.Z	2	0.137509607	0.085944
21	A.Z	3	-0.234934873	-0.676126
22	A.Z	3	0.05729576	0.206264
23	A.Z	3	0.12032096	0.040107
24	A.Z	3	-0.017188733	0.011459
25	A.Z	3	0.177616348	-0.160428
26	A.Z	3	-0.160427763	0.326582
27	A.Z	3	-0.085943605	-0.234911
28	A.Z	3	0.12032096	-0.028648
29	A.Z	3	-0.011459156	0.280747
30	A.Z	3	0.005729578	0.200534

Figure H.3 The V/V and F/E angle resultant from the measuring the RP for the Third Operator.

APPENDIX I MATLAB CODE FOR THE BOOTSTRAPPING

I1.png I1.png I1.png I1.png

Figure I.1 An illustration of bootstrapping code in Matlab

APPENDIX J CALCULATION OF K4 FACTOR IN THE MINITAB 17 SOFTWARE

- Open the “Statistics” from the toolbar.
- Click on the “Quality Tools” from the opened bar.
- Next from the opened bar click on the “Tolerance Interval”.
- In the opened window, choose “Summarized Data”.
- Enter the required data, per table 4.3 for “Sample Mean” and “Standard deviation” and set the number of 30 for the “Sample size” (the number of trial for the previous study).
- Click on the “Options”, in the opened window set the “Confidence Level” on 95.0, Minimum Percentage of Population in Interval per table 3.1, and the Tolerance Interval as two-sided.
- The results of the K4 factor will be appear on the “Work Sheet” of the Minitab.

APPENDIX K THE SCRIPT OF THE KRUSKAL-WALLIS TEST IN THE MINITAB 17 SOFTWARE

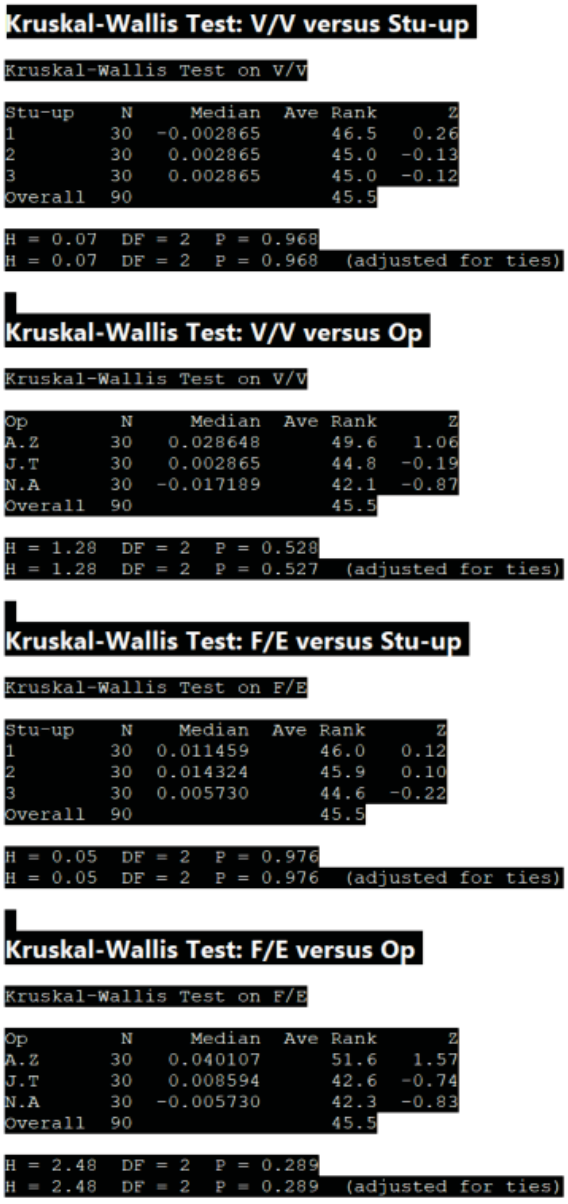

Kruskal-Wallis Test: V/V versus Stu-up

Kruskal-Wallis Test on V/V

Stu-up	N	Median	Ave Rank	Z
1	30	-0.002865	46.5	0.26
2	30	0.002865	45.0	-0.13
3	30	0.002865	45.0	-0.12
Overall	90		45.5	

H = 0.07 DF = 2 P = 0.968
H = 0.07 DF = 2 P = 0.968 (adjusted for ties)

Kruskal-Wallis Test: V/V versus Op

Kruskal-Wallis Test on V/V

Op	N	Median	Ave Rank	Z
A.Z	30	0.028648	49.6	1.06
J.T	30	0.002865	44.8	-0.19
N.A	30	-0.017189	42.1	-0.87
Overall	90		45.5	

H = 1.28 DF = 2 P = 0.528
H = 1.28 DF = 2 P = 0.527 (adjusted for ties)

Kruskal-Wallis Test: F/E versus Stu-up

Kruskal-Wallis Test on F/E

Stu-up	N	Median	Ave Rank	Z
1	30	0.011459	46.0	0.12
2	30	0.014324	45.9	0.10
3	30	0.005730	44.6	-0.22
Overall	90		45.5	

H = 0.05 DF = 2 P = 0.976
H = 0.05 DF = 2 P = 0.976 (adjusted for ties)

Kruskal-Wallis Test: F/E versus Op

Kruskal-Wallis Test on F/E

Op	N	Median	Ave Rank	Z
A.Z	30	0.040107	51.6	1.57
J.T	30	0.008594	42.6	-0.74
N.A	30	-0.005730	42.3	-0.83
Overall	90		45.5	

H = 2.48 DF = 2 P = 0.289
H = 2.48 DF = 2 P = 0.289 (adjusted for ties)

Figure K.1 An illustration of the script of the Kruskal-Wallis Test in the Minitab 17 software